Machine Learning to Optimize Embedded Adaptive Deep Brain Stimulation

Benjamin I. Ferleger

A dissertation
submitted in partial fulfillment of the
requirements for the degree of

Doctor of Philosophy

University of Washington

2020

Reading Committee:

Howard J. Chizeck, Chair

Jeffrey A. Herron, Chair

Andrew L. Ko

Program Authorized to Offer Degree:
Electrical and Computer Engineering

University of Washington

Abstract

Machine Learning to Optimize
Embedded Adaptive Deep Brain Stimulation

Benjamin I. Ferleger

Co-Chairs of the Supervisory Committee:
Professor Emeritus Howard J. Chizeck
Department of Electrical and Computer Engineering

Assistant Professor Jeffrey A. Herron
Department of Neurological Surgery

This thesis focuses on the development and application of novel machine learning approaches to the problem of optimization in adaptive deep brain stimulation. As brain-computer and brain-machine interfacing has rapidly developed in the past few years, attention in the relevant research has shifted from proof-of-concept to proof-of-feasibility. One of the first and, therefore, best-developed neurotechnologies is deep brain stimulation (DBS). DBS is a surgical intervention prescribed for several treatment-refractory neurological conditions. First, a stimulating electrode is chronically implanted into a condition-specific deep brain structure. The parameters of the stimulation provided by this electrode are then set by a clinician. Stimulation remains at these parameters continuously unless a patient actively chooses to disable their treatment. As has been repeatedly demonstrated, DBS is a safe and effective treatment for a number of movement disorders and is under active investigation for potential use in several psychiatric conditions.

DBS, however, is not a panacea. Battery replacement requires a revision surgery, and even rechargeable systems' batteries must generally be replaced at least once within a device's lifetime. Additionally, DBS therapy is associated with a number of unpleasant and sometimes dangerous side effects. These side effects can range from transient paresthesias to episodes

of depression and mania, and are broadly correlated with high levels of stimulation over long periods of time. In addition to concerns over battery life and side effects, the programming procedure for DBS is based primarily on a back-and-forth between clinicians and patients in a clinical setting. If we define "optimal" treatment as the most complete suppression of symptoms with the least manifestation of side effects, then achieving the corresponding settings is the goal of this procedure. The time consuming nature of this procedure, when considered in the context of clinical time constraints and patient fatigue, means that the parameters selected are far more likely to be the first passable setting than the truly optimal one. Patients are generally given the ability to disable their stimulation or select from a small range of amplitudes, but cannot actively reprogram their devices outside of a clinical setting.

One technique with the potential to alleviate concerns about side effects and battery life is adaptive deep brain stimulation (aDBS). aDBS refers to any method that uses feedback on a patient's state to modulate stimulation parameters in real time. This feedback could come in the form of gyroscope and accelerometer data in the case of movement disorders, or could be derived from neural signals that are correlated with the onset of symptoms. These signals are then processed and meaningful features extracted from them, which may in turn be used to determine the appropriate stimulation parameters. This ensures that stimulation is only applied as needed.

It is important to note that aDBS systems also intrinsically expand the state space for DBS programming, potentially adding yet more complexity to an already laborious procedure. As directional leads become more common in DBS devices, this expanded programming state space further reduces the likelihood of optimal settings being reached. A twin requirement to developing effective aDBS systems is thus the design of a streamlined procedure for parameter optimization in DBS programming. This may be accomplished through the introduction of an automated programming pipeline. Through the collection of quantified

data on symptom severity through the use of gyroscope or accelerometer data and the digitization of patient feedback on side effects, this pipeline could considerably speed testing. In addition, the digitization of the data required to analyze aDBS parameter performance could be integrated with modern optimization techniques, such that a personalized optimal treatment may be determined to within an increased degree of certainty.

This work details approaches for resolving these deeply interwoven problems in aDBS treatment through insights from the fields of machine learning and optimization. We begin by considering the current state of the art in adaptive deep brain stimulation, its accomplishments, but especially its limitations. The principal limitations are: a general reliance on distributed systems that hinder free movement in patients; a focus solely on computationally inexpensive, but potentially suboptimal, binary aDBS control strategies; and the lack of an effective pipeline to deploy optimization methods during or after programming. Furthermore, recognition that these limitations are fundamentally interrelated implies that an integrated approach is required.

The three key developments detailed in this work are thus themselves closely interrelated. Despite minor reductions in power savings, fully embedded binary aDBS is specifically designed to maximize therapeutic efficacy and ease of programming. Our results demonstrate that such a system is prepared for widespread studies in movement disorders. Our graded aDBS system yielded inconclusive results with regards to power savings and therapeutic efficacy. However, basing our approach to feature selection for symptom estimation from neural data on a model-free foundation has yielded promising evidence for relying on data-driven feature extraction. This approach to feature extraction intrinsically requires less direct programming, and instead maximizes the insights that may be gained from the data itself. Our development of a pipeline for automated programming of DBS parameters based on inertial measurements and patient feedback on side effects was designed to generalize easily into future integration with aDBS programming procedures. Finally, our computational ap-

proach to extracting information from a tablet- and mobile-based application demonstrates that semi- or fully-automated remote symptom assessment has the potential to significantly improve the future delivery of optimized, individualized treatment.

Throughout this work, integration is a key component of discussion and consideration. Each result extracted from the developments discussed herein represents a small step away from the current standard of care. Considered individually, these steps would be taken in completely different directions. It is the hope of the author that this work instead constitutes a realignment of these disparate goals and an explicit recognition of their inter-relatedness. Only by treating these problems as different faces of the same die can we arrive at truly optimized personalized treatment in aDBS.

TABLE OF CONTENTS

LIST OF FIGURES

GLOSSARY

θ (THETA) BAND: Refers to the 4-12Hz band of neural signals

α (ALPHA) BAND: Refers to the 8-12Hz band of neural signals

β (BETA) BAND: Refers to the 12-30Hz band of neural signals

γ (GAMMA) BAND: Refers to the 30-100Hz band of neural signals

ADBS: Adaptive deep brain stimulation; often used interchangeably with closed-loop deep brain stimulation (CL-DBS), although "aDBS" will be the preferred terminology in this work

BBCI: Bidirectional brain-computer interface

BCI: Brain-computer interface

BMI: Brain-machine interface

CDBS: Continuous or conventional deep brain stimulation

CL-DBS: Closed-loop deep brain stimulation, synonymous with aDBS (aDBS being the preferred terminology in this work)

DBS: Deep brain stimulation

ECOG: Electrocorticography

EEG: Electroencephalography

EMG: Electromyography

ET: Essential tremor

IMU: Inertial measurement unit (i.e., accelerometer and gyroscope)

IPG: Implanted pulse generator

LFP: Local field potential

MD: Movement, or motor, disorder

NM: Neural marker

TRS: Tremor rating scale

ACKNOWLEDGMENTS

I would like to thank a few people whose mentorship has been indispensable over the course of my academic career. Firstly, Dr. Janet Waldeck for pushing me to do more than I strictly "had to," well before I understood why that was important. Secondly, Professor David Borton, whose guidance through my undergraduate years provided me with pivotal insight into research. Thirdly, Dr. Brian Snyder for giving me the opportunity to take charge of a project and the freedom to design an approach. Finally, my PhD advisors and mentors, Professors Howard Chizeck and Jeffrey Herron and Dr. Andrew Ko, without whom this thesis quite simply could not have been accomplished.

I would next like to thank those whom I've had the good fortune to call my colleagues at the University of Washington. I'd like to thank Dr. Maggie Thompson, Dr. Tim Brown, Dr. Brady Houston, and Dr. Andrew Haddock for very, very patiently showing me the ropes. Additionally, thank you to Sabrina Sonnet and Sarah Cooper for the immense contributions made to several of the the papers foundational to this thesis.

I would also like thank our collaborators from other institutions: Professor Michael Tangermann and Dr. Sebastián Castaño-Candamil for both our deeply engaging and productive collaboration in graded aDBS, and for making me feel welcome while I was a visiting graduate researcher at the University of Freiburg; and Dr. Svjetlana Miocinovic, Professor Babak Mahmoudi, and Parisa Sarikhani for their insight and enthusiasm throughout our collaboration on the design of a platform for automated parameter selection in deep brain stimulation.

Finally, I would like to thank those institutions and organizations that have funded this research. Portions of this work were supported by a donation of devices and funds from

Medtronic and by Award Number EEC-1028725 from the National Science Foundation for the Center for Sensorimotor Neural Engineering, in addition to the BrainLinks-BrainTools Cluster of Excellence funded by the German Research Foundation (DFG, grant number EXC1086) and by the Federal Ministry of Education and Research (BMBF, grant number 16SV8012). I also acknowledge support in the form of computing resources from the state of Baden-Württemberg, Germany, and DFG through grants bwHPC, and INST 39/963-1 FUGG. The content is solely the responsibility of the author and does not necessarily represent the official views of the National Science Foundation, Medtronic, or the German Research Foundation.

DEDICATION

To Max, MC, Johnny, Lesley, Andy, and Rei for your love and support from very near and much too far.

To Andrew for always pushing me to walk where I talk.

To Vijeth for making sure I kept my head where it needed to be.

To Momona and Bora for making lab a place worth going into and getting out of.

To Laurel and Patricia for tea of many kinds and an utterly unique friendship.

Zu Sebastián, weil du mir geholfen hast, die Bächle zu meiden.

To Cousin Joey for making sure we get where we're going, and to Lexie for your steadiness while we got there.

To Jack, Linden, and Zac for truly unmissable interludes.

To Gene, Sam, Laura, Shauna, and Jessica for food, cthulhu, chickens, chess, and a home.

To Ma, Dad, Harold, Donna, Jonah, and Ruthie for everything I have and everything I am.

And, finally, to Katie – this would have been impossible without you. Thank you for your patience, your kindness, and for knowing when what I really needed was a kick in the ass. I love you.

Chapter 1

INTRODUCTION

The field of brain-computer or brain-machine interfacing (BCI or BMI) has arrived at something of a moment in the sun. Broadly referring to any attempt to circumvent the standard corporeal media standing between the brain and the outside world, BCI technology promises a direct link between the human nervous system and external machines. As such, BCI has the potential to represent a paradigm shift in how humans interact with the world. The recent maturation of the medical imaging and electrophysiological sensing tools required to extract neural data and the computational methods required to make sense of this data have reached a tipping point. No longer relegated to laboratories in a handful of academic institutions, private companies promising BCI-based technology have rapidly proliferated in the past few years. Their stated goals range from optimizing sleep and stress reduction to integrating artificial and biological intelligence. In the near term, however, much of the focus of this field remains where it began: in the generation of treatment strategies for those suffering from neurological injuries and diseases.

Among the most common and debilitating of these are the broad category of conditions referred to as movement disorders (MDs). This wide family of neurological disorders includes many conditions that have devastating effects through physical symptoms. Simultaneously, the loss of agency experienced by many patients diagnosed with these conditions often exacts a significant psychological toll on both those directly affected and their loved ones [1, 2]. Among the most widely known MDs are Parkinson's Disease (PD), essential tremor (ET), and primary dystonia, which together affect approximately 8% of the geriatric population worldwide [3, 4, 5]. Pharmacological treatments are effective in the early stages of these conditions, but the progressive nature of most MDs leads the efficacy of these treatments to

eventually fade [6].

When this erosion of treatment efficacy reaches a certain point, patients have an alternative in the form of deep brain stimulation (DBS) treatment. DBS represents the first and, to date, the most widely adopted chronically implanted invasive BCI device. In a surgical procedure, a small hole is drilled into the skull and a thin electrode inserted into a condition-specific deep brain structure. Electrical stimulation is then continuously delivered into the brain, ameliorating the patient's MD symptoms. Currently approved for use in several MDs [7, 8, 9] and obsessive-compulsive disorder [10], DBS is also being investigated for use in psychiatric conditions including Tourette's syndrome and major depression [11, 12, 13].

Despite its promise, however, DBS remains an imperfect treatment. From a design perspective, the most substantial drawback is that battery replacement presently requires a revision surgery to replace the relevant component of the implanted pulse generator (IPG) every 3 to 5 years [14, 15, 16]. Although rechargeable IPGs are quickly becoming the standard of care, even these will require occasional replacement. As chronically implanted devices, it is highly likely that most patients will need at least one such battery replacement surgery in their lifetimes. Another shortcoming of DBS, inherent in the treatment itself, is the incidence of unpleasant side effects. These range from motor and sensory effects including transient paresthesia [17], difficulty speaking [18, 19, 20], and balance or gait issues [21, 19], to chronic neuropsychiatric events and disorders including depression [19, 22], mania [22], and sexual behavioral disinhibition [23]. Taken together, 86% of patients experience some level of post-operative adverse effect related to DBS treatment, with severe irreversible effects occurring in nearly 5% [19].

Finally, DBS parameter selection generally depends on a time consuming back-and-forth between a patient and a clinician that amounts to a guess-and-check strategy. The clinician attempts a setting, asks the patient about side effects, conducts a clinical test to determine setting efficacy and, if the setting is ineffective or intolerable for the patient, tries the next setting [24]. This process comprises a breadth-first search of monopolar settings, with frequency and pulse width pre-selected. If no setting proves acceptable, frequency and pulse

width may then be modulated as well. Only after these settings have failed are bipolar settings investigated. The DBS parameter state space is thus immense, and evaluation of each setting within this space both time consuming and potentially inconsistent given the variability typical in MD symptoms. Optimal parameters, defined as the most complete symptom suppression with the lowest possible incidence of side effects, are therefore very unlikely to be found; rather, the first set of parameters that result in a tolerable level of side effects and reasonable amount of symptom suppression is generally the one selected.

It may thus be said that the current standard of care, referred to as continuous or conventional DBS (cDBS), suffers from three interrelated drawbacks: limited battery life, incidence of both transient and chronic side effects, and a high likelihood of selecting parameters that do not achieve the maximum treatment efficacy. The first cannot be completely eliminated without the introduction of a transcutaneous power supply, which in turn would come with complications including introduction of a new device, a requirement for a physical tether on the patient, and medical concerns about infection risk. These complications have precluded any real consideration of such a system. Any fully implanted electrical device will eventually require the replacement of its power source. However, minimizing the amount of power used would naturally increase battery life, substantially reducing the frequency of revision surgeries. Additionally, the incidence of side effects has been broadly correlated with the amplitude of stimulation received over a period of time [25, 26, 14]. The pathology of movement disorders is such that the clinical level of stimulation is not necessarily required at all times to suppress symptoms [27, 13]. This opens the door to the possibility that stimulation may be adjusted based on what activity the patient is engaged in or how severe their symptoms are during that activity. This may be considered the patient's state.

One approach to resolving the first two problems is the use of some form of feedback to modulate stimulation parameters in real time depending on patient state. This feedback may take the form of a sensor that directly reports symptom severity, such as an accelerometer, gyroscope, or electromyography (EMG) device to detect tremor. Alternatively, this feedback could be based on the collection of neural data through external sensors, like electroen-

cephalography (EEG), or implanted sensors, such as electrocorticography (ECoG). When paired with a machine learning algorithm to determine and extract neural markers (NMs) that correlate with patient state, these sensors are capable of a comparable level of patient state prediction. Broadly speaking, this closed-loop technique is referred to as adaptive deep brain stimulation (aDBS). Interchangeably referred to as closed-loop DBS (CL-DBS), aDBS has received increasing attention for its capacity to reduce overall stimulation and thereby extend the battery life of DBS devices. Previous studies have also indicated that lowering stimulation even temporarily can result in significant reductions in side effects manifestation and severity [26].

Interwoven with this attempt to provide a more nuanced, responsive treatment is the need to ensure the most effective treatment parameters are attained. Although real-time feedback on patient state allows for aDBS control systems to be developed, the actual effectiveness of this system is directly tied to how the device parameters are set during programming. The introduction of an aDBS control system increases the complexity of the programming process, adding several new parameters to assess in concert with the already-substantial state space of DBS programming.

One approach to ensuring optimal treatment parameters are found, while simultaneously preventing the ballooning of the DBS parameter state space with the addition of aDBS, is the introduction of automated programming techniques. Previous work has demonstrated that both computer-in-the-loop and brute-force fully-automated DBS programming are as or more effective than the current standard of care [28, 29, 30]. What has yet to be developed is a pipeline capable of testing advanced optimization techniques in this uniquely challenging problem space.

By developing a method to evaluate symptom severity using some set of biosensors, such as data derived from inertial measurement unit (IMU) recordings to determine tremor, one may pair this empirical data with digitized patient feedback on side effects. The combination of this data through a recording, synchronization, and feature extraction pipeline permits us to treat DBS programming as an optimization problem with quantifiable inputs. This,

in turn, opens up the entire field of optimization methods, which has the potential to allow clinicians to entirely replace the time consuming present method of DBS programming with a highly efficient approach that can be assured of an optimal outcome.

Although this will assist in the programming process itself, it does not necessarily alleviate all problems related to the tracking of disease. The progression of individual patients' MD symptoms is highly variable, but clinical visits to evaluate these symptoms must often be scheduled months in advance. This can result in patients making unnecessary visits to the hospital or, in an even worse scenario, suffering through uncontrolled symptoms for several weeks before their scheduled visits. One approach to resolving these issues is the creation of a system capable of remote symptom evaluation and quantification. To date, such methods have far been few and far between.

1.1 Specific aims

I will here document my work towards optimizing DBS treatment in movement disorders. The efforts within this work can be broadly broken into three specific aims, each attempting to demonstrate a different facet of treatment optimization. The first aim is the development and demonstration of a fully implanted aDBS system capable of functioning in freely moving patients. By eliminating the need for external sensors or processing, this development demonstrates that the simplest form of aDBS treatment, a binary system capable of disabling or enabling stimulation in real time without any external devices, is ready for deployment at large.

The second aim is an exploration of graded control systems for aDBS. Rather than the binary, all-or-nothing approach taken in the first aim, this approach takes as its baseline hypothesis that a binary system is an overly coarse control system in most cases. In contrast, a graded system with a range of settings between disabled and the clinically determined maximum value has the potential to provide additional power savings while further reducing the incidence of side effects.

Finally, the third aim details attempts to resolve issues with ensuring the effectiveness

of DBS therapy itself. In this aim, I discuss the creation of a platform for optimization in DBS parameter selection and a mobile- and tablet-based drawing application for remote tremor assessment. While this optimization platform streamlines the programming process for patients receiving DBS therapy, the drawing application allows for patients to complete MD severity evaluations at more regular intervals than permitted by clinical visits alone. When adopted, these developments may ensure that every patient's symptoms are effectively tracked and, when no longer controlled, that the patient may be scheduled for a streamlined reprogramming visit based on their individual disease progression rather than population-based estimates.

1.1.1 Aim 1: demonstrating a fully implanted binary adaptive deep brain stimulation system in freely moving patients

Ultimately, the adoption of an aDBS platform will depend on the ability to package it as an all-in-one system. The evidence available on adoption of health-related wearables suggests that systems dependent on these wearables may suffer from poor patient compliance due to questions of convenience, reluctance to wear the required device, and privacy concerns [31, 32]. Even with a fully implanted distributed system, it is quite likely that the patient will occasionally leave the required external processing device too far away to effectively connect and communicate with their implant. One workaround to each of these issues is the introduction of a "fail-safe setting" where, in the absence of an external connection providing feedback, stimulation parameters default to the clinical maximum. However, while this ensures that treatment will not fall below therapeutic levels, it also reverts such a system back to cDBS and thus negates any benefits to be gained from aDBS.

The most straightforward way to avoid these issues, then, is the implementation of a fully embedded system, wherein sensing, control, and stimulation parameter updates take place entirely "in-the-can" of the DBS device itself. By its nature, a fully embedded system will not be disabled or rendered ineffective due to a patient forgetting or refusing to use a symptom tracking wearable. Additionally, it frees the patient to move without the need of

any physical or wireless tether to an external processing device.

However, these advantages come with the loss of the easily interpreted patient state information a wearable provides, as well as the boost in computational power typical of an external data processing unit. In the case considered here, we are further restricted to a binary control system due to the limitations of the Activa PC+S. In approaching the problems presented by this aim, algorithm and control system design were of paramount importance. Chapter 3 includes consideration of the new concerns introduced by this technology, and outlines how a clinically-oriented algorithm may overcome these barriers. The results generated by the application of this algorithm lead to the conclusion that binary fully implanted aDBS is ready for widespread studies in MDs.

1.1.2 Aim 2: an exploration of graded adaptive deep brain stimulation strategies and techniques

Even with the development of a fully implanted system demonstrated in chapter 3, it remains incumbent upon researchers in this space to consider how this system may be further improved. The benefits promised by this binary system imply that even greater levels of optimization may be achieved in the delivery of aDBS treatment. These may be best delivered through the use of a graded control system.

Unlike in a binary control system, where a simple classification algorithm was sufficient for effective treatment, graded aDBS systems require that symptom severity itself be estimated in real time. Neural markers (NMs) were selected as the feedback system in order to most easily generalize to future, fully implanted systems. Chapter 4 therefore focuses on a pilot study to develop a graded aDBS system using solely this data source. Results from this study are considered, and subsequent developments in estimation of symptom severity from neural data are discussed. These developments imply that graded aDBS is at least as effective as binary aDBS, though further work is needed to determine how best to estimate symptom severity in real time using neural signals alone.

1.1.3 Aim 3: strategies and platforms for personalization and optimization in deep brain stimulation treatment

In this final section, we approach the problem of developing tools for the effective and efficient delivery of optimized DBS treatment. In a divergence from the first two aims, this section will focus most closely on patients receiving cDBS treatment. At present, stimulation parameters are selected in a highly laborious procedure that is unlikely to land on the most effective treatment for an individual patient. This is due in large part to the relatively limited number of settings that may be efficiently tested within a given programming session.

In chapter 5, we begin with the generation of a toolkit for future automated DBS parameter optimization. This chapter details the development of a pipeline that will enable rapid testing, evaluation, and updating when combined with modern optimization techniques in future studies. Through this pipeline, the programming procedure may be shifted from a laborious back-and-forth between clinicians and patients to a rapid and efficient process. The design of such a system has added importance in the context of directional leads, which are likely to become the standard in DBS probe design in coming years and add significantly to the size of the stimulation parameter state space. In addition, this chapter details the creation of a tablet- and mobile-based application for remote MD symptom assessment. This permits a far more informative picture of patient symptom progression to be established than is possible using only scheduled clinical visits, and may even be generalized into a remote DBS parameter updating tool. The combination of these two developments may in turn lead to a more personalized course of treatment and evaluation in patients receiving DBS treatment.

Chapter 2

STATE OF THE ART IN ADAPTIVE DEEP BRAIN STIMULATION FOR MOVEMENT DISORDERS

2.1 Movement disorders

Succinctly characterized by Stanley Fahn as neurological conditions resulting in an "excess of movement or a paucity of voluntary and automatic movements, unrelated to weakness or spasticity," MDs have an indelible effect on quality of life for those diagnosed with them [33]. It should be noted that individual members of this family of disorders do not necessarily share a causal basis. Rather, they are grouped by their shared pathological effects: the removal of control and agency one has over one's own body and movements. Although some MDs, such as Tourette's syndrome, are generally not degenerative, others, such as Huntington's disease, are progressive in nature. For many MDs, medications exist that can treat symptoms or slow progression for a time, but by their nature the severity of these conditions will eventually surpass the level where pharmacological interventions are effective.

2.1.1 Parkinson's disease

Parkinson's disease (PD) is a progressive disease affecting approximately 1% of the population over age 60 [4]. It is characterized by four cardinal motor symptoms: tremor, rigidity, bradykinesia, and postural instability [34, 27]. Additionally, psychiatric effects including dementia, depression, and anxiety are common [1]. In part due to the prominence of several individuals who have been diagnosed with the condition in the past few decades, PD has received an enormous boost in public awareness and funding to combat the effects of the condition. Due to its degenerative, debilitating, relatively widespread, and currently incurable nature, PD currently stands as one of the most extensively researched medical conditions.

2.1.2 Essential tremor

The vast majority of the work considered in this thesis is derived from studies with essential tremor (ET) patients. ET is the most common MD worldwide, affecting an estimated 4.6% of the global population over the age of 65 [3, 35]. Characterized by a postural and kinetic tremor in the 4-12 Hz range with peak frequency variable between individuals, ET is notably absent during rest in most cases [27]. In many patients, tremor severity is at first relatively limited and minor work-arounds may be found for most tasks, leading to its earlier designation as "Benign" Essential Tremor. However, in advanced cases, fine motor skills such as writing, sewing, and painting can become impossible. Eventually, even coarser activities like driving and handiwork can become difficult or dangerous to perform. In addition to the issues raised by the motor symptoms alone, the cognitive effects and psychological ramifications of the loss of agency encountered by patients diagnosed with ET can be devastating [36, 37].

2.1.3 Diagnosis and treatment in PD and ET

PD and ET are thus two of the most prevalent and best known MDs [3, 35, 4]. Though lacking a known etiological relationship, each presents as a progressive disease with a pronounced tremor component [27]. Each condition may be pharmacologically controlled in its earlier stages, using levadopa, dopamine agonists, anticholinergics, and MAO B and COMT inhibitors for PD and beta blockers, tranquilizers, and sometimes anti-seizure medications for ET. However, the degenerative nature of each of these conditions leads these pharmacological interventions to steadily lose efficacy over time.

These conditions were the first two in which cDBS was tested for therapeutic benefits [38, 39]. Numerous follow up studies have confirmed the efficacy of cDBS for each condition. As improvements have been made to cDBS devices and delivery of those devices, each have seen substantial reductions in the incidence of perioperative complications and improvements in long-term patient outcomes [8, 40, 41, 42, 43, 44]. The wealth of studies in the safety

and efficacy of cDBS provides a reliable background against which to compare the efficacy of newer, more advanced permutations of DBS therapy.

2.1.4 Symptom assessment and follow up

Although initial assessment of MD symptoms includes methods for differential diagnosis, the exact procedure for symptom assessment in MDs is condition-specific after diagnosis [27]. One commonality in the assessment procedure is the requirement that a clinician observe as a patient conducts a certain set of motor tasks that are known to present problems for those diagnosed with the MD in question [45, 46, 47]. This requires the patient to travel to a clinical location and conduct a series of tasks in the presence of a clinician, and therefore typically takes place only during scheduled clinical visits.

These tests are specifically designed to give clinicians the broadest possible understanding of the disease state for each condition. Although inter-rater comparison for patient state overall is broadly reliable, evaluation of performance on individual tasks can vary widely among multiple raters [48, 49]. Methods have been proposed that make use of inertial measurement data to develop a more quantified basis for tremor assessment, but these methods have yet to achieve widespread adoption [50, 51, 52, 53]. Additionally, MD symptoms vary significantly in severity based on factors as varied as hunger, fatigue, and circadian rhythm [54, 55]. The heterogeneous nature of many MDs means that these visits may or may not coincide with periods of disease progression in any given individual [27, 56, 57]. Although patient diaries are taken into account during assessment of disease progression, these are subject to problems in reliability and patient compliance, and cannot present a quantified assessment of symptom manifestation [58].

2.2 Deep brain stimulation

2.2.1 A brief history

Although records dating back to antiquity describe symptoms characteristic of movement disorders, modern medical understanding of MDs developed more fully through the late 19th and early 20th centuries [59, 60]. Those diagnosed with these generally progressive conditions had little in the way of treatment options, but by the beginning of the 20th century the literature on the rough symptomatic pathology of several MDs had matured enough for physicians to distinguish between them [59, 61]. Without modern imaging techniques, evaluation of patients diagnosed with movement disorders had to wait until they had passed away. These postmortem examinations revealed the existence of lesions and Lewy bodies in deep brain structures in several MDs, indicating that the root cause of these conditions likely lay within these structures [61, 62, 63].

A series of surgical interventions, both deliberately tested and accidentally discovered, were developed throughout the early-to-mid 20th century [64]. It was eventually determined that thalamotomy or pallidotomy – the destruction of part or all of the thalamus or globus pallidus – could lead to reduction in symptom severity for those suffering PD and other MDs [65, 66]. The discovery that levadopa treatment led to a substantial reduction in PD symptoms was essential in the development of modern understanding of its pathology [67, 61]. A renewed interest in these conditions then focused attention on the basal ganglia, uncovering some of the fundamental bases of movement in the process [61]. Although the surgeries developed through this period were effective in treating MDs, their irreversible nature and the risks and side effects associated with such interventions drove researchers to continue seeking alternative methods for treatment [61].

To determine the exact regions to be ablated, surgeries were sometimes prefaced by simulation of a lesion, either through application of chemicals or through high frequency electrical stimulation to temporarily deactivate target regions [64]. Irving Cooper, an early pioneer of both "chemotomy" and stimulation-based deactivation during target evaluation, was among

the first to propose chronic stimulation as an alternative to ablation [64]. Although his attempts were hamstrung by the limitations of electronics available at the time, this laid the foundation for French neurosurgeon Alim Louis Benabid and his colleagues. Benabid's work resulted in the first approval for implantation of a device specifically designed to chronically stimulate a deep brain structure for the treatment of Parkinson's disease in 1987 [38]. This technique was largely as effective as thalamotomy or pallidotomy, and its reversible nature made it far more appealing to both surgeons and prospective patients than the destruction of a portion of the brain had been. In the following years, as a similar procedure was investigated and approved for the treatment of patients diagnosed with several other MDs and psychological disorders, this method came to be known as deep brain stimulation (DBS).

2.2.2 Deep brain stimulation today

DBS has since been established as safe and effective in the treatment of Parkinson's disease [7, 43], essential tremor [8, 41, 42], dystonia [9], and obsessive-compulsive disorder [10], with additional studies being conducted in patients diagnosed with other neuropsychiatric disorders like major depression [11] and Tourette's syndrome [12]. Among the several models of DBS devices that are commercially available today, the essentials of the treatment itself are fairly standardized. After a surgery to implant a thin, flexible stimulation electrode probe into a condition-dependent sub-cortical target, high frequency ($\geq$ 90Hz) stimulation is continuously supplied to the target. Implantation carries risks inherent in all surgeries, including hemorrhage (1-2%) and infection (3-5%) [43]. However, follow up studies in MDs have generally concluded that the long-term benefits outweigh both perioperative and long-term risks [7, 8, 9]. As of 2019, DBS devices had been chronically implanted in an estimated 160,000 patients [68].

After implantation, the current standard of care in DBS begins with the patient and a clinician selecting stimulation parameters based on the patient's feedback on tolerable side effects, and the clinician's observation of symptom suppression. After this programming procedure, stimulation is left continuously active at these parameters. This procedure, in

which stimulation cannot be disabled without directly interacting with the device, is known as continuous, or conventional, DBS (cDBS). Presently, cDBS is the only method approved for use in most patients receiving DBS in the United States. Although, as outlined above, the benefits of cDBS are numerous and well-substantiated, the treatment is not a panacea. Transient side effects including paresthesias [17], difficulty speaking [18, 19, 20], and balance or gait issues [21, 19], and potentially chronic neuropsychiatric events and disorders including depression [19, 22], mania [22], and sexual behavioral disinhibition [23]. In addition, battery replacement, which in most devices must be conducted every 3 to 5 years, requires a revision surgery [14, 16]. These factors imply that cDBS therapy may still be improved upon.

2.3 Adaptive deep brain stimulation

Adaptive deep brain stimulation (aDBS) refers broadly to any DBS system that uses some sort of feedback to modulate stimulation parameters in real time [69, 70]. One of the earliest proofs-of-concept for this technique essentially comprised handing patients with PD a controller that enabled them to activate and deactivate their device as needed depending on their desired activity [71]. This limited level of this sort of control is now common, with most patients receiving DBS being given an accompanying wireless device that allows them to turn their stimulation on or off at will. Modern controllers generally permit the patient to increase or decrease stimulation amplitude within a limited window. This allows patients to deactivate stimulation when preparing for any activity during which their treatment will not be needed. This can result in substantial battery savings, and may reduce the incidence of side effects.

This simple structure may suffice in highly specific cases, such as when an individual with ET is about to go to sleep and thus can reliably assume they will not require DBS treatment for several hours [27]. However, for real-time modulation during an individual's activities of daily living, requiring explicit patient instructions for control can quickly become a significant burden. Furthermore, in the event a patient needs to activate their stimulation, the very motor symptoms they are trying to treat could become an impediment to successful

interaction with their device. A more responsive approach is the use of biometric data to infer patient and disease state in real time [69, 70]. These inferences may then be used to modulate stimulation accordingly. Although investigation of biomarkers for psychiatric disorders is an active realm of study, in this work we will restrict our considerations to MDs.

2.3.1 Inferring patient state and disease state in MDs

In MD patients, the most obvious and direct inference of patient state may be derived from devices that record the patient's movements [72, 73]. Such data allows for quantified information to be derived about a patient's symptoms and, by extension, for implications about treatment efficacy to be determined. The main benefit of using this form of data is the ease of interpretation. For example, ET frequently manifests as a 4-12 Hz upper limb tremor; therefore, a highly reliable estimate of relative tremor severity may be derived by simply assessing the power of this band from kinetic data [27]. If arm or hand movement is of principal interest, gyroscope and accelerometer measurements acquired from the inertial measurement unit (IMU) included in most commercial smartwatches is among the most straightforward ways to acquire this data [74]. Electromyography (EMG) data also may be used to acquire more detailed information from more varied sources [75].

An alternative, somewhat more indirect, approach uses biomarkers extracted from neural data, known as neural markers (NMs), to determine patient state [76, 77, 78, 79, 80]. Specific methods for data extraction include both noninvasive methods, such as electroencephalography (EEG), and invasive technologies, like electrocorticography (ECoG). Unlike movement data, neural data cannot necessarily be directly related to symptom severity based solely on inferences made by a human observer. Instead, this data must be processed and features extracted. These features may then be analyzed against either patient state (i.e., is the patient moving or at rest) or disease state (i.e., severity of hand tremor) through the application of signal processing and machine learning techniques. Although this requires significantly more work than depending solely on movement data, using neural data has the potential to "predict" patient state a few moments before the patient actually enters that state. This

lends neural data-based aDBS algorithms the capacity to preempt movement rather than responding to an uptick in symptom severity as it occurs.

2.3.2 aDBS stimulation control systems

Unlike cDBS, aDBS requires that some sort of control system be developed to provide the appropriate stimulation for a patient's state. Broadly speaking, this control system falls into one of two categories: binary or graded. In a binary aDBS (b-aDBS) control system, stimulation may be either completely "off" or "on" at clinically determined levels [79, 81, 80, 78]. The obvious benefit of this system is its simplicity. By reducing the question of adaptive treatment to its most basic possible form – whether the patient requires any stimulation or not – the accompanying data analysis architecture required may be reduced to a binary classification problem. However, this simplicity comes at the expense of specificity, and may still result in the patient receiving more stimulation than they necessarily require given their state.

A graded aDBS (g-aDBS) control system, by contrast, attempts to provide the stimulation parameters that are best equipped to treat the patient given their state at the time [82, 83]. This could take the form of a continuous feedback system, wherein the minimum required stimulation amplitude is derived from the biomarkers recorded on a continuous basis. Alternatively, this graded control could select from one of several predetermined stimulation settings known to optimally treat the patient when they enter a given state. In either case, this control system could provide assurances of optimal treatment in a far more nuanced fashion than binary aDBS allows. However, the data analysis techniques and algorithms required for such a system would be far more computationally costly than in a binary system.

2.3.3 Analysis architectures

Regardless of which signal source is selected from section 2.3.1 or which control system is chosen from section 2.3.2, some level of processing and data analysis will be required to generate the appropriate control signal. This signal must then be transmitted to the

stimulating electrode itself. There are two architectures for an aDBS analysis and signal generation system: a distributed system and a fully implanted system. In a distributed system, biomarkers are analyzed by an experimental computer which generates a control signal in response to these markers [84, 69, 78, 74, 76, 80]. This control signal is then transmitted to the DBS device itself. A fully implanted system, by contrast, conducts all collection, analysis, and control signal generation within the DBS device [79]. Such a system is also colloquially referred to as an "in-the-can" system.

The primary tradeoffs between these systems are mobility vs. computational complexity. In a distributed system, the data analysis and control signal generation techniques employed are limited only by the computational power of the external computer used. In most modern applications, it is also feasible for a cloud-based data analysis pipeline to be developed. Even in systems that promise immense bandwidth in terms of the data recorded, such a computational setup could reliably conduct extremely complex calculations at or near real time. However, in order for such a system to function, the DBS device must have some ability to communicate with this external computational system. Regardless of whether this system is wireless or has a physical tether, the patient's mobility is thus explicitly restricted to within a certain range of the external computational unit by any distributed system.

A fully implanted system, meanwhile, would permit the patient to move freely and without explicit thought given to their device. This frees patients from both the physical restrictions demanded by a distributed system and the requirement to remember their external device at all times during the day. However, a fully implanted system will inevitably result in limitations being placed on the complexity of the algorithms deployed. Despite significant advances in the field of implantable devices, any chronically implanted device will have only a fraction of the computational power the average smartphone has today. This means that algorithms used for fully implanted aDBS will require significant optimization before deployment, and may render more complex control systems completely infeasible.

2.3.4 Closing the loop

From sections 2.3.1, 2.3.2, and 2.3.3, it is apparent that there exist several options in the design of an aDBS system, each with their own unique benefits, drawbacks, and limitations. Previous work has demonstrated that aDBS systems may be reliably based on IMU data recorded from a patient's affected limb [74]. EMG and kinematic data have also been demonstrated as effective methods for evaluating DBS therapy effectiveness [85, 86]. Due to the wearable nature of IMU and other kinetic data collection methods, this analysis may only be conducted by a distributed system.

The use of NMs collected through invasive devices opens the door to the generation of fully implanted systems, if the proper hardware exists. In such a system, an implanted electrode – possibly even the stimulating electrode itself – could record neural data in the form of local field potentials (LFPs). NMs could be derived from this data and a control signal generated within the onboard computing capacity of the IPG itself [79]. Alternatively, this data could be streamed to an external device for the application of more complex computational methods [81, 80, 84, 78].

2.3.5 Medtronic Activa PC+S

One device meriting special attention due to its ubiquity in this work is the Medtronic Activa PC+S (**P**rimary **C**ell + **S**ensing). This investigational device, created by medical device developer and manufacturer Medtronic, is comparable in therapeutic capacity to the commercial Medtronic Activa PC. The IPG is implanted in the upper chest and a fully implanted connection to the stimulation probe wired through the neck. The DBS probe is comprised of four stimulating electrodes, and is capable of either bipolar stimulation (with one electrode the anode and another the cathode) or monopolar stimulation (in which the anode is taken to be the IPG case and, from a theoretical standpoint in stimulation mapping, assumed to be at $r \to \infty$). Stimulation pulse width, frequency, and amplitude comprise the remaining parameters to be tuned.

What differentiates the PC+S from the stimulation-only PC is threefold. First, the PC+S includes the capacity to sense neural data in the form of LFPs from the attached leads. A proprietary conversion turns this information into telemetry data. Through a wireless connection to the IPG, this data may be streamed to an external computer from both sites at 200Hz or from a single site at 422Hz. This data is sent via packets collected every 200ms and transmitted every 400ms in sets of 2. In addition to these streaming options, a limited amount of data may be recorded onboard the IPG from a single site at 800Hz and downloaded to a computer through the same wireless connection. A final option for data acquisition is through the use of a proprietary bandpower estimation method, and provides an estimate of the power of a given band of neural data every 200ms (5Hz). The details of this final option are considered more fully in section 3.3.1. The streaming capacity of the system is bidirectional, allowing one pre-selected stimulation parameter, selected from amplitude, frequency, and pulse width, to be modulated in real time through instructions given by an external experimental computer. Streamed neural data may thus be either collected passively by an external computer, or integrated into a distributed aDBS system.

Second, the PC+S includes the capacity for a second recording lead in the form of a Medtronic Resume 2 ECoG lead. This lead makes use of the wired connection reserved for a second stimulation probe in the original PC if a clinician were to determine a bilateral course of DBS therapy were in order for a patient. The strip may be placed over any region of the cortex, permitting the collection of data from a second source.

Third, the PC+S includes the capacity to use an onboard binary classification algorithm to turn stimulation to a maximum or minimum amplitude based on the bandpower estimate discussed above. The details of this method will be expanded upon below in section 3.3.1. This capacity of the PC+S enables a fully implanted binary aDBS system to be deployed, allowing a patient to move freely with an aDBS system active and without the need for external sensing or a distributed data processing platform.

The PC+S is therefore a potentially powerful platform for the development of either a simple, binary fully implanted control system or a more complex distributed control system.

However, there are a few known drawbacks to this particular architecture. The first is a high noise floor for data recorded from the ECoG strip, restricting useful cortical data to those bands under about 50Hz. This precludes most of the gamma band from proper exploration for potentially useful NMs. A second drawback of this system is its relatively limited streaming capacity. Being restricted to no more than 2 channels at 200Hz or a single channel at 422Hz places an outsized burden on the accompanying algorithm to compensate for the sparsity of data. Finally, the restriction of the onboard control system to a binary classifier precludes the development or examination of results with a graded aDBS system during free movement, limiting the ability to explore the effectiveness of these more nuanced control systems. Nonetheless, as one of the first investigational tools of its kind, the PC+S is an extremely useful platform, which has served as the bedrock for all results in chapters 3 and 4, and much of the testing involved in the developments outlined in chapter 5. A diagram of the system may be found in fig 2.1.

Figure 2.1: An illustration of the Activa PC+S system, incorporating the IPG in the upper chest with wired connections to the ECoG strip over M1 and DBS probe in the thalamus. The IPG is equipped with data streaming and limited data storage capacity.

Chapter 3

FULLY IMPLANTED BINARY ADAPTIVE DEEP BRAIN STIMULATION

3.1 Distributed aDBS systems

A common thread in previously explored aDBS systems is a reliance on either external sensors or a distributed system for signal processing and control signal generation [84, 69, 78, 81]. External sensing, such as neural data collected with surface EEG or IMU data from a smartwatch affixed to a patient's treated wrist, provides easily defined and understood real-time feedback on symptom severity and patient activity [70, 81]. Distributed data processing structures use data streamed out to an external PC from implanted sensors, such as LFP data recorded using chronically implanted ECoG strips, in order to infer the patient's state through the deployment of machine learning algorithms on an external experimental computer or other computational device [78, 80, 76, 83]. The use of a distributed system allows the application of powerful data processing and machine learning techniques on notoriously noisy, non-stationary neural data. This permits development of highly accurate algorithms to predict patient state [80, 83].

Unfortunately, each of these system architectures entails significant drawbacks. External sensing systems require a patient to wear some symptom-tracking device at virtually all times, which is unlikely to serve in a translational capacity due to the likelihood of patients either forgetting to charge the required device, forgetting the device itself, or even their unwillingness to wear it altogether [31]. Likewise, distributed systems tether patients to an associated data processing device, limiting mobility in cases where the tether is a physical wire and, with wireless systems, running into the same translational problems encountered with wearable devices [87]. Additionally, both wearable and distributed systems raise clear

privacy and security concerns due to the streaming of personal health information. Perhaps even more concerningly, such a system architecture enables an increased potential for malicious third-party interference with the device itself [32].

3.2 Considerations for fully implanted aDBS systems

A fully implanted system, in which internally detected biomarkers are processed in the IPG itself and an on-board algorithm applied to modulate stimulation parameters in real time, promises the capacity to resolve each of these issues [79]. This system would eliminate concerns about a patient remembering their external devices by making the process entirely internal and automated, with the added benefit of intrinsically resolving issues of privacy and security during chronic treatment. Due to the necessity of using only internally recorded data, however, these systems would lack the ease of interpretability in programming ensured by wearable systems. Furthermore, the limited processing power available on implanted devices relative to modern computers and mobile devices leads to substantial reductions in the sheer processing power available to fully implanted systems. These factors have previously limited the translational applicability of fully implanted aDBS. Additionally, these hardware restrictions require that only a binary control system be used, precluding more nuanced treatment.

Here is detailed the first translation-oriented training procedure for a fully embedded aDBS control system for use in MDs, additionally constituting one of the first examples of a fully implanted aDBS system in freely moving ET patients. Previous attempts to develop fully implanted aDBS algorithms relied solely on the on-board capacity of the implanted system for training, leading to issues in reliability, repeatability, and interpretability [79, 88]. Through a straightforward distributed training procedure permitting reliable collection of training data, a supervised machine learning algorithm optimized for clinical considerations was used to train intrinsically personalized aDBS classifiers in two patients. These classifiers were then uploaded to the patients' devices and their performance evaluated through IMU data analysis and patient feedback. This system greatly simplifies the training procedure

itself while simultaneously increasing reliability and transparency of classifier training. The following sections are largely comprised of the content of an article published in the Journal of Neural Engineering detailing the design, implementation, and testing of an embedded aDBS system for tremor [89].

3.3 Implementation of a fully implanted aDBS system in ET

3.3.1 Device specifications

The on-board classifier of the Activa PC+S is limited to using a bandpower estimate of a given band of LFP data, calculated in a proprietary hardware design. The band must be of the form $c \pm r$ with $c \in \{2.5, 5, 7.5 \ldots 97.5, 100\}$Hz and $r \in \{2.5, 8, 16\}$Hz, with an estimate generated every 200ms (5Hz). Two different bandwidths may be collected from the DBS probe and the ECoG strip, respectively, resulting in a state estimate $\hat{X} \in \mathbb{R}^{4\times 1}$ defined as

$$\hat{X} = \begin{bmatrix} x_{DBS,1} \\ x_{DBS,2} \\ x_{ECoG,1} \\ x_{ECoG,2} \end{bmatrix}$$

Furthermore, due to the limited processing capacity of the IPG itself, we are restricted to a binary linear classifier to determine whether stimulation amplitude should be set to a pre-determined "LOW" value (set in this work to 0.0V in both patients) or "HIGH" value (a clinician-determined, patient-specific amplitude), with other parameters (frequency, pulse width, stimulation electrode configuration) held constant. Stimulation ramping slew rate for the on-board system cannot be explicitly set. Rather, the time for the system to ramp to its maximum amplitude must be selected as one of 1, 2, 4, or 8 seconds. Ramping time was set to 1 second for both patients to minimize time between movement onset and treatment.

3.3.2 Distributed training architecture

Despite the streaming capacity of the Activa PC+S, previous efforts towards using the device's fully embedded aDBS capacity required the researcher to rely solely on the on-board capacity of the device to record data in order to obtain training data, on which more detailed information may be found in section 2.3.5 [79]. This data could then be downloaded to a proprietary tablet, from which it had to be transported by USB to an experimental computer for analysis.

In contrast, our system is structured such that, during collection of training data, neural and IMU data are streamed wirelessly to an experimental computer. This allows for accurate and reliable timestamped data collection, and permits the instantaneous review of all training data to easily determine if a test must be repeated. When satisfactory results have been obtained, the classifier is uploaded to the IPG itself for evaluation of aDBS in free movement. A diagram of this system may be found in fig. 3.1.

3.3.3 Supervised training data collection

Since only neural data may be used in our classifier and the presence of stimulation is known to alter neural dynamics, data must be collected in each state with stimulation both active and disabled. In order to take these considerations into account, training data must be collected with patients in each state of the form [*Stimulation State, Patient State*], amounting to A) [*Off, Rest*], B) [*Off, Action*], C) [*On, Rest*], and D) [*On, Action*].

To obtain data during each of the four possible patient states, 30 seconds of data were collected with the patient at rest with hands in lap with stimulation active and stimulation disabled, and 30 seconds while the patient was continuously conducting the finger-to-nose task of the Fahn-Tolosa-Marin (FTM) tremor rating scale (TRS) with stimulation active and stimulation disabled [45]. These two minutes' total data were used to train an intrinsically personalized classifier. Immediately following data collection, a visualization of the time series of the bandpower estimate data akin to that in fig. 3.2 and cross-validated accuracy

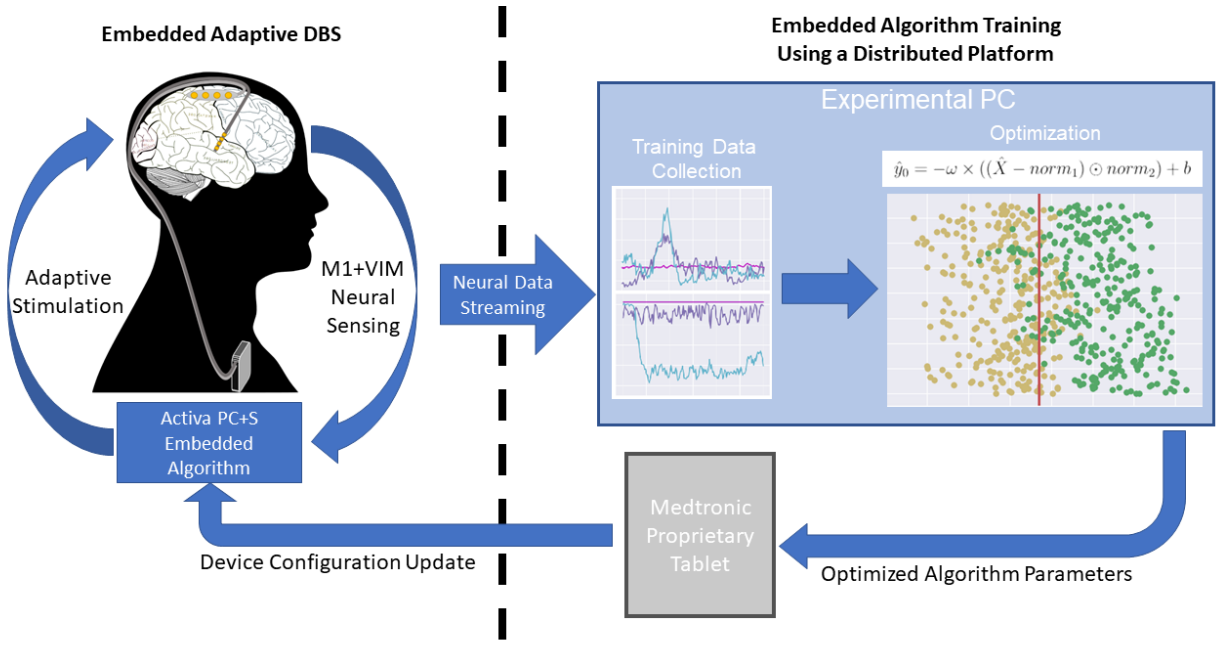

Figure 3.1: A diagram of our distributed training procedure using the Medtronic Activa PC+S. During the training procedure outlined in section 3.3.3, neural data is streamed wirelessly to an experimental PC on which initial data review is conducted. When satisfactory data has been collected, optimized algorithm parameters are trained and transported via USB to a proprietary tablet device. A configuration update to the Activa PC+S itself supplies it with the trained, personalized classifier. The embedded aDBS system then uses its sensing capacity with this classifier to modulate stimulation.

of a classifier trained on this data was available for review. This may be used to inform the researchers' decision to repeat individual tests if necessary. The structure of the training data collection was arranged to allow for individual states to be recorded independently, as opposed to repeating the full procedure.

3.3.4 Band selection and algorithm design

The primary task of the algorithm is to differentiate between when stimulation must be set to "HIGH", and when it may be left "LOW". The objective is therefore to determine when

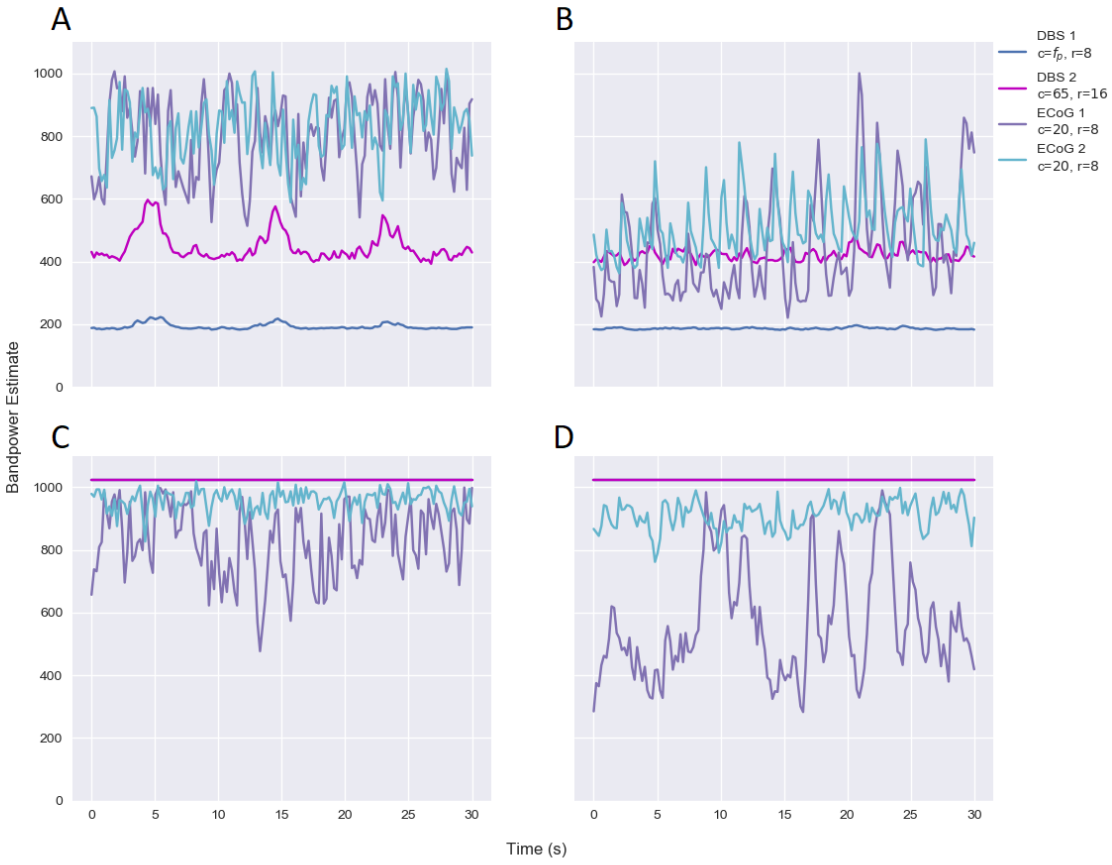

Figure 3.2: Time series training bandpower estimates of neural data used for Patient 1 for recordings, of form [*Stimulation State, Patient State*], of states A) [*Off, Rest*], B) [*Off, Action*], C) [*On, Rest*], and D) [*On, Action*]. Channel legend in upper right. Each set is 30 seconds in length, with bandpower estimate being an integer value between 0 and 1023. Differences between the *Rest* and *Action* states are readily apparent for ECoG data within stimulation states, with clear differences between the behavior across stimulation states. In the DBS channels, note the differences between signal behavior during *Rest* and *Action* with stimulation *Off*. During stimulation *On* in (C) and (D), the configured bandpower estimates for both DBS channels are saturated; this is indicated by the solid lines at the maximum value the system may output. This implies that the DBS channels provide both an effective indication of whether stimulation is active, and useful information when it is not.

a patient requires stimulation to treat their symptoms which, in ET patients, may be said to be the difference between when the patient is at *Rest* and generally without tremor, and when they are in *Action* and thus experiencing tremor.

Additionally, as the classifier has no explicit way to "know" whether stimulation is active or disabled, some method of indirect inference for device state must be provided. To allow the algorithm to determine whether stimulation was active or disabled, $x_{DBS,1}$ bandpower estimate was set to the patient-specific, clinically determined stimulation frequency ($c = f_{patient}, r = 8$). $x_{DBS,2}$ bandpower estimate was set to measure thalamic γ-band ($c = 65, r = 16$), previously demonstrated to correlate with movement [90]. Although suppression of thalamocortical coupling between the γ-band of the cortex and lower frequency bands of the VIM have been demonstrated to strongly correlate with movement [91], the noise floor in the Activa PC+S ECoG strip precludes effective measurement of this range. Instead, both $x_{ECoG,1}$ and $x_{ECoG,2}$ were set to record β-bandpower ($c = 20, r = 8$) from alternating pairs of the 4 linearly arranged ECoG electrodes available, desynchronization of which is known to correlate with movement onset, thus indirectly indicating onset of tremor in ET [80, 92, 93].

With $\hat{X}$ thus defined, an unbiased linear classifier was trained to differentiate between the 60 seconds of data collected during the *Rest* recordings and the 60 seconds collected during the *Action* recordings. A linear projection $\hat{y}_0 \in \mathbb{R}$ was defined with $\omega \in \mathbb{R}^{1\times4}$, $b \in \mathbb{R}$, $norm_1 \in \mathbb{R}^{4\times1}$, and $norm_2 \in \mathbb{R}^{4\times1}$ of the form

$$\hat{y}_0 = -\omega \times ((\hat{X} - norm_1) \odot norm_2) + b$$

so as to maximize the variance between the means of $\hat{y}_{0,Rest}$ and $\hat{y}_{0,Action}$. A sample above 0 was classified as *Action* and below 0 as *Rest*.

Finally, under the clinically informed theory that it is preferable to have stimulation unnecessarily active than to risk it being absent when needed, the classifier was biased in favor of keeping stimulation *On* by $\lambda = \frac{1}{5}$ the standard deviation of the projection from training data. This was accomplished by adding λ to that projection, thus creating the final projection $\hat{y} = \hat{y}_0 + \lambda$. This fraction was determined through analysis of previously recorded

data for distributed aDBS systems and found to consistently reduce false negatives without excessively increasing the overall error rate.

3.3.5 Tremor severity characterization and analysis

Gyroscope data from each task was extracted from IMU data streamed via Bluetooth at 100Hz from a smartwatch fastened around the patient's dominant wrist and timestamped upon receipt by an experimental PC. This data was split into 400ms intervals, a $4-12$Hz bandpass filter applied to extract only tremor-related data [27], and Welch's method applied to x, y, and z components individually to obtain the frequency domain of the inertial data. The area under the curve of each of the 3 components was approximated with the trapezoidal method, and the sum of these values used as our ground truth for semi-instantaneous IMU-based tremor severity assessment, denoted χ. Average level of tremor S, normalized for duration of test τ and thus defined as

$$S = \frac{\sum \chi}{\tau}$$

was derived for each test state. Tremor suppression J was defined as the fraction of tremor severity reduction as compared to tremor with stimulation *Off*, such that tremor suppression for a given control system may be defined

$$J_{system} = 1 - \frac{S_{system}}{S_{Off}}$$

3.3.6 Quantifying reduction in energy use

Energy use per unit time was calculated using the total electrical energy delivered (TEED) methodology proposed by Koss et al. [94] adapted to control for test duration τ, such that

$$TEED_{system} = \frac{voltage^2 \times frequency \times pulsewidth}{impedance \times \tau} \times seconds$$

Although actively running the classifier on the Activa PC+S results in a small increase in power demand, this value is not explicitly calculable *in vivo* [95]. Energy savings with aDBS

will therefore be quantified solely as the percentage of TEED saved in aDBS versus cDBS, such that relative energy saved may be estimated as $E_s = (1 - \frac{TEED_{aDBS}}{TEED_{cDBS}}) \times 100\%$.

3.3.7 Methods for evaluation of therapeutic accuracy

For the quantified portion of classifier evaluation, patients were asked to begin at rest with hands in their lap. At a semi-randomized timestamped prompt, the patient was asked to conduct the finger-to-nose task of the FTM [45] continuously until the next prompt, at which point they were asked to return to rest. IMU data was streamed continuously throughout the experiment, while stimulation amplitude was recorded on the Activa PC+S device during experiments and downloaded for analysis.

A false positive ϵ_+ was said to occur when stimulation amplitude rose above $\frac{1}{2}$ of a subject's clinically prescribed settings during a rest period, while a false negative ϵ_- was defined as stimulation amplitude below this level during a period of movement. Total error rate $\mathcal{E}$ was defined as the total number of errors divided by the duration of test τ, such that

$$\mathcal{E} = \frac{\sum \epsilon_+ + \sum \epsilon_-}{\tau}$$

This protocol was conducted with stimulation disabled, cDBS control system active, and aDBS control system active. Following this controlled experimental protocol patients were asked to stand and move freely for some minutes without IMU or neural recordings in order to determine qualitatively whether they could detect a difference in the quality of their treatment or in the manifestation of side effects.

3.4 Performance of fully implanted system

3.4.1 Subject information

Two subjects diagnosed with ET were implanted with the Activa PC+S (see section 2.3.5). These subjects, hereafter referred to as Patient 1 (P1) and Patient 2 (P2), were enrolled in studies at the University of Washington Medical Center. Patient information and clinical settings are outlined in table 3.1, with ECoG lead localization visualized in fig. 3.3.

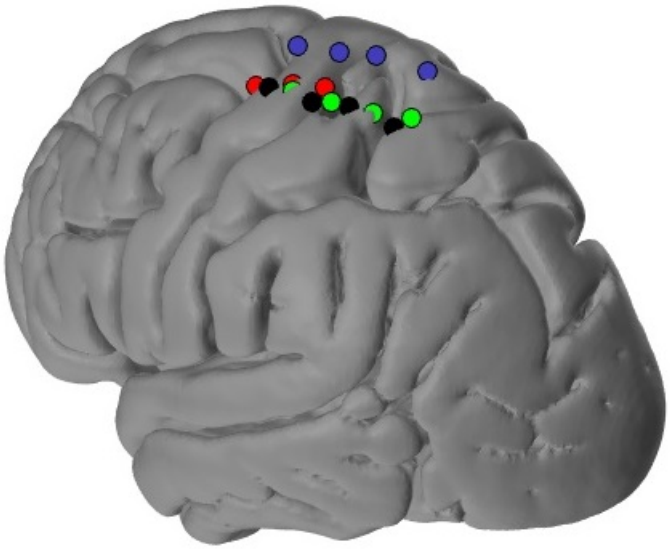

Figure 3.3: ECoG lead localization for P1 (red), P2 (purple), P3 (black) and P4 (green). Electrodes were placed based on median nerve somatosensory evoked potential phase reversal. Note that in P1, P2, and P3 the targeted hand and wrist region of the motor cortex was accurately covered; in P2, the strip more closely covered the shoulder, neck, and head region. Only P1 and P2 were involved in the study discussed in this section.

Table 3.1: Fully implanted aDBS patient information and clinical DBS settings, comprising amplitude, frequency, pulse width, and stimulating electrode configuration settings.

Patient	**Age**	**Sex**	**Dominant Hand**	**Ampl. (mV)**	**Freq. (Hz)**	**PW (μs)**	**Electrode Configuration**
P1	84	M	Right	3900	140	90	2+/0- (bipolar)
P2	70	M	Right	2100	140	90	1- (monopolar)

3.4.2 Distributed training procedure

As described in section 3.3.3, the data collected was made immediately available for review following recording of all 4 states. In each patient, review of the data visualization and cross-validated classifier performance led to the determination that one state, different in each

patient, was excessively noisy. The individual test pertaining to that state was repeated, and the classifier trained from the new set of states uploaded to the device.

The versatility of our distributed training system ensured that the entirety of the procedure, including explaining procedure and tests to subject, recording training data, reviewing data and repeating tests if needed, training classifier on selected data sets, and uploading classifier to patient device, was completed in under 20 minutes in each patient. This training time included repeat data collection for one state in each patient when initial data review revealed insufficient classification accuracy. This indicates that the brevity of the training process was due largely to the rapidity with which data could be analyzed and the ease of collecting more at-will with the distributed system

3.4.3 Effectiveness of biased classification algorithm

For the training data, a false positive is said to have occurred if a sample labelled *Rest* is above the threshold, while a false negative is said to have occurred if a sample labelled *Action* is below the threshold. Total error rate is the average of these rates, as equal training time was spent in the *Rest* and *Action* states. Biasing the threshold resulted in a 12.7% increase in average error rate; however, this constituted a 28.2% decrease in average false negative rate. Training data distribution and classification in each patient are presented in fig. 3.4, and the full results of biasing are detailed in table 3.2.

Biasing the classifier towards the *On* state reduced overall accuracy; however, this was exactly the intent. As may be seen in the analysis of training data, biasing resulted in marginal increases in overall error rate while cutting false negative rates for an overall sensitivity of 91.8%. It should be noted that total error rate was somewhat divergent between our patients, most likely due to the variation in ECoG lead localization during implantation. It is a testament to the robustness of our biasing system that the clinically relevant false negative rate was kept at the low levels seen. In our analysis of therapeutic accuracy during testing, we found that 96.4% of the time stimulation was required, it was provided. This increase in sensitivity may have to do with alteration of neural dynamics during stimulation ramping

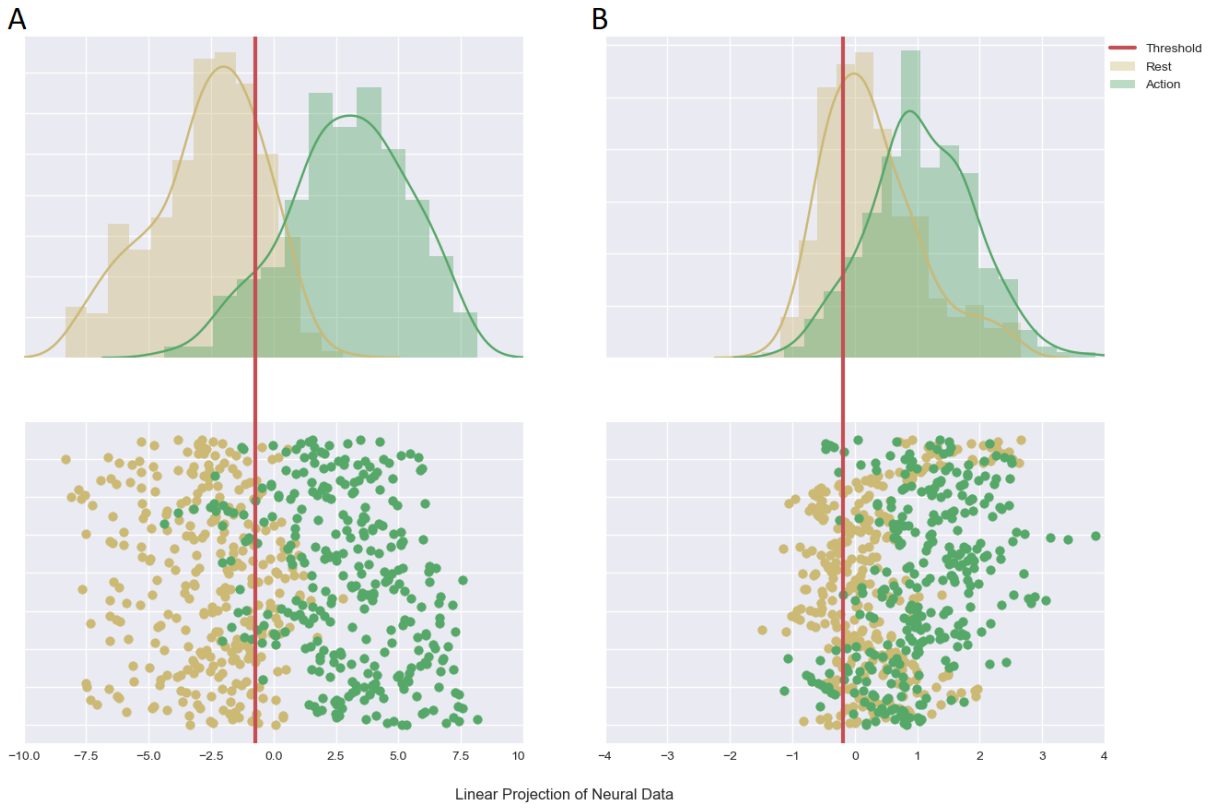

Figure 3.4: Kernel density estimation with histogram in training data for A) Patient 1 and B) Patient 2, with *Rest* data for both stimulation settings combined in yellow and *Action* data for both stimulation settings combined in green. The unbiased classifier control system would return *On* for any point over 0 and *Off* for any point beneath 0. Our patient-specific biased threshold, seen here as a red line down each figure, demonstrates that appreciably more of the *Action* state is classified as requiring stimulation than the unbiased system would recognize.

periods. Although the effect appears to be an increase in the likelihood of an *On* control signal, giving little clinical reason to examine it more closely, it is nonetheless an interesting occurrence that may be considered further. Quantification of classifier longevity, defined as the number of weeks a given classifier remains clinically effective, will require longitudinal studies and will be a focal point of future work.

Table 3.2: **Effects of biasing on training data**: Though overall error rate is increased by a marginal amount, clinically relevant false negative rate is substantially reduced in both patients, indicating that biasing our linear projection effectively increases treatment reliability by clinical considerations.

Measure	Unbiased	Biased
P1 training error rate	0.122	0.143
P2 training error rate	0.342	0.380
P1 training false neg. rate	0.130	0.090
P2 training false neg. rate	0.097	0.073

3.4.4 Therapeutic performance during controlled testing

For testing data, it was determined that therapeutic classifier average total error rate was $\mathcal{E} = 0.468$. However, over 92% of these errors were comprised of clinically permissible false positives; average false negative rate was $\mathcal{E}_- = 0.036$, indicating that stimulation was almost always being supplied at therapeutic levels during our experimental procedure. Use of the aDBS control system resulted in a 30.8% average drop in energy use by the neurostimulator. Complete results may be found in table 3.3, with stimulation and tremor severity during experiments displayed in fig. 3.7.

During their free movement period, subjects clearly and accurately differentiated between when stimulation was disabled and when some stimulation control system was active. However, they reported no differences in treatment efficacy between aDBS and cDBS. As data recording was not active during the free movement period, accuracy and specificity of aDBS could not be quantitatively evaluated. One patient reported experiencing a brief paresthesia in their right hand on two occasions with aDBS active. Neither reported any side effects with cDBS active.

Average tremor suppression across both patients with cDBS $J_{cDBS} = 0.361$. Average tremor suppression with aDBS $J_{aDBS} = 0.481$ for a 33.2% improvement with aDBS over

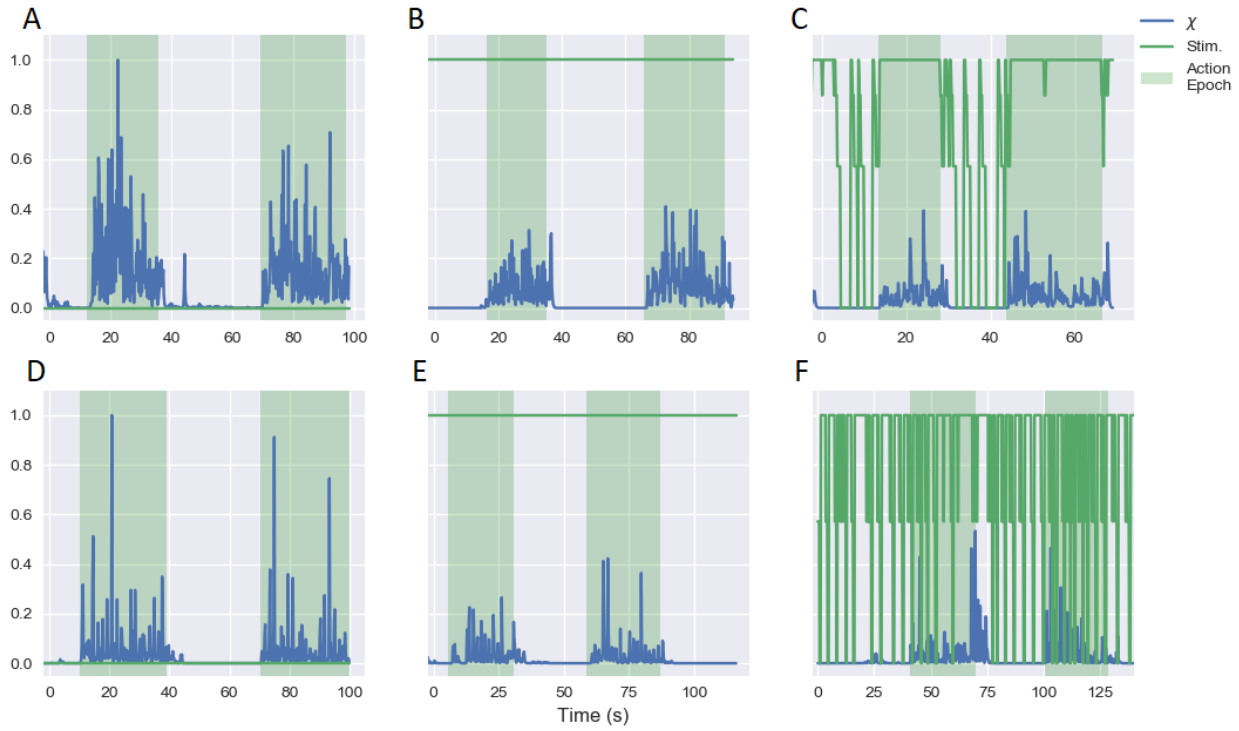

Figure 3.5: Stimulation amplitude (green line), normalized by clinically determined maximum amplitude, and tremor severity χ (blue line), normalized to the maximum value in any state, with stimulation disabled, enabled and with aDBS active (respectively, A, B, and C in Patient 1 and D, E, and F in Patient 2). Green background indicates patient was asked to perform finger-to-nose task, while blank background indicates patient instructed to rest with hands in lap. Although stimulation fluctuates substantially throughout experiment, note that it is consistently on during movement epochs, consistent with the desired effect of biasing the classification algorithm.

cDBS. This is in line with previous findings that aDBS is more effective in tremor suppression than cDBS [84, 80]. Detailed results are included in table 3.3.

Our results indicate that aDBS can reduce the stimulation power necessary to effectively treat tremor. However, it is important to note that such systems require additional sensing components and expanded signal processing capabilities of the embedded firmware. These additional hardware components would result in higher power usage than a cDBS device if

Table 3.3: **Efficacy of aDBS**: The extremely low false negative rates, paired with a significant reduction in overall stimulation, appear to have led to a substantial increase in tremor suppression in aDBS over cDBS.

Patient	**1**	**2**
Percentage TEED saved	34.0%	27.5%
Overall error rate	0.361	0.575
False negative rate	0.030	0.042
cDBS tremor suppression	0.596	0.125
aDBS tremor suppression	0.740	0.221

excluding stimulation. Prior work has demonstrated that, for the Activa PC+S when using typical stimulation parameters, a 6% reduction in stimulation "on-time" is all that is required to offset the power cost of the additional hardware and processing [95]. As stimulation was disabled 49% of our quantified test in P1 with 48% of the test in the "rest" state and 36% in P2 with 56% of the test in the "rest" state, we can comfortably assume our system delivered net power savings.

Nonetheless, longitudinally assessing the power savings of these systems in a patient's less rigidly structured activities of daily living will be required to make a final determination of the overall potential of aDBS to improve battery life, and should be a focus of future work. Given the trends in the development of lower-power integrated circuits and more efficient microprocessing units, even biased aDBS algorithms that disable stimulation very conservatively will most likely offset any power cost of the added hardware and processing.

In keeping with previous findings for ET [84, 80], our quantified analyses of symptom severity indicated that aDBS was substantially more effective in tremor suppression than cDBS on average, albeit with less substantial tremor reduction in P2 than in P1. This divergence may be partly due to P1 having considerably more severe tremor without treatment, reducing the relative amount that treatment can observably reduce symptoms in P2. This

may be similar to the "floor" effects found in aDBS for PD [79].

Although the cause of this increased efficacy is not currently well understood, our working hypothesis relates it to the tolerance and habituation effects previously described in DBS of the VIM [96, 97, 98]. The regular shifts in stimulation parameters characteristic of aDBS may have the added benefit of acutely interrupting this habituation, although further studies will be needed to assess the validity of this hypothesis. A related follow up question requiring larger subject pools will be whether aDBS is more effective in all patients, improves tremor suppression in some individual patients more than others, or if it is more effective depending on stimulation target, such as the VIM vs. the subthalamic nucleus.

That aDBS treatment was at least as effective as cDBS was supported by our patients' reports in their periods of free movement, during which they noticed no substantial differences in treatment efficacy. When paired with our quantitative results implying the superiority of aDBS treatment over cDBS, this suggests that, while the differences in therapeutic efficacy may be below the threshold of perception for most patients already receiving cDBS, an aDBS system may be able to operate with a lower maximum amplitude than that used in cDBS systems, thereby reducing overall stimulation to an even greater extent. This will further increase the already substantial energy savings promised by aDBS systems. Additionally, as previous work has indicated that "context-dependent" fully implanted aDBS systems can effectively differentiate between several patient states, such as gait holding an object vs. gait with hands naturally at sides [99], a more quantified treatment of our freely moving period will be a component of further work.

The transient paresthesia experienced by Patient 1 is most likely an indicator that the ramping rate for stimulation was set too high [69]. This issue may be resolved through a straightforward addition to the patient programming phase. Rather than prioritizing reaching maximum stimulation level as quickly as possible, a "maximum tolerable rate" test should be implemented in future training procedures in order to ensure patient comfort is maintained during aDBS.

3.5 Evaluating potential short-term effects of binary aDBS

One clinically observed phenomenon with potential implications for binary aDBS in ET is the "rebound effect" [100, 101, 44], a seeming inversion of the washout period well documented in PD [102]. Immediately following deactivation of DBS, the rebound effect manifests as a transient increase in tremor severity which eventually settles into a pre-stimulation baseline of tremor, referred to here as the "steady state." This sudden cessation is a relative nonissue in patients receiving cDBS, but in binary aDBS could be expected several dozens of times per day depending on patient activity. Given this paradigm shift in the nature of treatment provided, a more in-depth consideration of rebound is warranted.

Clinical observations of the rebound effect in existing literature have been mixed. Kronenbuerger et al. [71] did not observe rebound in their ET patients, Patel et al. [97] saw rebound effect in demyelinating sensorimotor peripheral neuropathy but not ET patients, and Hariz et al. [101] and Reich et al. [100] observed rebound in only a subset of their ET patients. In all of these studies, only clinical TRS's were used to assess the presence of rebound. These tests are often subject to issues of inter-rater reliability for movement disorders, especially in writing and drawing tasks [48, 49]. This indicates a need to find a more quantitative and intrinsically reproducible approach to assessing tremor severity. A recent study by Paschen et al. [44] marked the first use of IMU data to quantify the curve of rebound. In the subset of their patients who experienced rebound, this study found that tremor severity peaked some 2 minutes after cessation of stimulation and reached steady state after about 30 minutes. This means that, on the timescale on which the above binary aDBS system was active, we would not have had sufficient time to examine rebound effect or its immediate consequences on treatment efficacy.

Within this section, largely covered in work presented at the Engineering in Medicine and Biology Conference in 2020 [103], I detail a study attempting to characterize rebound effect in a more explicitly quantifiable way. Using tasks specifically chosen to generate a maximal tremor response, clinical and IMU-based assessment were conducted on patients to

determine the arc of rebound effect.

3.5.1 Patient information and data collection

Three patients implanted unilaterally with the Activa PC+S served as subjects. Relevant patient information may be found in Table 3.4. IMU data collection was conducted using a procedure identical to that described in section 3.3.5.

Table 3.4: **Rebound effect patient information**, including age, sex, months since implantation surgery was conducted, and the time before the study for which stimulation was continuously active. Note that, while patients 2 and 3 disabled their devices for sleep, reactivating them each morning, patient 1 preferred to leave his continuously active except during set medical or experimental appointments when disabling it was required.

Patient No.	**Age (yrs)**	**Sex**	**Mo. Since Imp.**	**Time Stim. On**
P1	84	M	39	3 months
P2	70	M	24	5.5 hours
P3	82	M	29	4 hours

3.5.2 Experimental protocol

Each "task session" comprised patient completion of two tasks: the spiral-drawing and the line-drawing tasks of the FTM (examples in Fig 3.6) [45]. A tablet-based application was used for all tremor data collection. Each experiment involved a series of task sessions completed at approximately 5-minute intervals over a period of 38-42 minutes, including 1 to 2 sessions when stimulation was activated and 6 to 7 sessions after stimulation was deactivated. Video recordings of the patient completing each task were collected for later analysis by clinicians. IMU and neural data were streamed continuously throughout experiment.

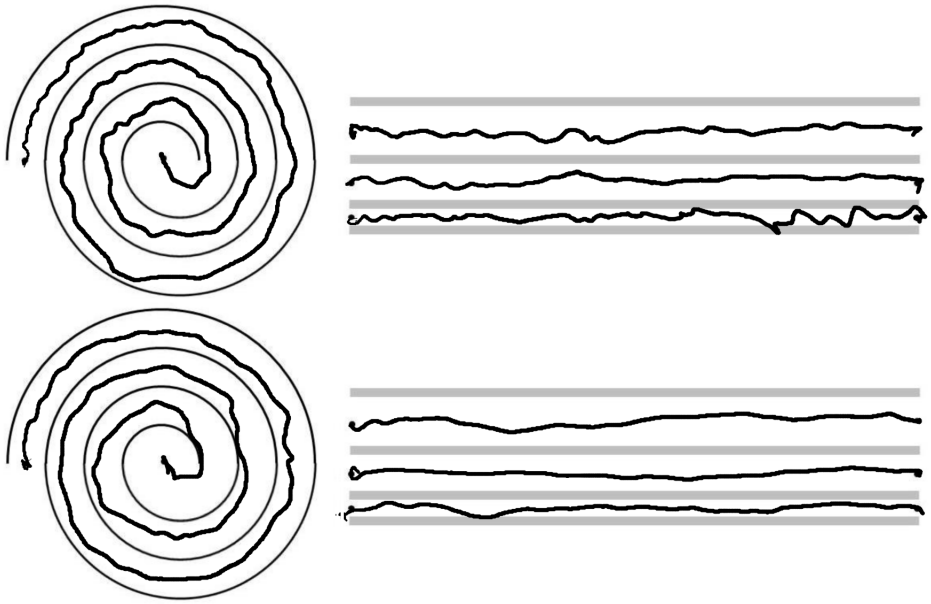

Figure 3.6: Example spiral and line drawing portion of the FTM test in Patient 1 both without stimulation (top) and with DBS treatment active (bottom).

3.5.3 Tremor severity analysis and characterization

Recordings of patients completing the tasks were shuffled and shown to 2 clinicians for rating. The averaged results were taken as the clinical analysis of tremor severity over the course of the experiment. IMU-based tremor assessment was conducted in the same manner as outlined in section 3.3.5.

3.5.4 Quantification of rebound effect

Rebound effect clearly manifested in all 3 patients by both clinical and IMU assessment, the latter of which may be seen in Figure 3.7. Mean time-to-peak by clinical measurements $T_{cp} = 10$ minutes ($SD = 5.7$); mean gap between peak severity and steady state severity in FTM point scale (total range = $[0, 4]$) $\Delta s_c = 0.83(SD = 0.24)$. Mean time-to-peak by gyroscope measurements $T_{gp} = 6.65$ minutes ($SD = 0.80$); mean percent gap between peak

severity and steady state severity $\Delta s_g = 94\%$ $(SD = 26\%)$.

In contrast with previous research on rebound effect, all 3 of our patients clearly presented with some level of rebound effect. Though possibly due to coincidence, this may also be due to the specific tasks used in our study. The activity-dependent nature of ET symptom severity and the high level of variability in which activities most consistently generate tremor means in some cases rebound effect may have gone under- or unreported. Selecting tasks that are themselves highly likely to cause tremor, especially fine-motor tasks like drawing and writing, may result in rebound becoming more apparent in patients in whom the effect has previously appeared less pronounced or even absent. Future work should investigate whether rebound effect may contribute to understanding of the pathophysiological basis of ET itself.

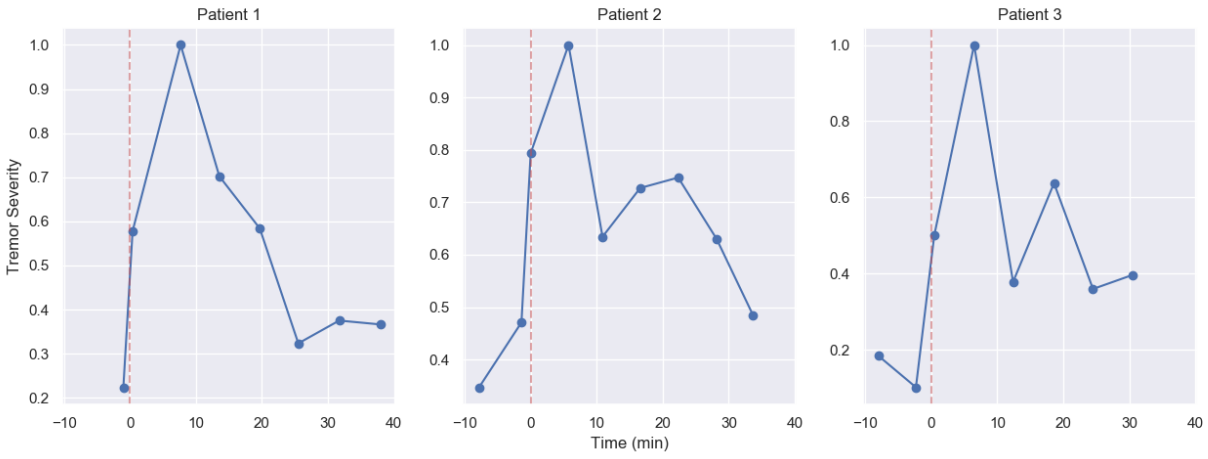

Figure 3.7: Tremor severity in each patient over course of experiment, as determined with IMU data generated by combining spiral and line data. Stimulation disabled at 0, indicated by red line. Variations in Y-axis scaling are due to differences in subjects' individual symptom severity and variations in task durations. Note the clear peak taking place some minutes following cessation of stimulation, followed by a settling to steady state over the ensuing half hour.

3.6 Binary aDBS in context

Here we have considered one of the first examples of a fully embedded aDBS system in freely moving ET patients, and the first with a distributed training procedure and biased classification algorithm. In addition to demonstrating the efficacy of this system, our evidence supports earlier work indicating that aDBS is quantifiably more effective than cDBS in experimental settings without substantial differences in patient perceived treatment efficacy. Subsequent work has further reinforced the efficacy of chronic fully embedded aDBS in patients diagnosed with ET [104].

Of note here is the simplicity of the algorithms designed and applied. With fairly minor expansions upon some of the most elementary methods available for data analysis and classification, a functioning binary aDBS system was demonstrated with sizeable savings in battery use and an unexpectedly substantial improvement in overall treatment efficacy. In the short term, this combination of increased overall efficacy, a novel translation-ready training procedure, and a clinically-oriented classification algorithm indicate that fully implanted binary aDBS systems are approaching the level of clinical efficacy necessary for population-wide deployment.

Binary aDBS may thus be said to provide a substantial and much-needed improvement on cDBS treatment in terms of battery savings and potentially in both treatment efficacy and chronic side effect mitigation. However, its restrictive control system almost certainly falls short of truly optimized treatment. Furthermore, although rebound effect did not manifest in our patients during the above binary aDBS trials, this may have been due to the relatively restricted time period over which this treatment setting was evaluated. A chronically implanted binary aDBS system may thus require rebound to be considered more fully, as our findings indicate that it manifests more widely than previously thought.

Rather than prompting the pursuit of further, minor advancements in binary aDBS, my interpretation of these results is that the focus of future work should shift towards more nuanced, graded aDBS systems. In the following chapter, I will consider and discuss this

approach, reviewing a pilot study for the deployment of a graded aDBS control system that seeks to ameliorate these concerns using presently available hardware. Subsequently, I will consider a tremor prediction algorithm based upon the results taken from the above study on rebound effect. The combination of these twin developments has the potential to substantially increase the feasibility of a deployment-ready graded aDBS system based solely on neural data.

Chapter 4

AN EXPLORATION OF GRADED ADAPTIVE DEEP BRAIN STIMULATION STRATEGIES

4.1 Graded aDBS: an alternative approach

As discussed in prior chapters, DBS is an established clinical treatment for refractory stages of several MDs including PD and ET [8, 7, 9]. In a standard clinical context, DBS parameters (amplitude, frequency, pulse width, and electric field shape) are periodically determined for each patient by a trained expert. This recurring, yet infrequent, adaptation accounts for post-surgical transient states and disease progression. However, it is insufficient for adapting to behavioral contexts and neurophysiological changes occurring on day-to-day or minute-to-minute timescales. As an alternative to cDBS strategies, aDBS systems use motor state surrogates to provide an online adaptation of DBS parameters. Such strategies decrease stimulation when it is not required, and thus may ameliorate DBS-induced side-effects as well as increasing treatment efficacy [105, 84, 26, 89, 80].

The previous chapter contained a discussion of a straightforward data collection procedure and clinically-oriented, biased binary classification algorithm for fully implanted binary aDBS. These developments demonstrate that training and deploying a binary aDBS algorithm is both eminently feasible with presently available investigational devices and that such a system is a meaningful improvement upon the existing standard of care in both battery life and in treatment efficacy [89]. However, binary aDBS systems may introduce new concerns, such as rebound effect and potential side effects related to stimulation ramping rate [89, 103].

In this chapter, I will discuss an alternative approach to aDBS treatment based on a graded aDBS control system. Rather than restricting treatment to a simple "on/off" sys-

tem, graded aDBS refers to a control system based on several intermediary settings being made available in an effort to minimize stimulation at a given time and, by extension, to continuously optimize treatment. The next three sections of this chapter, dealing with a pilot study on a graded aDBS control system, are comprised of the contents of a journal article published in Frontiers in Human Neuroscience [106]. The following section, which considers a more responsive and reliable method for symptom estimation from neural data, includes substantial portions of a conference paper presented at the Engineering in Medicine and Biology Conference in 2020 [103].

4.2 A model-free approach to feature selection for graded aDBS

4.2.1 Data-driven neural marker selection

A key component of any aDBS system is a reliable motor state and symptom severity estimate, which can be directly quantified in movement disorders using IMU or surface electromyography (EMG) [81, 75]. Alternatively, motor state surrogates can be extracted from neural signals, removing any need for external sensors [107, 108, 109]. These motor state surrogates, here termed neural markers (NMs), can be measured from LFP of subcortical or cortical areas [84, 110, 111, 112, 79]. A well known example of NMs extracted from LFPs is the power of the beta-band (12-30 Hz), which – despite unclear causal relation and action mechanisms – is correlated with PD symptoms including bradykinesia and rigidity [113, 114, 115, 111, 116]. Likewise, cortical band-power features have also been found to correlate with motor symptoms' severity in PD and ET [117, 93].

Pioneering studies of aDBS for PD animal models utilized control strategies triggered by action potentials in the primary motor cortex (M1) or internal globus pallidus [118]. Later studies in human patients implemented unidimensional power-band features driving threshold-based controllers, yielding symptom suppression comparable to cDBS strategies, while having a significantly shorter effective stimulation time, as shown by Little et al. [84, 119]. Likewise, Rosa et al. implemented a proportional control strategy based on the

same oscillatory NMs, obtaining similar results in terms of symptom suppression and reduced net stimulation [82]. These studies stand out among the first approaches on aDBS systems for humans. In more recent contributions, Velisar et al. have improved upon them by utilizing fixed dual-threshold control implementing hysteresis which accounts for fast variations in the control signal [83].

The aforementioned studies follow a top-down approach for the identification of NMs by following *a priori* pathophysiological group-level knowledge about the disorder. While these surrogates facilitate the understanding of underlying neural dysfunctions, their practical value for controlling an aDBS system may be limited when it comes to an individual patient. This is due to the highly heterogeneous phenotype of most MDs, indicating that a globally applicable NM optimally suited for all patients may not exist [120]. Such a universal NM seems even more elusive in a more semiologically complex disease like PD, where research has been focused on symptom-wise NM identification.

In contrast, data-driven approaches used in the field of BCI can be used to determine subject-specific NMs using machine learning [121, 122, 77], thus improving motor state characterization of individual users [123]. Initial work in this direction has been presented by Connolly et al. [124], who implemented machine learning methods to decode stages of PD in an animal model based on band-power and cross-frequency features. In more recent studies, Tan et al. [125], and Yao et al. [126] have argued convincingly in favor of a bottom-up approach for identification of NMs and discussed the implications that this may have on an aDBS system. However, the offline nature of their study's implementation leaves open the question of the suitability of such an approach in a real-time scenario.

The threshold-based and proportional control strategies for aDBS considered thus far generally disregard any state transition information or the temporal evolution of the symptoms and of the corresponding NMs, since the next control signal is determined based on just a single NM state measurement (the NM at the current time point). However, several authors have suggested temporal dynamics of beta-band power embedded in beta-burst characterization as potential source of dynamics-aware information [127, 128, 129]. Dynamics-aware

control strategies have also been explored, including model predictive control for ET in an aDBS system based on IMU information [53], coordinated-reset in PD patients and animal models [130, 131], phase-dependent burst stimulation [132], or context-triggered strategies based on event-related desynchronization [76]. These studies are an important indication for considering patient-specific temporal dynamics for control of aDBS systems.

Developing novel aDBS systems is a challenging endeavor. For example in PD, the characterization of robust NMs by itself is a difficult task, mainly due to the significant variability in symptom presentation between patients. Furthermore, the temporal dynamics in PD are non-trivial due to the DBS *washout*—a decaying clinical effect of DBS therapy observed after stimulation withdrawal—which affects different symptoms at different timescales [133]. In contrast, ET has several characteristics that render it a simpler scenario for aDBS development compared to PD. Notably, ET symptoms are generally restricted to kinetic and postural tremor, and although rebound effect should be considered when stimulation will be suddenly disabled for prolonged periods [44, 103], the DBS washout effect itself is more rapid than in PD. Additionally, as the prevalence of ET is significantly greater, it is easier to investigate: a recent meta-study found that ET affects nearly 5% of the population over 65, compared to under 2% of the same demographic diagnosed with PD [3, 4].

Discussed in this section is the design of a proof-of-concept study of a novel closed-loop aDBS system with model-free control. This represents the first aDBS system that implements both 1) characterization of NMs based on machine learning and 2) a dynamics-aware, graded control. As such, it attempts to address the most significant unresolved challenges in aDBS, as outlined in chapter 3.

4.2.2 Experimental setup and session design

Experiments were conducted in five sessions performed with three right-handed, male patients diagnosed with ET: two sessions each with patient 1 (P1, sessions denoted $S1_1$, $S1_2$) and patient 3 (P3, sessions denoted $S3_1$, $S3_2$) and one session with patient 4 (P4, session denoted $S4_1$). All patients were unilaterally implanted with the Activa PC+S investigational

device (see section 2.3.5). The ECoG recording electrode configuration was determined in a different study as the most effective for achieving volitional control of DBS, with the same patient population here presented [80]. ECoG array location may be found in figure 3.3.

Excepting stimulation amplitude, DBS parameters were kept unchanged from clinical settings, and thus vary between subjects, as found in Table 4.1. The same table shows the time elapsed between implantation surgery and execution of the corresponding experimental session, and amount of data collected per session.

Training data was collected during a cDBS parameter optimization procedure carried out for a parallel study (please refer to [28] for further information). Patients sat at rest in a chair with hands in their laps; for each *trial*, the experimenter prompted patients to move the dominant hand to a patient-specific tremor-eliciting *posture*, where it was held during a 10 s interval, followed by a 30 s *rest* period. For the tremor-eliciting *posture*, patients were instructed to conduct the "arms extended" and "wing-beating" postural tests of the TETRAS test [134]. If these tests did not generate sufficient tremor, patients were asked to hold a posture they knew to be especially troublesome while untreated. Specifically, for P3 and P4, the "wings" posture was most effective, while for P1 the act of holding a screwdriver to a fixed point was most effective.

Although different DBS configurations were applied throughout the stage, only trials performed during DBS-off were used as training data. From these trials, only *posture* segments were used. Restricting our analysis to the posture condition only is not a useful distinction in a clinical aDBS system. However, for this pilot study, we aim to prioritize NMs that do not represent kinetic activity. In a scenario where one would consider both posture and rest conditions, then the derived labels y would be structured as two large clusters of tremor activity corresponding to these conditions. The tremor would vary within each of them, but the largest variation might be between them. So if both conditions are considered, any NM that we extract to capture variations in tremor might be related to tremor itself (and would be an appropriate feedback signal for the aDBS system), or might be related only to posture and rest conditions but unrelated to any pathology. The latter would be unsuitable

as a feedback signal for the control system because the tremor label would have acted just as a label of rest/posture conditions, and not as a label of pathological tremor. The total numbers of rest-posture trials collected during this stage can be found in Table 4.1.

Following the training run, the b-aDBS and g-aDBS approaches were applied online. Analogous to the training stage, a computer screen signalled patients to remain at *rest* for a 20s duration at a timestamped prompt. Following this, patients were to assume and hold their patient-specific tremor-inducing *posture* for a 30s duration by another timestamped prompt. In total, 6 complete rest-posture trials were collected for each controller type during this online stage, corresponding to 5 minutes in total.

In the final phase of the experimental sessions, the clinical efficacy of the aDBS strategies was compared to cDBS and DBS-off, using parts A and B of the FTM scale [135]. The FTM tests were captured on camera and the videos were evaluated offline by two blinded clinicians. Due to logistical constraints, this clinical assessment was performed only for cDBS and g-aDBS in sessions $S1_1$, $S3_1$, and $S3_2$.

Table 4.1: **Information about experimental sessions**, including: months since implantation (MSI), therapeutical cDBS parameters (amplitude, frequency, and pulse width), total amount of *rest* and *posture* trials, and the resulting time segments utilized for training the tremor decoding model (N_c).

Session	**MSI**	**Ampl. (mV)**	**Freq. (Hz)**	**PW (μs)**	**Trials**	N_c
$S1_1$	13	3900	130	90	20	200
$S1_2$	16	4100	130	90	20	200
$S3_1$	5	2900	140	60	20	200
$S3_2$	12	3100	140	60	30	83
$S4_1$	22	2500	140	90	22	220

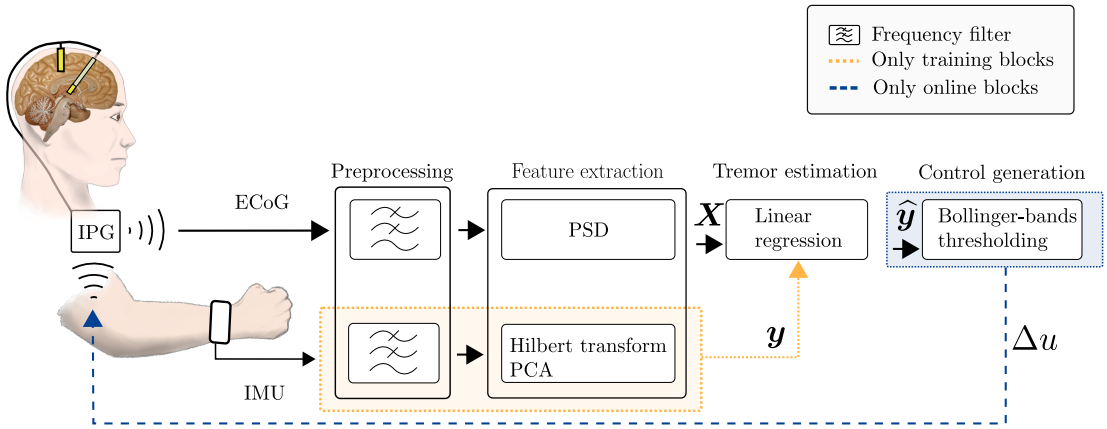

Figure 4.1: Diagram of the implemented data-driven aDBS system, for training and online stages. Firstly, ECoG data and IMU data are collected for training the tremor estimation model. During the online stage, the tremor estimated by the trained linear regression model of Equation 4.1 is used for generating the DBS control signal in Equation 4.2.

4.2.3 Signal acquisition

LFP data was recorded from a single ECoG channel with a sampling rate of 422 Hz. Data was streamed at 400 ms intervals from the Activa PC+S unit to an RF receiver connected through USB to an external computer, where all relevant computation was conducted. Angular velocity and linear acceleration were recorded in three orthogonal spatial directions at 100 Hz using the IMU contained in a smartwatch fastened onto the subject's right wrist, resulting in six IMU channels. Since ECoG and IMU data were acquired with different systems at different sampling rates, signals had to be aligned with respect to a common timestamp. This alignment was updated with the beginning of each rest-posture trial. IMU signals were band-pass filtered with a 5-th order butterworth filter in the band corresponding to pathological tremor.

The aligned IMU and ECoG signals were segmented into ten continuous, non-overlapping 1 s epochs per trial, such that up to 220 epochs were available per patient. An artifact rejection stage was applied, removing segments containing ECoG signals with a peak-to-peak amplitude ≥ 3 mV. For training data, segments belonging to the transient stages of

movement—i.e., transitions between rest and posture conditions, and vice versa—were removed from the analysis. Such segments were identified by detecting epochs where any IMU channel showed a standard deviation of more than 5 times the IMU channel-wise average standard deviation across epochs, in the tremor frequency band.

Table 4.1 shows the final number of epochs N_e available for training of the tremor decoding model. Note that for $S3_2$, approximately 72 % of the epochs had to be rejected due to artifacts and inconsistent patient pose during the posture condition. For the rest of the sessions, all data collected during *posture* was utilized.

4.2.4 NM identification based on machine learning methods

The proposed aDBS system is grounded on two main functional building blocks: (a) the continuous estimation of semi-instantaneous tremor intensity based on individual spectral features extracted from ECoG signals, processed by a machine learning algorithm and (b) a model-free control strategy that adapts the stimulation amplitude based on temporally local statistics of tremor prediction. Descriptions of both functional building blocks and the specific methods used to implement them are detailed below. All methods were implemented using the publicly available MNE python module[136].

The appearance of ET has been linked to dysfunctions in the cortico-thalamic-cerebellar loop. Specifically, anomalies in the connectivity and band-power activity of the motor cortex have been identified as physiological surrogates of the disease[137, 138, 139]. Therefore, this approach uses the band-power of several bands of ECoG signals recorded from M1 as the information source to learn patient-specific NMs for the proposed data-driven tremor estimation.

In contrast with other sections, where tremor was determined as described in section 3.3.5, an alternate approach to tremor evaluation was taken here. Let $y \in \mathbb{R}^{N_e}$ be a vector containing average tremor intensity measured at N_e time windows, as characterized from an IMU. We propose to find a linear projection vector $w \in \mathbb{R}^{N_f+1}$, where N_f is the number of

frequency bins of the ECoG signal, such that

$$\hat{y} = w^T X \tag{4.1}$$

with $\hat{y} \in \mathbb{R}^{N_e}$ denoting the predicted tremor intensity at N_e time windows, and $X \in \mathbb{R}^{N_f+1 \times N_e}$ a matrix containing the spectral power of selected frequency bins computed from N_e time windows recorded from an ECoG electrode placed over M1, and a row containing only ones, for bias estimation. Tremor intensity y is an autocorrelated process since contiguous time points are not necessarily independent; however, for the sake of simplicity in our proof-of-concept system, we assume that the measurements of y have sufficient temporal distance such that the samples are independent and identically distributed. Under this assumption, the weights w can be estimated by solving the optimization problem $argmin_w ||y - \hat{y}||^2$.

This ordinary least mean square regression problem can be solved analytically, resulting in a weight vector $w = (XX^T)^{-1}Xy$.

4.2.5 Control signal generation robust to non-stationary dynamics

In the closed-loop study by Little et al. [84], thresholds on NMs to switch DBS on or off had been determined manually. Similarly, the proportional control strategy by Rosa et al. [82] uses pre-estimated band-power ranges to determine a linear mapping to DBS amplitude. These approaches were successful, even in experiments involving freely moving PD patients, and are referents in the field.

Those fixed mappings between observed NMs and amplitude, however, presuppose the underlying neural system as a stationary process. This assumption is problematic in aDBS: The dynamics of band power NMs are context-dependent and change upon, e.g., sitting, walking, or during transitory movement state [140, 53]. In addition, they are co-modulated by other processes, such as the circadian rhythm or medication intake [141]. Therefore, we propose a time-varying mapping of $\hat{y}$ to the DBS-amplitude, based on local *high* and *low* tremor intensity states, derived from moving statistics of the estimated tremor. Specifically,

we define an increase or decrease in DBS amplitude Δu by

$$\Delta u = \begin{cases} u_i, & \text{if } \hat{y} > \delta_h^t \\ u_d, & \text{if } \hat{y} < \delta_l^t \\ 0, & \text{otherwise} \end{cases} \tag{4.2}$$

where $u_i \in \mathbb{R}^+$ and $u_d \in \mathbb{R}^-$ are scalars that respectively indicate an increase or decrease in stimulation amplitude, and $\delta_h^t, \delta_l^t \in \mathbb{R}^+$ are the corresponding time-varying thresholds at time point t.

We use the Bollinger bands method [142] to compute δ_h^t and δ_l^t. It is widely used in financial analysis for detecting trends in assets pricing, characterizing relative high and low states while taking local volatility into account. In our case, the same principle is used to detect whether the current tremor estimation delivered a relative *high* or *low* intensity state, based on a short term history of the estimated tremor $\hat{y}$. Specifically, $\delta_h^t = a_N(\hat{y}_t) + Kstd_N(\hat{y}_t)$ and $\delta_l^t = a_N(\hat{y}_t) - Kstd_N(\hat{y}_t)$, where $K \in \mathbb{R}^+$ is a scaling constant, $a_N(\hat{y}_t)$ is the moving average of $\hat{y}$ computed in the time interval $[t-N, t]$, and $std_N(\hat{y}_t)$ defines the standard deviation of $\hat{y}$ in the same period of time.

Two alternate approaches for determining the control signals u_i and u_d, inspired by the threshold-based aDBS and proportional aDBS systems used in [84], [82], and [83], were considered. In the data-driven *binary aDBS* (b-aDBS), only DBS "on" and "off" states are considered, i.e., $u_i = -u_d = A_{cDBS}$, where A_{cDBS} corresponds to the patient-specific DBS amplitude optimized by a trained expert for clinical cDBS therapy. In the data-driven *graded aDBS* (g-aDBS), a more granular control of the DBS amplitude is provided by $u_i = -u_d = 0.5\,V$, which is the minimum voltage change Δu implementable in the available hardware platform. In both cases, the stimulation amplitude is restricted to the interval $[0, A_{cDBS}]$.

Recall that, in a standard clinical context, the FTM is among the most widely-used TRS's for assessing the tremor intensity in ET patients and the corresponding efficacy of DBS or standard pharmacological treatment. We will use the FTM scale as one of the assessment criteria for our developed systems. The FTM assessment is divided into several items that

evaluate axial symptoms, motor activities (such as drawing or water pouring), as well as tremor intensity in specific limbs. These items are scored with integer numbers from 0 (no tremor), up to 4 (tremor amplitude $> 2\,\mathrm{cm}$). For more details about the FTM scoring system, we refer the reader to the original publication [135].

4.2.6 Signal characterization and tremor decoding model

For obtaining tremor labels y, the envelope of the band-pass filtered IMU signals was extracted as the magnitude of the Hilbert transform. Average channel-wise IMU power was computed for each of the epochs by averaging the envelope across time. The resulting $N_e \times 6$ matrix was subsequently standardized along the first dimension. Finally, principal component analysis (PCA) was performed and the signals were projected onto the principal component associated with the largest eigenvalue of the corresponding decomposition, thus yielding a scalar representation of tremor intensity, used as the ground truth label y for training and validating the regression model in Equation 4.1.

For extracting neural features, the power spectral density (PSD) of the ECoG signal was computed for each epoch using the Welch method based on the fast Fourier transform computed with 256 coefficients. Only spectral features in the interval $[3-25]\,\mathrm{Hz}$ were considered for further analysis, resulting in fourteen $1.56\,\mathrm{Hz}$-wide frequency bins. The motivation for limiting the analysis to this frequency band lies on the spectral properties of stimulation and muscle artifacts, which are sometimes detectable in the $> 25\,\mathrm{Hz}$ rhythms. Even though ECoG signals are rather robust to muscle artifacts compared to non-invasive recordings such as electroencephalographic signals, the pilot character of our study called for a more conservative approach to the experimental setup, which further enforced this design decision. Since NMs discussed in the literature are also typically found in this frequency range, it may be assumed that limiting the spectral analysis to this band does not erode the significance of results obtained.

A subset of the fourteen ECoG spectral features were used to construct a patient- and session-specific training data set X. The subset was determined using what is generally

known as the greedy forward feature selection method. In this method, the full spectral feature set was iteratively pruned until the regression model's performance ceased to increase. In each iteration, the least important feature, as characterized by the corresponding weight in w, was removed and the linear model was re-trained with the remaining features. Using a chronological 5-fold cross-validation procedure without sample shuffling, the decoding performance was assessed using the Pearson correlation coefficient ρ between y and $\widehat{y}$. If a performance increase with respect to the previous iteration was observed, the pruned feature was left out and the iterative procedure was continued. Otherwise, the pruning stopped.

The moving statistics determining δ_h^t and δ_l^t were computed using a time window of 2 s and a standard deviation scaling constant $K = 2$. These hyperparameters were not optimized per patient but fixed prior to the study based on analysis of *a priori* data. A control signal was issued according to the rules defined in section 4.2.5 every time a new data package was available, i.e., every 400 ms.

4.3 Graded control in vivo

4.3.1 Model-free neural marker selection

Figure 4.2 shows the average PSD calculated for training data and the corresponding correlation ρ between band-power in each frequency bin of the ECoG signals and labels y. Features selected are highlighted in green. The spectra show a high inter-patient variability: for P3 and P4, the spectrum is characterized by a prominent beta peak, whereas in P1 an alpha-band component is dominant. There is also pronounced intra-patient variability across sessions in terms of the absolute spectral power. The frequency band of prominent spectral peaks, however, is constant across sessions for each subject, i.e., alpha-band for P1 and beta-band for P3.

Power band features revealing the strongest correlation with tremor intensity vary considerably between patients: for $S1_1$, $S3_2$, and $S4_1$ the frequency bins with the strongest correlation are in the alpha- and theta-band, whereas for $S1_2$ and $S3_1$ the most informative

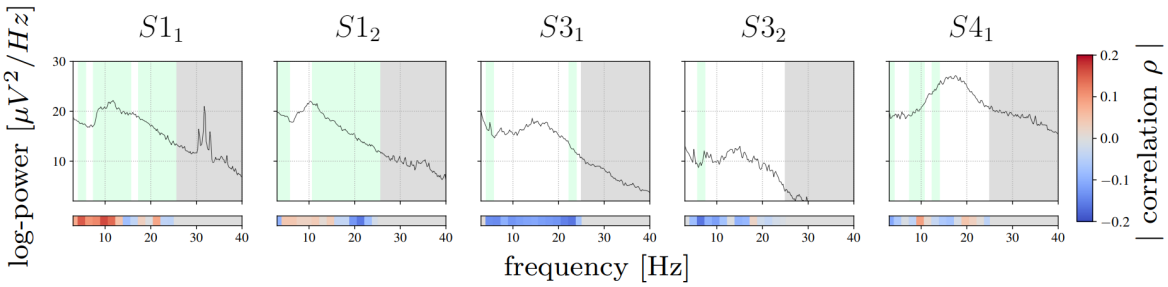

Figure 4.2: Session-wise averaged PSD computed for training data. Bars on the bottom show the Pearson correlation achieved between each frequency bin and true tremor labels y. Highlighted in green are the frequency bins selected by the feature selection algorithm. Marked with gray are frequency bins that were not used for the analysis.

frequency bins are found above 10 Hz, mainly in the high beta-band.

In contrast, features selected for inclusion in the tremor prediction model were found all across the spectrum analyzed. The absence of spectrally compact features may be explained by the high redundancy of neighboring frequency bins and as the feature selection procedure typically selects only one out of multiple bins with redundant information.

Figure 4.3 shows a representative example of the robustness of the spectral features used for tremor decoding under different DBS conditions. Specifically, it depicts a segment of ECoG data recorded during the online phase of $S4_1$. The stimulation artifact is clearly visible, but does not impede measurement of low-frequency components due to saturation of the amplifiers or sub-harmonics of the stimulation.

4.3.2 Tremor estimation accuracy

Table 4.2 shows the average Pearson correlation coefficient between estimated and true tremor intensity. For $S4_1$, no IMU data was available during the online stage, and consequently tremor decoding accuracy scores cannot be reported. For $S3_2$, no online stage was executed for b-aDBS due to logistical constraints. As a baseline, the average correlation between the theta-band power and true tremor intensity, a well known NM for ET stemming

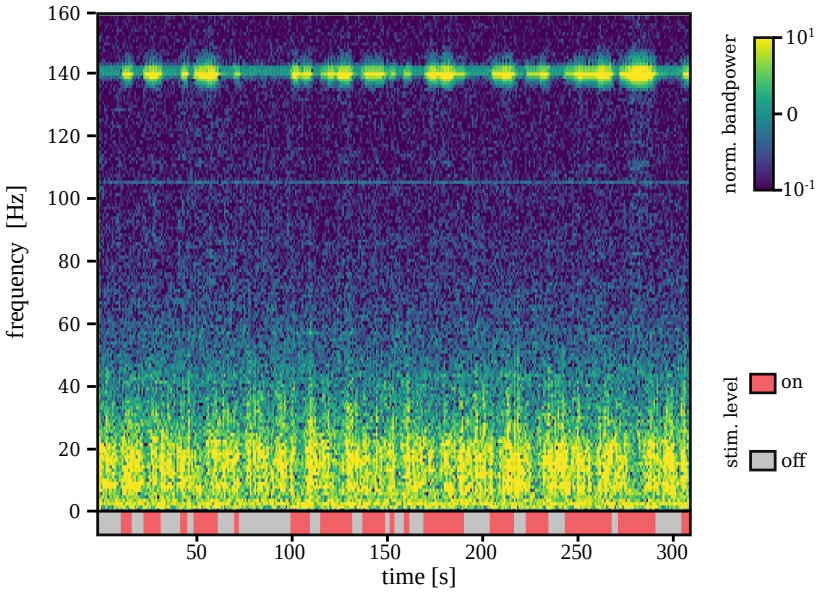

Figure 4.3: Time-frequency representation of the ECoG signal during stimulation on and off for a representative example ($S4_1$). Although stimulation artifacts are clearly visible, signal is not saturated and lower-frequency components are measurable even during stimulation on.

from group-level studies [143] is also considered. All scores derived from the training stage were computed using a 5-fold crossvalidation without shuffling. Statistical significance was defined at an uncorrected $p < 0.02$ for the probability that the score was obtained by chance under a bootstrapping procedure for 1000 label shuffles.

It can be observed that the proposed data-driven tremor decoding model achieved a significant correlation in four out of the five sessions for the training stage. During the online stage, in three out of four sessions conducted, statistically significant decoding performance was obtained. Although data-driven decoding performance of the data-driven model is broadly superior to the fixed theta-band power, the correlation achieved was relatively weak in all sessions analyzed.

	Training Stage			Online Stage	
Session	**theta-only**	**Data-driven**	**Rel. band(s)**	**b-aDBS**	**g-aDBS**
$S1_1$	0.22*	0.21*	theta, alpha	-0.15	-0.10
$S1_1$	0.16	0.22*	beta	0.05	0.12*
$S3_1$	-0.14*	0.29*	theta, beta	0.29*	0.35*
$S3_1$	-0.18	0.05	theta	n/a	0.20*
$S4_1$	-0.06	0.39*	alpha	n/a	n/a

Table 4.2: Average linear correlations between estimated and true tremor intensities using only θ bandpower and data-driven band selection. Statistical significance (indicated by *) is defined at an uncorrected $p < 0.02$ obtained with a bootstrapping procedure with 1000 label shuffles. Additionally, column *informative band* shows the frequency band with the largest correlations with tremor intensity, according to Figure 4.2.

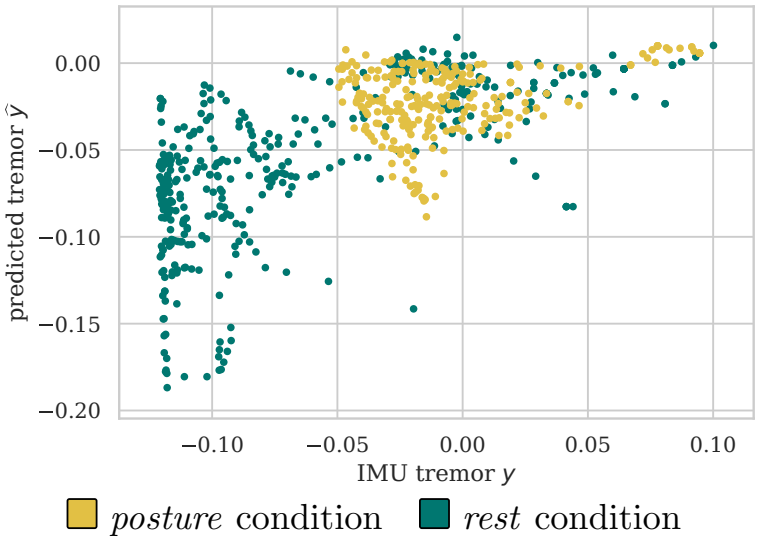

Figure 4.4: Example scatter plot for $S1_1$ of predicted versus measured tremor intensities discriminated between *posture* and *rest* conditions

4.3.3 Control signals distribution

Figure 4.5 shows an illustrative example of the control signal, including the Bollinger bands, as well as measured and predicted tremor. As expected, predicted and measured tremor intensity increased during the *posture* condition, which ensured delivery of stimulation at most times.

Figure 4.6 shows the average stimulation time during the online stages, compared to the equivalent cDBS strategy. It can be observed that for all types of controllers, the average time stimulated was considerably lower than that of the cDBS strategy. Furthermore, there is an indication for low intra-subject variability of average stimulation, whereas inter-subject variability might be larger. The total stimulation duration of b-aDBS and g-aDBS strategies was similar within patients.

4.3.4 Tremor suppression in online stage

Figure 4.7 compares tremor intensity suppression $(1 - y)$ between all stimulation strategies during online stages, under *posture* condition. Each box shows the standardized mean difference of the pairwise comparison (top) and the p-values of the corresponding Mann-Whitney rank test (bottom). If standardized mean difference is negative, no values are shown. For $S3_2$, no significant difference was established among all considered conditions, whereas for $S1_1$ and $S3_1$, adaptive strategies achieved tremor suppression superior to that in cDBS and improved upon DBS-off. For $S1_2$, all stimulation strategies improved upon DBS-off, but no differences could be found among them. Although we expected aDBS to perform as well as cDBS and better than DBS-off, cDBS only performed better than DBS-off in $S1_2$, and slightly worse in $S3_1$, suggesting a suboptimal setting of therapeutic parameters in cDBS. Overall, all significant differences reflect a small to moderate effect.

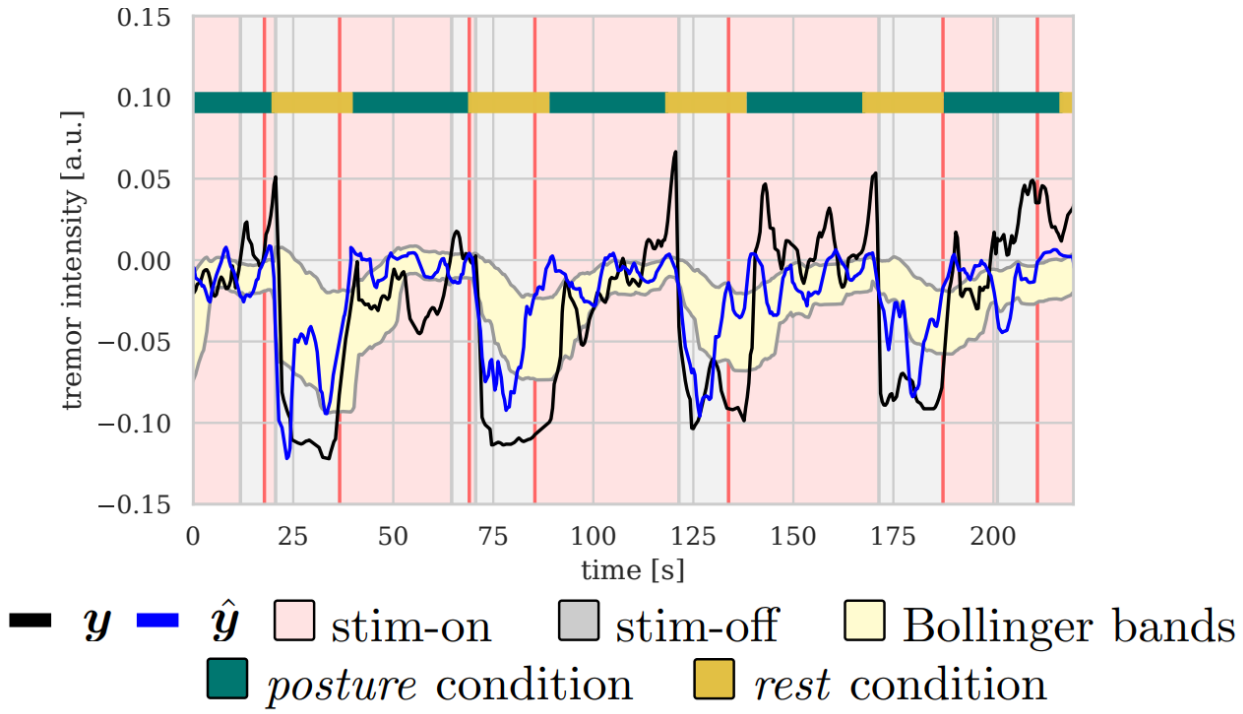

Figure 4.5: Illustrative example of the control signal for b-aDBS computed during the online stage of $S3_1$. There is a clear correlation between *posture* condition and tremor intensity, both predicted and measured, thus, triggering stimulation mainly during *posture* condition.

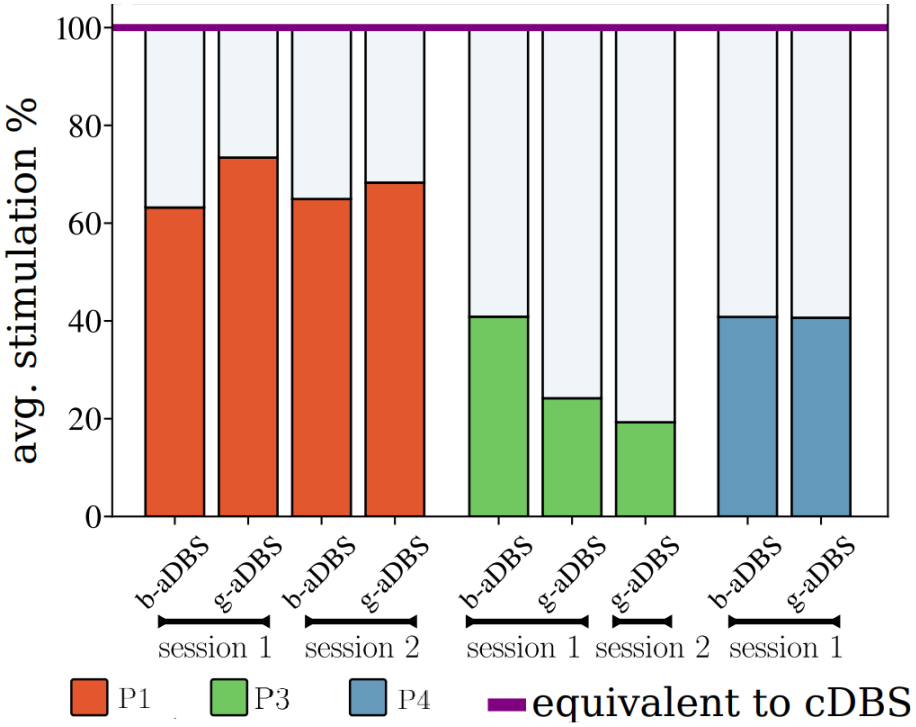

Figure 4.6: Average time stimulated relative to the stimulation using the equivalent cDBS strategy.

4.3.5 Clinical tremor assessment

Table 4.3 shows the FTM scores averaged for both clinical raters. Axial scores reported here comprise the sum of face, tongue, head, and trunk tremor scores. The scores for left/right upper/lower tremor comprise the sum of scores obtained during rest, posture, and action (finger to nose and toe to finger). For subtests with a discrepancy between clinical raters greater than one point, we marked the averaged value (*) and provided both individual scores in parentheses.

Considering the total FTM score per session, the proposed g-aDBS strategy did not lead to worse FTM score than DBS-off. The g-aDBS system achieved at least a moderate symptom suppression in two out of the three online sessions analyzed ($S1_1$ and $S3_1$). In these two sessions, cDBS and DBS-off did not vary significantly in performance, while the

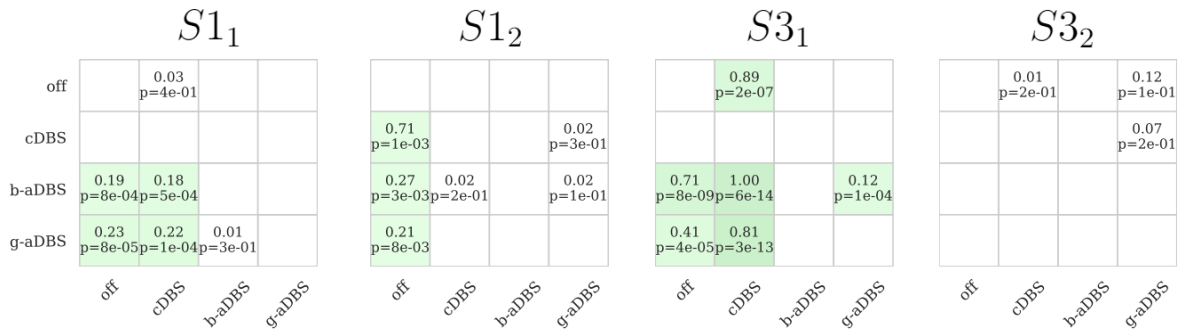

Figure 4.7: Pairwise comparison of tremor intensity under different stimulation strategies during the online stage (only *posture* segments). In each box, top number indicates the effect size and bottom number the corresponding p-value obtained with the Mann-Whitney rank test, comparing the method on the y-axis against the corresponding method in the x-axis. Only positive effect sizes are shown. Green boxes indicate uncorrected p <0.05. For the comparison, 1 s windows extracted from the 30 s posture intervals of the 12 trials executed for the online stage.

g-aDBS score improved moderately for $S1_1$ and markedly for $S3_1$. For $S3_2$, g-aDBS did not improve symptoms compared to DBS-off, while cDBS treatment improved symptoms by 2 points, indicating a moderate tremor amelioration.

A closer look at the sub-tests of FTM reveals that at least one point of improvement (mild tremor amelioration) between g-aDBS and the baselines cDBS and DBS-off was obtained for axial and upper lateral scores for $S1_1$. For $S3_1$, handwriting, drawing, and pouring liquid with the right hand were the sub-tests for which g-aDBS achieved a mild improvement. Interestingly, g-aDBS in $S1_2$ did not worsen any symptom by more than one point (mild worsening). However, it improved drawing with the right hand by one point, compared to DBS-off. In the other sub-tests, differences were at most 0.5 points, which is within the expected fluctuations over the course of a day [144] and indicates a marginal effect upon symptoms.

The b-/g-aDBS strategies were driven by NMs for right hand tremor (location of the IMU) extracted during *posture*. Consequently, it is important to analyze the specific scores for

	$S1_1$			$S3_1$			$S3_2$		
Test	**cDBS**	**OFF**	**g-aDBS**	**cDBS**	**OFF**	**g-aDBS**	**cDBS**	**OFF**	**g-aDBS**
Axial	1.5	1.5	0	0.5	0	0	0.5	0	0
Speech	1	0.5	1	0	0	0	0	0	0
Written	0.5	0.5	0.5	0	2.5	0.5	0.5	1.5	1
L. upper	4.5	3.5	3.5	2* (1/3)	1* (0/2)	1.5	1	1* (0/2)	1.5
L. lower	0	0.5	0.5	0	0	0	0	0.5	0.5
L. draw	3	3	3	1.5	1	1	1.5	1	1.5
L. pour	3	3	3	0.5	0.5	0	0	0	0.5
R. upper	3	4* (5/3)	3* (4/2)	3.5	3	3	2.5* (4/1)	3	3
R. lower	0	0	0	0	0.5	0.5	0.5	0.5	0.5
R. draw	1.5	1	1	2	2	1	1.5	2	1
R. pour	1	1	1	1	1	0	0.5	1	1* (0/2)
Total	19	18.5	16.5	11	11.5	7.5	8.5	10.5	10.5

Table 4.3: Averaged scores of parts A and B of the FTM assessment for sessions $S1_1$, $S3_1$, and $S3_2$. Scores marked with a $*$ indicate a discrepancy of more than 1 point between the scores assigned by each of the clinicians, followed by the individual scores in parenthesis. Due to logistical constraints, FTM assessment is only available for g-aDBS.

this item of the clinical evaluation individually. Clinical raters assessed right hand postural tremor under DBS-off for all the sessions as either absent (FTM score 0) or slight (FTM score 1, corresponding to a tremor amplitude of less than 0.5 cm). Under cDBS, it was reported that in $S1_1$ and $S3_2$ tremor improved, while for $S3_1$ no difference could be established. The evaluation of the g-aDBS strategy showed the same improvement as for cDBS with the exception of one clinical rater who stated that for $S1_1$ tremor increased to moderate (0.5 to 1cm tremor amplitude).

4.4 Discussion on pilot study graded aDBS performance

4.4.1 Using machine learning for data-driven decoding of tremor

Using our data-driven approach, tremor intensity could be decoded from spectral information contained in M1 ECoG signals, yielding a correlation value ranging from 0.21 to 0.39 in all training trials where statistical significance was attained. This is a significant improvement compared to tremor decoding using solely theta-band power, in which a significant decoding performance was achieved in only two sessions. It is noteworthy that in one of the two sessions where theta-band power was informative about tremor intensity, a negative correlation was found. This supports the hypothesis that top-down approaches to NM selection generalize poorly as well as demonstrating the ambiguity and unreliability derived from this method. One observation confirmed by the D'Agostino's K^2 test is that the kurtosis and skewness of tremor y and estimated tremor $\hat{y}$ deviate from a Gaussian distribution. This calls the generalized effectiveness of the Pearson correlation coefficient into some question. However, the absence of long tails and outliers in our data set and the fact that only the relative differences in correlation are meaningful in this approach indicate that the selected decoding performance score may be relied upon in our use case.

This decoding approach demonstrates that informative features are present in power of frequency bins found in the range of $[3 - 25]$ Hz, and that tremor estimation from neural data should not be subject to a single frequency band selected *a priori*. In addition to demonstrating the necessity for data-driven NMs identification for aDBS systems in ET, this has important implications in the development of aDBS systems for more phenotypically heterogeneous disorders such as PD, where patient- and symptom-specific characterization of motor symptoms from neural data may improve aDBS even further.

This method further identified non-stationary dynamics contained in the NMs used. Variations of global spectral features were observed across sessions, as was heterogeneity in the spectral feature information content as described by the varying intra-patient correlation scores between power in individual frequency bins and the tremor intensity across sessions.

Such variability in the feature information content and in tremor decoding performance within subjects—for example $S3_1$ and $S3_2$—suggests an underlying mixture of processes that might correlate with tremor intensity, but that cannot be captured from spectral features extracted only from one contralateral ECoG channel in M1. Consequently, multimodal and multidimensional data-driven NMs should be explored.

4.4.2 Generation of dynamics-aware control signal

The model-free control strategy implemented in our system accounted for non-stationary dynamics of tremor estimation. Although the number of patients included in the study is too small for a statistical analysis, those sessions conducted indicated that accounting for non-stationary dynamics may allow for identification of local tremor states. Their existence may explain symptom suppression achieved by our g-aDBS system in a wider variety of conditions during the FTM evaluation, compared to cDBS and DBS-off.

Our control strategy does not account for non-stationary dynamics in the NMs space, but rather directly in the space where tremor estimation is found. However, different neural features may be governed by different non-stationary dynamics stemming from factors such as the circadian rhythm, current physical activity, medication, and surgery-induced stun-effect. Therefore, accounting for non-stationary dynamics directly in the NM space might provide a more robust feedback signal. This should be subject to future examination, where a longer time horizon will enable the study of multi-timescale dynamics.

4.4.3 Clinical assessment

From a clinical perspective, the g-aDBS strategy performed better than cDBS in two out of the three sessions assessed with the FTM scale. Unfortunately, one of the limiting factors in our study is that only the g-aDBS strategy, and not b-aDBS, was evaluated using the FTM scale. In general, the clinical evaluation of motor diseases requires a highly trained clinician and a lengthy assessment protocol. These requirements play a major role in time-constrained situations such as those encountered in typical experimental sessions.

From the patients' perspective, they could clearly differentiate between no stimulation and active stimulation, but could not identify substantial differences between cDBS and g-aDBS. In b-aDBS, patients reported occasional paresthesias in their treated upper limb. This mainly occurred while stimulation was ramping up from 0 to the maximum amplitude due to the ramping rate required to keep b-aDBS effective [69].

4.4.4 Technical implications in a clinical aDBS

Our system achieved a reduction of at least 24% and as much as 80% of stimulation time. According to Khanna et al. [95], the breakeven point of the Activa PC+S regarding power consumption in closed-loop mode is at a reduction of 6%. Therefore, our system allows a considerable reduction in power consumption well above this threshold. Another typical constraint when implementing aDBS in clinical grade systems is that the available platforms have low computational capacity, which limits the complexity of the algorithms that can be used. Fortunately, most computationally expensive parts of our system can be implemented by a fast Fourier transform (power spectrum estimation) and a linear projection (tremor estimation model). Both operations are relatively inexpensive and are easily implementable in simple embedded systems contained in modern DBS.

4.4.5 Limitations and open questions

The greatest limiting factor of this contribution is the small sample size and partially conflicting outcome regarding the efficacy of the clinical cDBS condition used as control. Specifically, according to the FTM scale, cDBS performed better than DBS-off in only one session, suggesting that cDBS suffered suboptimal therapeutic parameter settings. This may also define a ceiling for the effect of aDBS and calls for a larger clinical study, where the efficacy of the proposed system can be drawn as a statistically sound conclusion.

Another important consideration is clinical safety of our approach. Although our patients did not report any side effects during treatment with aDBS (besides transient parethesias) and we do not think that our strategy does presents any risks not encountered in existing

aDBS strategies, the safety profile of our approach is still an open issue and should be further investigated with a larger cohort of patients.

From a technical point of view, there are also several open questions to consider. First, we limited the training segments to the *posture* condition only. This allowed us to obtain a model that effectively decodes tremor intensity during tremor-inducing conditions and should not contain discriminative information about the posture itself or movement onset. If *rest* segments had also been included, our model would potentially have learned to decode the motor task (going from *rest* to *posture* and vice versa). Although detection of movement onset may provide additional information for controlling the system [76, 125], our main goal was to obtain an aDBS system relying on symptom surrogates. This design decision limits the generalization of our approach to other postural conditions, which should be subject to further investigation.

Our system can account for spectral fluctuation of a specific NM in the short term, since the Bollinger-bands consider a history of its activity. A large contextual change (e.g., falling asleep), however, may render the chosen NM uninformative and would limit our approach. In this case, an adaptation of the decoder (i.e., using a different NM) will be necessary. Furthermore, by limiting our training data collection to postural data, we implicitly limited generalizability to long term use. Both the re-evaluation of longer term efficacy of the Bollinger bands system and extension of training data collection to include a more varied set of patient states should be subject to future studies. Finally, limiting the features to spectral power of M1 signals might reduce the decoding power of the underlying machine learning model. To improve upon this limitation, future systems should include more complex features, for example as used by Yao et al. in their most recent work [126].

4.5 Tremor prediction from neural data in rebound effect

As is apparent from the sections above, a robust method for tremor estimation from neural data is a prerequisite for the design of any effective graded control system. Such estimation would require that neural data be collected in concert with IMU data, and an algorithm de-

veloped to determine symptom severity using neural data alone. As also demonstrated in 4.2, population-scale determination of the appropriate NMs for this sort of control system generally yields suboptimal results. It has previously been assumed that such data is extremely difficult or even impossible to obtain given the significant variability and unpredictability of intra-patient symptom severity in most MDs, which may fluctuate due to factors including fatigue, hunger, and circadian rhythm [54, 55]. This likely contributed to the mixed clinical results found in section 4.3.

With the more thorough treatment of rebound effect outlined above in section 3.5, however, we believe that a predictable and repeatable method for collecting this data on a patient-specific basis has been discovered. In that section, we discussed rebound effect primarily in terms of its potentially disruptive effect on binary aDBS algorithms. Serendipitously, rebound effect itself presents an ideal testbed to develop tremor severity prediction algorithms directly from neural data by providing a predictable method for analyzing a wide spectrum of patient-specific symptom severity in a relatively short time frame. In concert with symptom severity data collection as outlined in this section, neural data was recorded during these tasks. These data sets were then used to determine whether real-time intra-patient symptom severity could be predicted solely from neural data.

4.5.1 Data collection and experimental protocol

Patient information and IMU data acquisition may be found in section 3.5.1. In addition to this inertial data, LFP data was recorded and streamed to an external experimental computer from VIM and the primary motor cortex (M1) simultaneously from one pair of electrodes at each site at sampling rates of 200Hz. All data was timestamped upon receipt, guaranteeing synchronization of neural and IMU data. IMU-based tremor estimation as calculated in section 3.3.5 was used as ground truth for local symptom severity. The experimental protocol may be found in section 3.5.2.

4.5.2 Neural data processing, feature extraction, and tremor estimation

Neural LFP data was collected at 200Hz from VIM and M1 throughout the experiment. Data was split into task-dependent periods (spirals, lines, or no set task). Welch's method was then applied to each period during which a task was being conducted. Transformed data was further split into θ, α, low-β, and high-β sections for both VIM and M1 data. The area under the curve of each section was taken and divided by the amount of time required to perform the task in order to control for variations in the duration of each task. This process generated 8 features in total, detailed in Table 4.4.

Table 4.4: Neural power bands selected as features for estimation of tremor severity.

Feature	**Band (Hz)**
VIM θ	4-8
VIM α	8-12
VIM low-β	12-20
VIM high-β	20-30
M1 θ	4-8
M1 α	8-12
M1 low-β	12-20
M1 high-β	20-30

4.5.3 Linear regression for tremor estimation from neural data

Linear regression was applied to each data set in order to predict tremor severity. Entire task sessions were considered, such that each sample represents the neural and IMU data collected over the course of spiral drawing and line drawing. Accuracy was assessed using the coefficient of determination R^2.

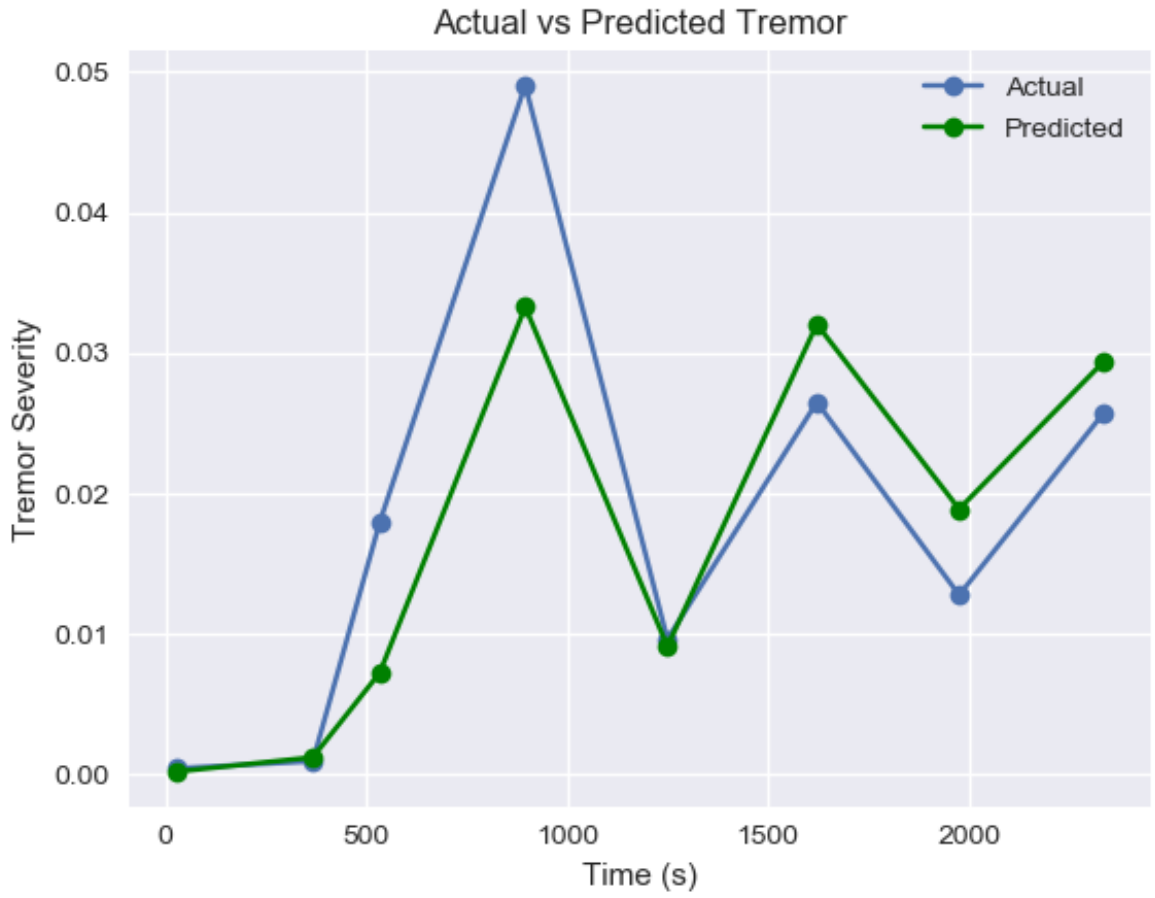

Figure 4.8: Estimated and actual tremor during Patient 3 spiral drawing task using combined data from spiral- and line-drawing tasks, with $R^2_{P3} = 0.79$.

This estimation was highly accurate, with average coefficient of determination $R^2_{avg} = 0.82$, $SD = 0.14$. Although all results were promising, accuracy in P1 was found to be perfect ($R^2_{P1} = 1.0$); however, the risks of over-fitting on so small a data set are hard to ignore. An example depicting predicted vs. actual tremor in Patient 3 across the entire experiment may be seen in Fig 4.8.

In aDBS systems based on implanted sensors, graded aDBS systems remain under-investigated in part because there is a lack of data on how to properly estimate tremor

severity from neural signals alone. Our highly promising preliminary results in this arena indicate that there may exist a method to effectively correlate neural activity and tremor severity on an individual level. The focus of this initial study precluded more in-depth analysis of this data or attempts at estimation of tremor severity on shorter timescales. Nonetheless, our results indicate that such an algorithm is eminently feasible, suggesting that graded aDBS systems may be trained using one of the very phenomena they are designed to help prevent. The intrinsically personalized algorithms stemming from these tests add support for a more individualized and data-driven approach to aDBS development.

4.6 Integration of graded control and optimization into embedded aDBS

Here we have detailed and discussed the development and evaluation of a graded control system for adaptive deep brain stimulation in essential tremor patients. Fundamentally speaking, the design requirements of such a system differ from those of a binary aDBS system only in the respect that the control signal must be capable of more settings than the simple "on/off" classification problem considered at length in chapter 3. Attendant upon this new requirement, however, are several layers of complexity added due to the need for a method to estimate symptom severity with far more specificity than required by a binary system.

The benefits of the binary system lay primarily in its simplicity: one need only determine, in the broadest possible terms, if a patient needs any stimulation or if it is unnecessary. A graded system, by contrast, relies on a far more specific reading of symptom severity that must be conducted in real time. This significantly increases the weight placed on algorithm design and data analysis methods, which has previously hindered the ability to

The key advantage of our approach to this problem was in recognizing the hindrance posed by focusing on population-scale feature selection. Our fundamental innovation in this regard was the development and demonstration of a model-free NM selection method. This bottom-up approach to feature selection resulted in an intrinsically individualized tremor estimation system with more accurate settings than achieved by comparable, top-down methods. De-

spite the inconclusive results stemming from our control system itself, our analysis of our system's performance lends significant weight to the argument for data-driven NM selection methods.

These results also provide further impetus for device manufacturers to invest in implantable devices capable of more complex control systems. As demonstrated in chapter 3, the most computationally costly portion of developing an embedded aDBS algorithm – training – may be conducted on an external experimental computer. Additionally, in the process of classification using the system described in this chapter, a fully embedded binary system already calculates a linear projection based on neural data. By removing the classification step and implementing a symptom severity prediction algorithm as opposed to the linear projection currently used, one could easily generate a continuous control signal based solely on this prediction. The limitation, then, is in the availability of such a setting within the device itself.

One concern with this system that has not yet been addressed is the increased complexity that any aDBS system places on the already-laborious parameter selection process. In the next chapter, we will approach issues concerning the present programming procedure with an eye towards interoperability with future aDBS systems. This chapter will cover the development of an automated cDBS programming pipeline based on application of optimization theory and the deployment and testing of a tablet- and mobile-based application to track MD symptom progression remotely. The former will demonstrate that parameter selection may be conducted in an efficient and reliable manner with a guarantee of optimal treatment, while the latter will show that remote tracking of patient symptom progression and, by extension, treatment efficacy may be mostly automated itself.

Chapter 5

STRATEGIES FOR OPTIMIZATION IN DEEP BRAIN STIMULATION TREATMENT

5.1 Efficient delivery of optimized treatment

The preceding two chapters of this thesis have focused on the meaningful improvement upon existing cDBS treatment provided by binary, fully-implanted aDBS, and strategies for further improvements through graded aDBS. However, despite the highly promising results described in these chapters, the question of actual deployment has not yet been approached. This chapter will instead approach these issues in the context of optimized DBS treatment.

These issues comprise two sides of the same coin. The first lies with the manner in which deep brain stimulation is programmed. Far from being optimized, this process often takes on something of a guess-and-check character that rarely results in ideal treatment parameters being selected. The second is the way in which MD symptom severity is tracked on a chronic basis. Despite significant variability in rates of progression across individuals diagnosed with a given MD, evaluation of their symptoms relies on observations during clinical visits that must be planned months in advance. In the context of the COVID-19 crisis, this requirement that patients commute to a clinical setting has shifted from merely inconvenient to potentially dangerous.

At present, DBS parameter tuning is a time consuming and poorly structured process. Patients are required to travel to a clinical setting to be evaluated by a trained clinician for programming with the goal of determining settings that strike a balance between tolerable side effects and effective tremor suppression. The programming process begins with arbitrarily selected frequency and pulse widths being applied, followed by a sweep of all monopolar settings available. If none of these settings prove satisfactory, variable frequency

and pulse width settings may be tested, followed by bipolar settings. This process possesses a guess-and-check character that may result in a local minima, but very rarely achieves truly optimal parameters. Sections 5.2, 5.3, and 5.4 discuss the strides made towards generating a pipeline for the optimized selection of treatment parameters with a mathematical guarantee of overall efficacy. In both procedural efficiency and treatment effectiveness, this represents a considerable improvement upon the current standard of care.

Section 5.5 discusses the development of a novel mobile- and tablet-based diagnostic tool to track movement disorder symptoms chronically [145]. At present, MD symptom severity and, by extension, therapy effectiveness is evaluated only during sporadic and sometimes arbitrarily scheduled clinical visits. Here, we attempt to resolve this inconsistent approach to symptom assessment with the development of a novel system that permits remote assessment of tremor. In addition, this section details an algorithmic approach to symptom assessment, in a pilot attempt to categorize tremor from a purely mathematical and quantified standpoint. This process both increases the interpretability of results and spares clinicians from the requirement to evaluate patients manually.

5.2 Parameter selection in DBS

Manual programming in DBS is an extremely time consuming and inefficient process [28, 29]. Initial programming of the DBS device takes place several weeks or months after implantation to allow for any lesion effect to dissipate [146, 147]. Patients must then return to a clinical setting, where a clinician conducts what amounts to a trial-and-error sample of the various stimulation settings available [24]. The two required inputs to determine overall treatment efficacy at a given set of parameters are 1) the severity of tremor and 2) the manifestation and severity of side effects. The dominant procedure presently requires that, after each stimulation setting, the clinician evaluates the patient's symptom severity and asks for patient feedback as to side effects. This process is repeated until the clinician and patient are satisfied with the parameters selected.

Even with the relatively modest number of parameter and electrode configurations avail-

able to be set in most presently deployed DBS probes, this process can take several hours. This can understandably lead to fatigue and frustration in both patients and clinicians. As a result, there is a high propensity to select the first passable setting rather than pursuing a truly optimal set of parameters. Indeed, retrospective work has demonstrated that suboptimal parameter settings are the most common reason for patient dissatisfaction with DBS therapy [148]. In addition to being a highly inefficient process, this implies that the current parameter selection procedure also rarely achieves optimized treatment settings.

Future updates or adjustments to a patient's device are limited by the requirement that a patient return to a clinical setting. Access to such a setting varies widely between patients, and the variable disease progression common in MDs means that arbitrarily scheduled visits may not reflect an individual's disease progression [54, 55]. A formal reprogramming has been demonstrated to improve upon outcomes in a majority of cases, but issues of access to care and the lack of any tool to track efficacy of all settings tested across multiple visits render such a course of action unlikely [29]. Instead, when a patient does arrive for an update, changes to settings are usually restricted to incremental shifts in amplitude or frequency. The manual DBS parameter selection process is therefore inefficient, time consuming, and highly unlikely to achieve the maximum possible treatment efficacy either at initial setting or in subsequent clinical visits.

One approach to resolving this problem is the automation of DBS stimulation parameter selection [28, 149]. By using some quantified measure of tremor severity that may be collected more quickly than standard clinical rating scales allow, in addition to real-time patient feedback on side effects through a straightforward computer interface, the problem statement may be rephrased. This permits the application of advanced methods drawn from the field of optimization. Previous work has already demonstrated that, even using a simple brute-force parameter selection algorithm, automatically selected DBS parameters are as or more effective than clinically selected ones [28]. Building upon this work, this section discusses the generation of a platform for more advanced optimization methods to be tested and deployed. This platform exploits the integration of real-time patient feedback on side effects and tremor

severity ratings extracted from IMU data to generate a rapidly acquired estimate of treatment efficacy. Using this framework, algorithms may be deployed and exchanged freely, permitting an immense range of optimization methods to be tested quickly and easily. It is hoped that this framework will enable future studies to demonstrate that automated programming of DBS parameters provides an improvement in both speed and effectiveness over traditional, manual methods.

5.3 Tremor rating scale estimation from IMU

5.3.1 Digitization of clinical rating scales

Clinical tremor rating scales remain the standard for evaluation of MD symptom severity. The usefulness of these scales is dependent in large part on their relative ubiquity and generalizations that may be derived from these scores [45, 150]. A patient may not present with the exact same symptoms in any two tests, but their overall condition will likely remain within a certain, known range for a period of several weeks or months depending on disease progression [151]. This is sufficient for a clinician to recommend and prescribe a course of care in the near term.

Such scales are not without their drawbacks. The most apparent are that inter-rater reliability can be inconsistent, especially in fine motor tasks, and that the evaluation process is intrinsically time consuming [48, 49]. One solution to both of these issues is the generation of a TRS estimation algorithm through some sort of digitally acquired data. This may take the form of data extracted from a tablet- or mobile-based drawing task, as described in section 5.5, or through analysis of kinematic or inertial data acquired through the use of an IMU fastened to a patient's wrist [28, 85, 145, 152].

In the IMU-based tremor estimation methods described in previous chapters, this estimation was primarily used for measuring relative severity between variable patient states and stimulation settings. Ground truth was therefore considered less important than maintaining computational simplicity for the sake of real-time feedback on symptom severity. In contrast,

our aim with an automated DBS parameter programming system requires that some form of ground truth be defined such that a guarantee of clinical efficacy may be maintained. The aim here is therefore to develop a regression algorithm capable of estimating absolute tremor severity as defined by an established tremor rating scale.

5.3.2 Generation and comparison of IMU-based FTM estimation algorithms

10 patients diagnosed with ET were observed and rated during clinical tests for tremor at Emory University. Evaluations were conducted with the patient at rest with hands in their lap (*Rest*), holding a "wing beating" posture (*Posture*), and conducting the finger-to-nose task (*Kinetic*), each from the Fahn-Tolosa-Marin tremor rating scale [45]. During these tests, each with a set 10-second duration, IMU data was streamed at 100Hz using a commercial smartwatch and timestamped on arrival at an experimental PC.

With slight abuse of notation for consistency with chapter 3, we denote our ground truth for clinical rating score as χ and our estimate of that score derived from our input features as $\hat{\chi}$. The x, y, and z components of both accelerometer (a) and gyroscope (v) data were used as raw data. The four features selected for signal analysis were median tremor band magnitude, mean tremor band magnitude, root mean square of the raw channel, and root mean square of the rate of change of the raw channel. These features were extracted from each channel and the results summed for gyroscope data and accelerometer data separately, resulting in a feature space $X \in \mathbb{R}^8$ (enumerated in table 5.1) [28]. These were lined up against our ground truth FTM scale $\chi \in \{0, 1, 2, 3, 4\}$, with 0 corresponding to no tremor and 4 corresponding to tremor amplitude $> 2\,\text{cm}$ [135]. Our objective was the generation of an estimate $\hat{\chi}$ from X. Due to variations in how FTM scores are calculated, regression algorithms had to be individually trained for each of the *Rest*, *Postural*, and *Kinetic* tests.

Linear regression (LR) calculated using minimized residual sum of squares, random forest regression with 30 trees and minimizing mean squared error (MSE), and support vector regression (SVR) with a radial basis function kernel were each tested. Cross-validated coefficient of determination R^2 and MSE were considered a direct measure of accuracy and an

inverse measure of specificity, respectively. Results from each are summarized in table 5.2, while example results from each regression method may be seen below in figure 5.1. Random forest regression performed best for the *Rest* and *Kinetic* cases, while SVR was most reliable for *Postural* assessment. In each "best" case, accuracy was within the bounds of inter-rater reliability for FTM assessments [49].

Table 5.1: **Features from IMU data**: This table comprises a list of all features extracted from IMU data for FTM estimation. Individual features are the sum of each method along each channel (i.e., median gyroscope tremor band magnitude refers to the summed median magnitude extracted from each of the x, y, and z channels of the gyroscope).

Median gyroscope tremor band (4-12 Hz) magnitude
Mean gyroscope tremor band (4-12 Hz) magnitude
Median accelerometer tremor band (4-12 Hz) magnitude
Mean accelerometer tremor band (4-12 Hz) magnitude
Root mean square of gyroscope
Root mean square of rate of change in gyroscope
Root mean square of accelerometer
Root mean square of rate of change in accelerometer

5.4 Automated cDBS programming

5.4.1 Development of an automated programming pipeline

The basic structure of an automated DBS programming system is a method to determine overall treatment efficacy, an optimization algorithm capable of determining what the next stimulation setting should be, and an interface capable of communicating directly with the DBS device to ensure that the new settings are uploaded in the most efficient manner possible. With a given stimulation setting, overall treatment efficacy must first be quantified. Paired with prior knowledge about previously evaluated stimulation settings, this quantification

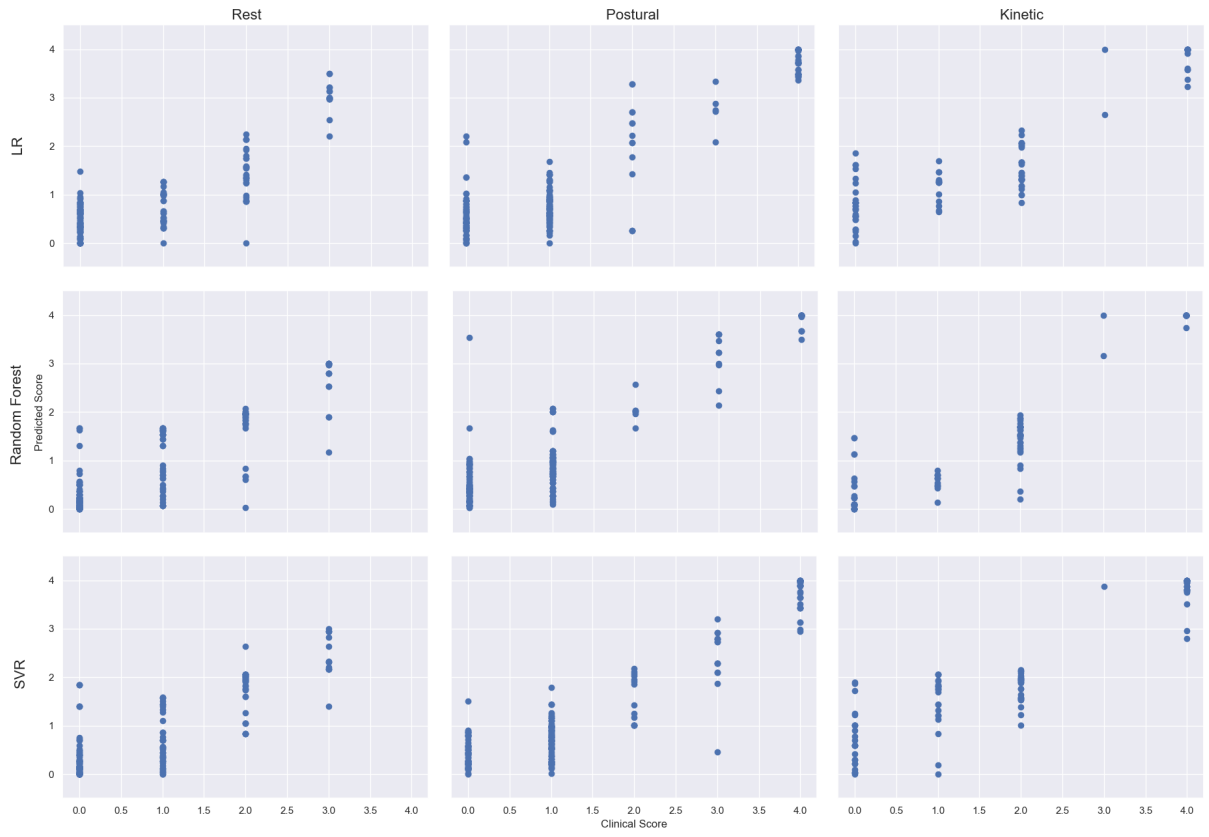

Figure 5.1: Results for FTM estimation from IMU data using linear regression (LR), random forest regression, and support vector regression (SVR) for the Rest, Postural, and Kinetic states.

Table 5.2: R^2 **MSE for each algorithm tested**: This table details the coefficient of determination (R^2) and mean squared error (MSE) for linear regression (LR), random forest, and support vector regression (SVR) in each state. Best results for each state in bold. Accuracy for all algorithms is well within the bounds for inter-rater reliability in tremor rating scales.

Algorithm	Rest		Postural		Kinetic	
	R^2	MSE	R^2	MSE	R^2	MSE
LR	0.69	0.30	0.84	0.30	0.82	0.40
Random forest	**0.73**	**0.24**	0.84	0.27	**0.88**	**0.27**
SVR	0.68	0.31	**0.86**	**0.27**	0.82	0.40

serves as cost function of an optimization algorithm. This algorithm will search for optimal settings with a guarantee of efficiency.

The basic inputs required to evaluate DBS treatment efficacy are 1) tremor severity and 2) side effect manifestation. An interface to automate this procedure would therefore require both a reliable method to extract quantified estimates of tremor severity and an interface allowing rapid input of side effects. This interface may be seen in figure 5.2.

The results described in 5.3 indicate that a reliable estimate of FTM score may be extracted from only 30 seconds of data per state. This satisfies the first requirement and does so with a sufficiently small amount of data to be considered highly efficient. Using the simple and straightforward dropdown menu seen in figure 5.2, each of the 13 most common side effects may be entered and quantified as $s \in \{0, 1, 2, 3\}$, with 0, 1, 2, and 3 indicating no, mild, moderate, and severe side effect manifestation, respectively. These 13 side effects then constitute a single vector $S \in \mathbb{R}^{13}$, which may be factored into optimization alongside the previously defined $\hat{\chi}$. From this, we may define our presently unknown cost function $J(\hat{\chi}, S)$.

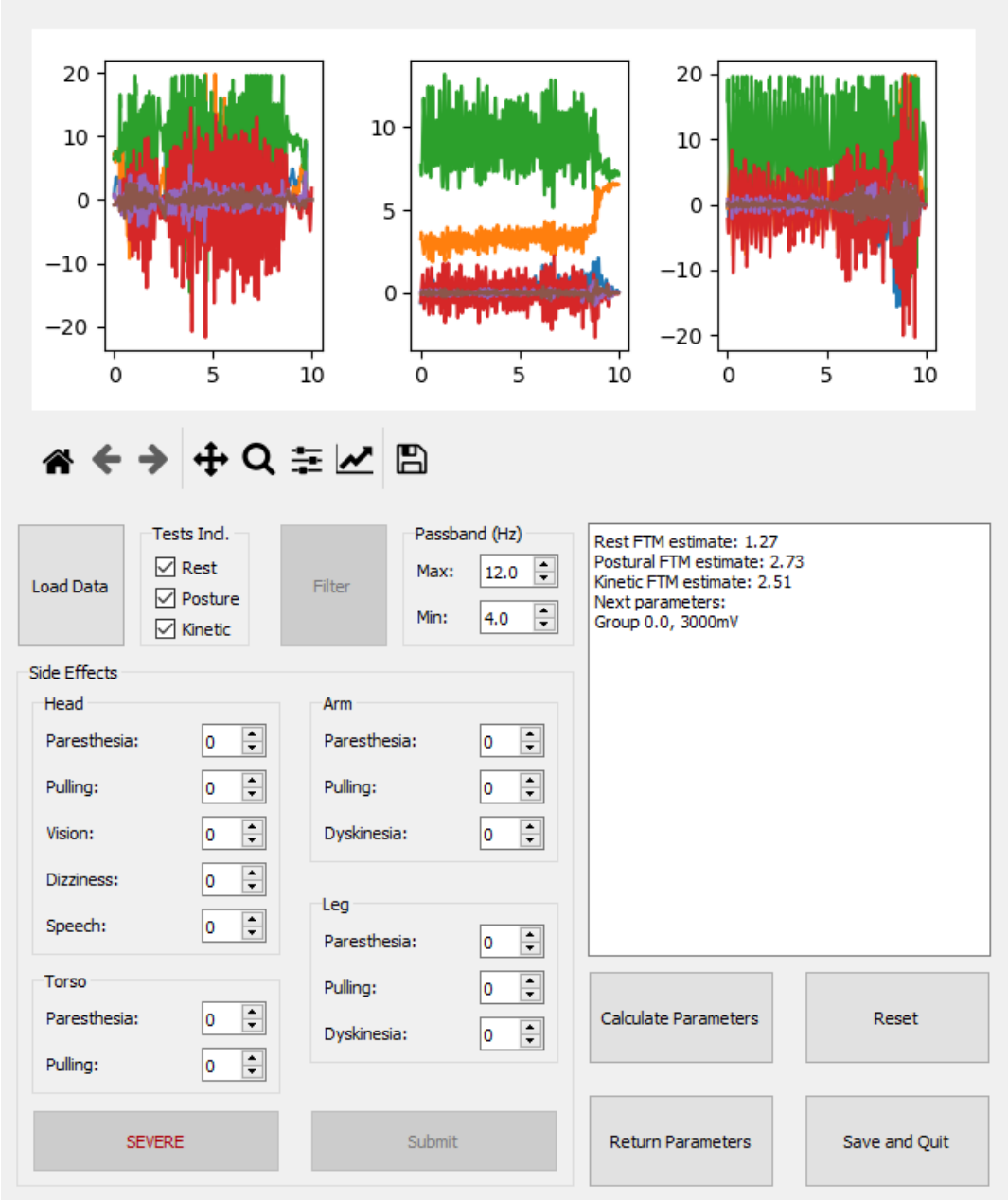

Figure 5.2: Interface for calculation of FTM estimate and side effect inputs. FTM estimates, in text in the textbox on the right side of the interface, are extracted from the raw IMU data, visible in the figure at the top of the interface. Side effect severity for each of the 13 most common side effects of DBS may then be input using the dropdown menu in the bottom left of the interface. After submission, the FTM estimates $\hat{\chi}$ and side effect severity S are incorporated into an optimization algorithm that directs what the next stimulation settings should be.

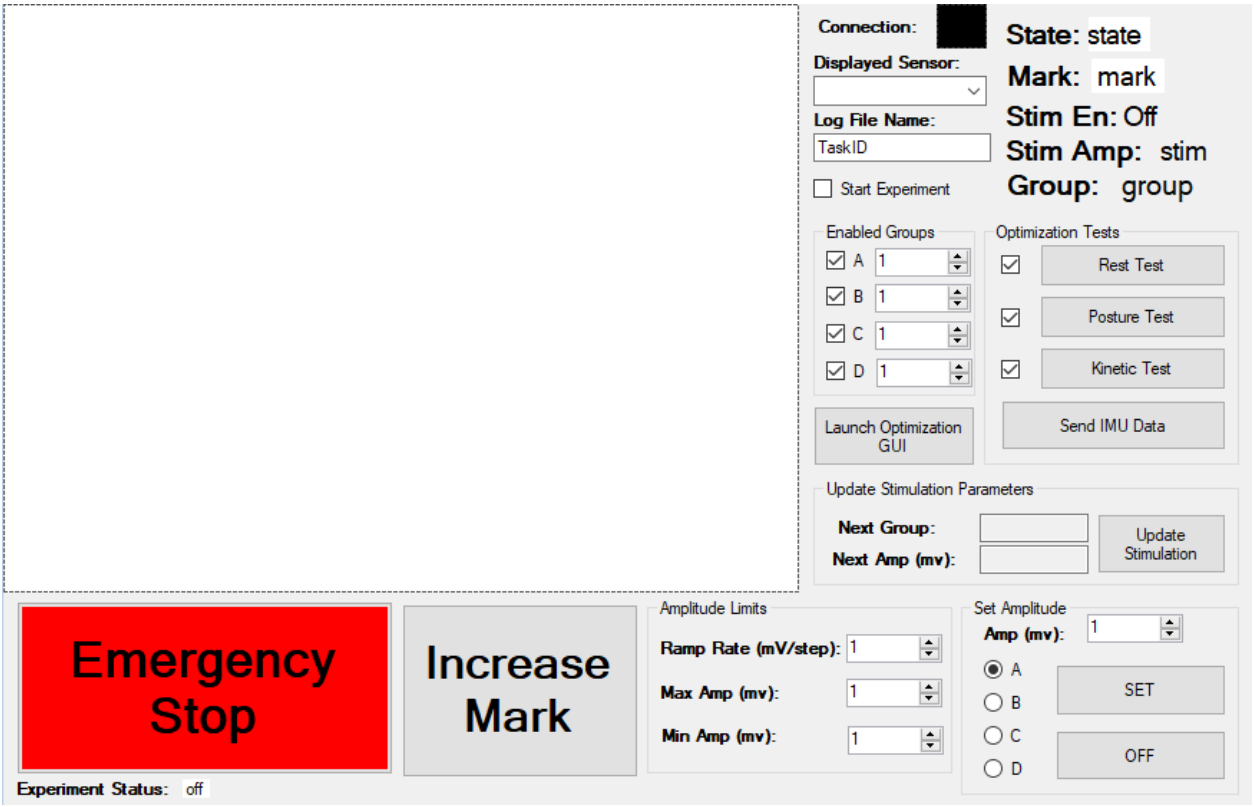

Figure 5.3: Interface for collection of IMU data and interaction with DBS device. IMU data is collected during 10 seconds with the patient conducting *Rest*, *Posture*, and *Kinetic* tests from the FTM scale, using the three buttons at the center right of the interface. This data is used in the optimization algorithm behind the interface in figure 5.2 to determine next stimulation settings, which are returned to this interface for review and activation using the buttons directly below those used to begin the tests. This interface also permits the user to set stimulation at will, set maxima and minima to ensure patient comfort, and, if needed, cease stimulation instantaneously using the "Emergency Stop" option.

The final component of the interface, the capacity to quickly and effectively interact with the DBS device used, may be seen in figure 5.3. This interface is derived from the Medtronic Activa PC+S interface described in previous work and generalized to work with the Activa PC [74, 81, 76, 28, 99, 80]. This interface serves to collect IMU data, package it for analysis, receive instructions as to the next stimulation settings, and implement those settings.

5.4.2 Future deployment of optimized automated cDBS programming system

The system described in this section is prepared for deployment in any patient implanted with the Medtronic Activa PC or PC+S neuromodulatory device. Using Bayesian optimization to develop an active map of symptom severity, this interface will allow for the evaluation of far more stimulation parameters than presently permitted by time constraints on DBS programming. The introduction of a straightforward and reliable pipeline for automated cDBS programming has the potential to make this process both significantly more efficient and more likely to reach optimal stimulation settings. Nonetheless, there are still improvements to be made. As discussed in section 5.3, accuracy for all tests was well within the bounds of inter-rater reliability for FTM assessments. However, the lowest MSE for each algorithm tested, which hovered around 0.25 , indicates that an error of ± 0.50 points on the FTM scale of 0-4 will be commonplace during programming. This implies that, although the interface itself is prepared for immediate use, the features currently used to develop $\hat{\chi}$ may be further improved upon. The further analysis and review of IMU data will be a focus of future work. Benchtop testing implies that this framework for optimized automated programming is a much needed step towards ensuring that patients receive individually optimized treatment.

5.5 A distributed, tablet- and mobile-based diagnostic tool for MDs

5.5.1 Symptom evaluation and tracking in MDs

Although specific tests for symptom analysis in MDs vary condition to condition, each involve having the patient conduct a series of tasks in the presence of a clinician [47, 45]. This places a considerable time demand on both clinicians, who must either be present to conduct tests or review recordings taken by others, and patients, who must make their way to a clinical setting for these tests. In the context of the COVID-19 public health crisis, the prospect of in-person visits and tests has shifted from inconvenient to potentially life-threatening, especially given the advanced age typical of patients diagnosed with MDs [34, 3].

One solution to this is the introduction of a remote tremor evaluation system making use

of a digitized tremor assessment method [153, 154, 155, 156]. By making use of a tablet- or mobile-based data-collection application, MD patients may be asked to complete a simple task at clinically determined intervals from the comfort of their homes. Through cloud-based storage and an accompanying application for fully remote review by a clinician, data collected through such a system may be used to clearly and consistently track symptom progression.

One additional benefit of the work described above is the clear, quantifiable data acquired using the drawing application. In several tremor rating tests across multiple MDs, inter-rater reliability has been called into question, especially with regards to drawing tasks [49, 48]. Additionally, there is substantial evidence that symptom severity in several MDs fluctuates over time, and even within a single day, based on factors related to hunger, fatigue, and circadian rhythm [54, 55]. These factors call into doubt the use of a one-off test in analyzing MD symptom severity progression.

With the recent increase in the relevance of telemedicine, especially as regards older patients with underlying conditions, it is also reasonable to suggest this system could sit at the center of a completely remote DBS parameter programming regime. Manual DBS parameter updating is a time consuming task for both patients and clinicians. Although computer-guided and automated systems for DBS programming have been demonstrated in the past, these systems still require that the patient be present in a clinical setting during a programming session [30, 28]. The simplicity and wide applicability of drawing tasks makes a tablet-based remote programming system ideal for minor updates when treatment parameters become sub-optimal between scheduled clinical visits. Furthermore, the results of each test could be completed with a "clinician-in-the-loop" by having a clinician in a remote location review results of tests immediately upon conclusion of each task.

In this section, I present a pilot study of a system for remote MD diagnosis and symptom analysis from an application using drawing tasks common in MD diagnostic tests. This application may be run on mobile, tablet, or touch-enabled PC platforms. Using the tablet-based version with three patients, we demonstrate that a fully remote data collection system may be used to assess, and even diagnose, ET.

5.5.2 Drawing and replay applications

The application, written for maximum adaptability across both tablet and mobile platforms, comprises a start screen where the subject may enter their patient and test code, digital versions of a pre-determined drawing task, and a final screen used to confirm this de-identified data has been sent securely to the cloud for storage. All data is redundantly backed up locally. Tasks may be completed with either a stylus or the subject's finger. Touchscreen data is collected at a maximum of 120Hz and comprises a timestamp, the starting and ending points of the line segment completed at the timestamp as defined by the pixel location on device, and the average pressure applied by the subject to the surface of the device during this segment.

The spiral- and line-drawing tasks of the FTM TRS are used here as our drawing task [45], examples of which may be seen in Fig. 5.4. However, these may be exchanged on demand for any task for which there exists a background image, or for any task that may be run on a blank background. Drawing tasks may be reviewed remotely using a Javascript-based application that may be run on any modern browser by dragging and dropping the desired recording into the application. Although making use of a browser, this review application is run entirely locally and is therefore intrinsically secure.

5.5.3 Subjects and procedure

29 trials across 3 male subjects diagnosed with ET (age 70-84 years) recruited with informed consent for ongoing studies at the University of Washington Medical Center with appropriate IRB supervision, and 45 trials across 2 male and 1 female healthy subjects (age 27-33 years) were conducted, the latter group comprising three of the authors of Ferleger et al. [145]. Tests were conducted on a commercial tablet with accompanying proprietary stylus. Subjects were asked to keep arms and sides of palm elevated from any surface. Subjects were instructed to complete the tasks as quickly as possible without sacrificing accuracy and to press as gently as possible on the surface of the device to limit the ability to use the stylus as a "crutch"

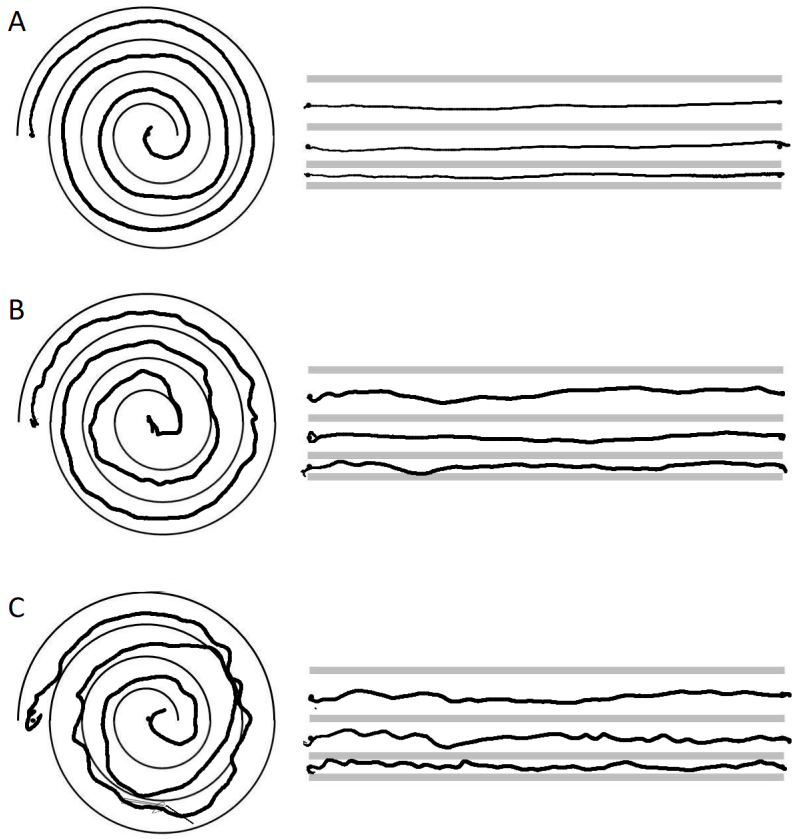

Figure 5.4: Examples of spiral review data accessible after completion of the replay application, taken from A) a healthy subject, B) an ET subject with DBS treatment active, and C) the same ET subject without treatment. Note the clear differences between healthy (A) and treated ET (B) samples, potentially indicating sub-optimal treatment settings. An advantage of our system is that a clinician reviewing these spirals remotely could recommend a reprogramming session as they deemed necessary, rather than relying on arbitrarily scheduled visits.

against tremor. This also allows collection of pressure data, which has been demonstrated to increase accuracy in differential diagnosis of Parkinson's disease compared to pure coordinate data analysis [157].

5.5.4 Feature extraction and classification

In order to differentiate between healthy and tremor-diagnosed subjects, 17 total features, a subset of which may be seen in Fig. 5.5, were extracted from combined spiral- and line-drawing data sets. First, the number of times a subject lifted their pen during a task was determined. Data was then split such that only periods of continuous contact would be considered for other features. From these were extracted several base features, including drawing velocity (pixels/sec), acceleration (pixels/sec^2), and pressure. Additional features were derived from this base set, comprising both features found to be useful in tremor analysis from other works [158] and wholly original features. Recursive feature elimination with cross-validation was used to evaluate and rank features. Two classification algorithms, logistic regression and linear discriminant analysis (LDA), were tested for their ability to differentiate between spirals taken by healthy subjects and subjects diagnosed with ET.

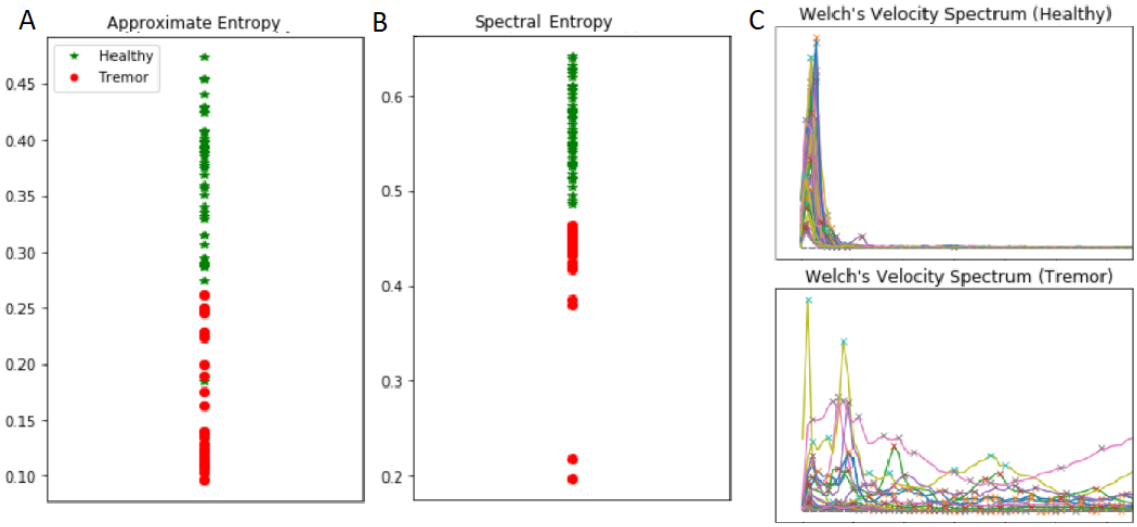

Figure 5.5: Scatter plots of subset of feature used in diagnosis algorithm. Samples of healthy (green stars) and ET (red circles) subjects showing A) the approximate entropy of the discrete cosine transform (DCT), B) the spectral entropy of the DCT, C) normalized Welch's transform of drawing velocity may be seen in all samples from healthy (top) and ET (bottom) subjects, from which the number of peaks was extracted. ET subjects had many more peaks occurring at far higher frequencies than healthy subjects.

5.5.5 Cloud-based data storage and analysis

All data was collected by the tablet-based application. Data from both healthy subjects and subjects diagnosed with ET was successfully loaded to the cloud and backed up locally. The replay application was successfully tested on all data. Analyses were conducted entirely remotely. This implies that a remote system is capable of recording all required information to help inform a "clinician-in-the-loop" DBS programming system. This finding lends weight to the idea that DBS parameters may be updated remotely within a limited scope. Future work will expand on the level of patient feedback that the program supplies, allowing for information on side effects to be easily sent in for clinical review.

5.5.6 Classification algorithm performance

Two classification algorithms, LDA and logistic regression, were applied to classify sample spirals and lines as coming from either "healthy" or "tremor" populations. First, 2-dimensional principal component analysis (PCA) was conducted on the entire set of features for dimensional reduction. Cross-validated accuracy on this reduced space was 93%; a representation of this, with LDA conducted on the entire set, may be seen in Fig. 5.7. Next, cross-validated accuracy on the full set of features was analyzed and the most useful feature extracted through recursive feature elimination. The best performing set of features yielded an accuracy of 98.3%. A ranked list of all features in decreasing order from most to least useful to our classifier may be found in Table 5.3, with effect of each feature on our model detailed in Fig. 5.6.

5.5.7 Implications for remote tremor assessment

Using both previously validated and newly developed features, this platform represents the first fully mobile MD assessment tool. Initial classification accuracy in ET is highly promising and represents a proof of feasibility for touchscreen-based MD assessment. While conducted on a relatively small number of subjects, the longitudinal nature of the data illustrates the

Table 5.3: Table of features in order of usefulness to our classifier

Accuracy Rank	**Feature**
1	Velocity Amplitude
1	Velocity Spectrum Peaks
1	Pressure
4	Smoothing
5	Acceleration Amplitude
6	Seasonal Autoregressive Integrated Moving Average (SARIMA)
7	DCT Detrend Fluctuation
8	DCT Fractral Dimension
9	DCT Spectral Entropy
10	DCT Singular Value Decomposition
11	Num. Velocity Changes
12	DCT Standard Deviation
13	DCT Approximate Entropy
14	DCT Permutation Entropy
15	DCT Sample Entropy
16	Jerk Amplitude
17	DCT Autoregression

potential for tracking MD progression over extended periods.

Remote evaluation in particular has significant implications for the tracking and treatment of MDs and other neurological conditions and diseases. A questionnaire on "side effects" could be incorporated with relative ease to extend the effective mapping of treatment efficacy, as could a questionnaire aimed towards extending use of this application to neuropsychiatric conditions. This may be used to persistently track treatment efficacy without the need for

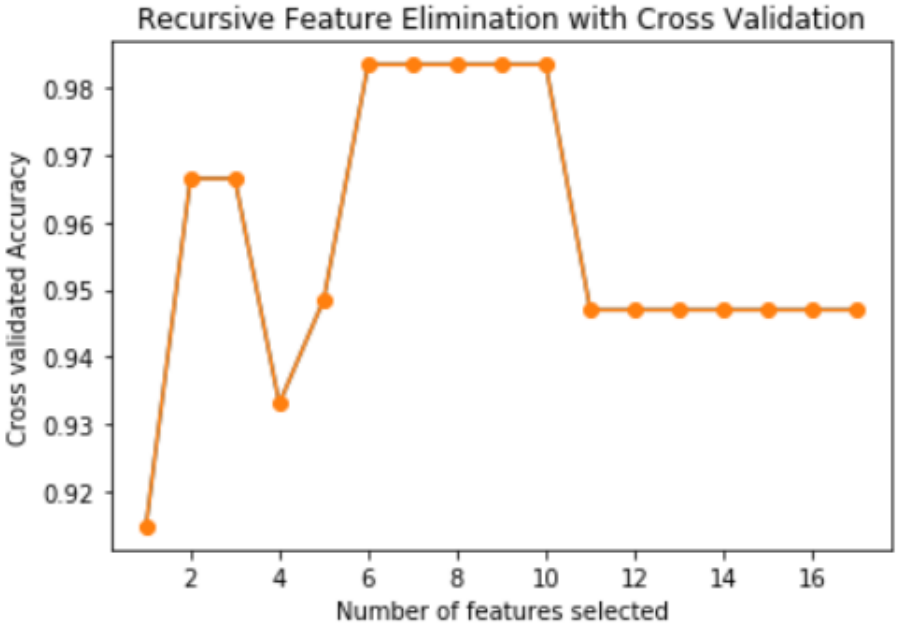

Figure 5.6: Accuracy of classification algorithm as a fraction between 0 and 1, with n features used. Order of features is identical to that seen in table 5.3. Note that using more than 6 feature contributes nothing to classification accuracy, indicating that many features may not be needed for analysis and may even add disadvantageous levels of noise.

frequent clinical visits that would previously have been a prerequisite for such a map. In the context of the global health crisis and considering the age of most patients diagnosed with MDs, remote tracking of disease progression is not only more convenient, but safer. Future studies in this space should specifically be designed to evaluate patient compliance and capacity for tracking disease progression remotely.

Larger populations of both age-controlled healthy subjects and subjects diagnosed with MDs will be recruited for future studies. This larger population will also permit nuanced analysis of symptom severity as opposed to the system's current binary diagnostic capacity, enabling any smartphone or tablet to serve as a tool for symptom tracking. Indeed, subsequent work has already demonstrated that differentiation between healthy subjects, those diagnosed with ET and untreated, and those diagnosed with ET and treated with cDBS may be accurately and efficiently conducted, as the confusion matrix in fig 5.8 from Sonnet et al.,

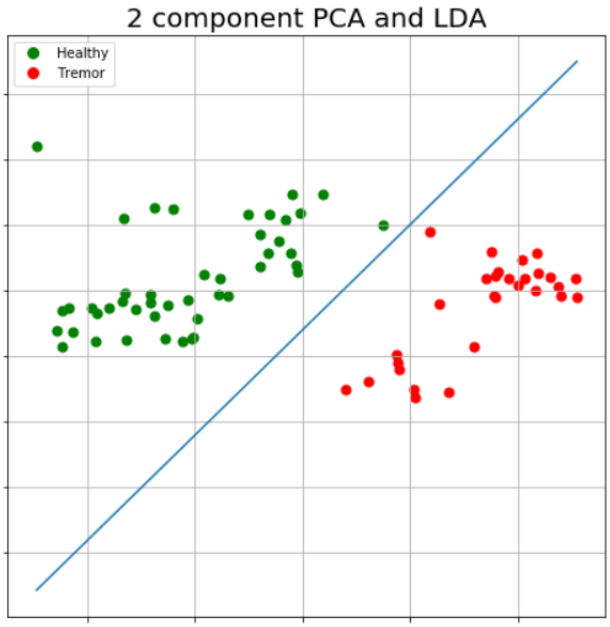

Figure 5.7: 2D PCA dimensional reduction of the original 17 features taken from healthy (green points) and ET (red points) subjects, with a line constituting the LDA classifier generated from the entire data (blue) set projected onto the space.

2020 [159] clearly demonstrates. In future examinations, MD tests in addition to the FTM will be analyzed to determine which are best suited to this system. This will also permit generation of differential diagnostic algorithms to assist physicians in cases where a diagnosis is unclear.

This larger population pool will also allow for the deployment and analysis of remote programming tools for aDBS systems, in which DBS parameters are modulated in real time based on biofeedback about patient state [79, 80, 160, 81]. As aDBS systems see more widespread use in MDs, the increased complexity of these systems may necessitate more frequent tuning than is viable with a purely clinic-based treatment. Integrating our system into both the symptom-tracking and parameter-tuning aspects of such a regimen significantly streamlines the procedure for treatment by enabling minor updates to be conducted completely remotely with a "clinician-in-the-loop" programming paradigm.

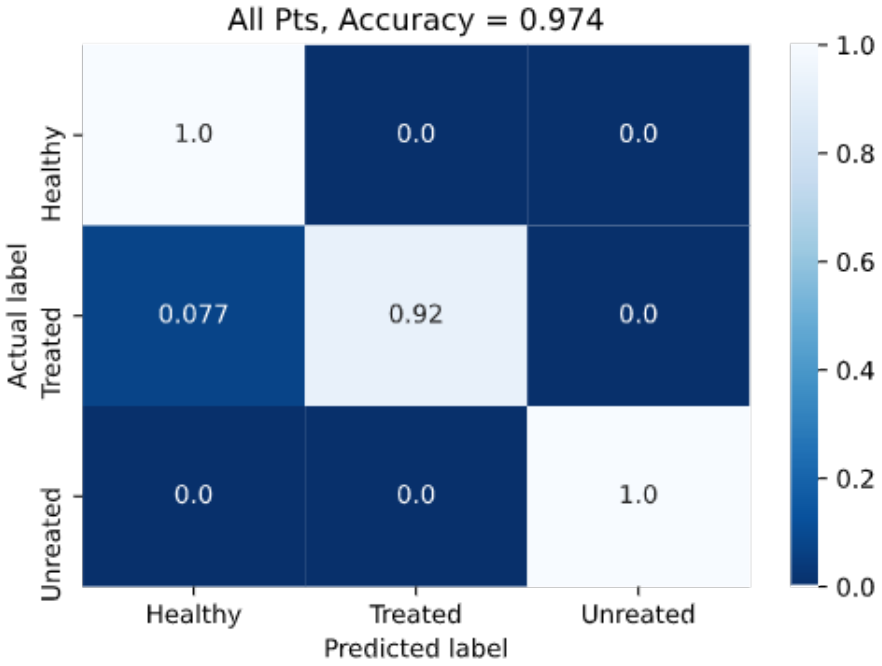

Figure 5.8: Plot of a confusion matrix for a randomly selected testing subset of the full data set, divided into "Healthy" samples with no known MD, "Treated" samples from patients diagnosed with ET and treated with cDBS therapy, and "Untreated" samples from the same population set with all treatment disabled. This confusion matrix is derived from the results of a gradient boosting classification algorithm whose design and deployment is considered more fully in Sonnet et al., 2020. The matrix shows that a small portion of samples from treated patients were misclassified as healthy subjects. This is expected as, if patients' treatment is perfectly effective, their spirals should be indistinguishable from those of healthy subjects. It also indicates that, in most samples, tremor was not fully suppressed with cDBS therapy.

5.6 Generalization to optimized aDBS treatment

As detailed in previous chapters, there is no way to ignore the increased complexity that aDBS systems introduce. The requirement that personalized classifiers be designed and evaluated for each patient carries with it an intrinsically increased burden during programming of DBS devices. The longevity of tremor-detection algorithms on which most binary aDBS systems are built has been demonstrated to be quite high [88]. However, these classification

systems will eventually require parameter updates.

Automated programming and remote symptom tracking thus approach each side of the coin first discussed at the beginning of this chapter. Through the deployment of advanced optimization methods and the efficient tracking of disease progression through a novel, remote diagnostic tool, cDBS parameter effectiveness may be optimized during clinical visits and tracked for when an update is required. These represent two substantial improvements upon the existing standard of care. However, it remains for future work to deploy these systems and test them at-large. As this testing is conducted, these systems may also be further integrated, generating the capacity for remote automated parameter updates.

These developments also lend themselves well to generalization in the context of aDBS. The automated programming system discussed above intrinsically collects large volumes of personalized data on treatment efficacy depending on patient state. However, there is always the potential that a setting ideal for suppression of symptoms during one patient state may not be ideal in the other two states. If, instead, IMU and side effect data were coordinated with neural data collection, algorithms could be designed to optimize treatment in real time depending on patient state. This could be incorporated into the optimization algorithm itself with relatively little overhead.

Subsequently, the remote tremor assessment tool described above could be altered slightly to incorporate an assessment of the neural data-based classifier. This would permit the tracking of both algorithm accuracy and effectiveness of tremor suppression on a chronic basis. Automation of DBS parameter selection and chronic tracking of MD symptom severity are thus much more than improvements on the existing standard of care in and of themselves. They are also integral stepping stones towards personalized, optimized deep brain stimulation treatment.

Chapter 6

CONCLUSIONS

In this dissertation we have described the current state of the art in deep brain stimulation therapy, recognizing the substantial benefits of this vital treatment for neurological disorders, but with special attention paid to its drawbacks and limitations. With an eye towards the broader context of personalized medical treatment, we have extracted from these limitations several key needs that have not yet been met, and defined three aims to approach these omissions. These aims – the development of a deployment-ready fully embedded binary adaptive deep brain stimulation system, the design and evaluation of a graded adaptive deep brain stimulation control system based on a model-free approach to algorithm design, and the creation of automated programming tools and remote symptom tracking – comprise three faces of the same die. Recognizing the inextricably linked nature of these aims is the fundamental keystone around which this work has been constructed.

6.1 Significance of this work

In our demonstration of a fully embedded binary aDBS system, we integrated an understanding of the therapeutic context of DBS into our system design. This resulted in an easily trained and tuned system specifically biased to minimize the potential for stimulation to be erroneously deactivated when it was needed by a patient. In this process, we demonstrated that a quickly and easily trained biased binary aDBS system provides treatment nearly all of the time it is required while simultaneously providing substantial stimulation power savings. In an unexpected discovery, we further determined that aDBS is far more effective in tremor suppression than conventional DBS. This suggests that rebound effect, previously suspected of potentially hazardous interference with binary aDBS systems, may

not manifest on the stimulation timescales common within these systems.

The simplicity of these binary systems implies that they may reliably be based on top-down feature selection strategies, an implication firmly supported by our own results. However, our results demonstrate that, when designing a graded control system based on neural data-based estimation of untreated symptom severity, top-down approaches to feature selection may be less effective than developing an individualized, data-driven algorithm. Although results in terms of power savings and symptom suppression were inconclusive with our Bollinger band-based control system, demonstrating that a data-driven approach can yield benefits in symptom severity estimation lays a solid foundation upon which to base future work on just such a model-free approach. Additionally, our discovery that neural data may be used to reliably estimate symptom severity during rebound effect implies that this downstream effect of DBS may itself be used to generate symptom severity estimation algorithms.

Finally, we approached the problem of optimization in DBS treatment with special attention paid to its eventual generalization into a fully automated programming platform. Our first step was the development of an accelerometer and gyroscope-based tremor assessment tool capable of determining a patient's clinical movement disorder rating within the range of inter-rater reliability. By pairing this with a rapid and straightforward interface for side effect input and quantification, we established a pipeline for efficient tracking of treatment effectiveness during programming, specifically designed to permit future deployment of modern optimization techniques. Introducing a simple drawing application for the chronic tracking of symptom manifestation and, by extension, treatment efficacy is directly related to the corresponding need for increased data acquisition in personalized treatment.

6.2 Generalization to future directions in personalized treatment

Perhaps the single most important conclusion we may take from this dissertation is the recognition that strategies for optimized treatment cannot succeed in a vacuum. No individual technique or application will suffice to "solve" the problem of optimized aDBS in a

one-size-fits-all fashion. Rather, researchers must focus on the integration of many methods, as we have attempted to do here. Without evidence of effective and reliable binary aDBS, medical device manufacturers cannot be expected to develop the much more complex systems required for embedded graded aDBS. The increased complexity posed by aDBS systems makes automated programming a prerequisite for clinicians and patients to adopt these systems at-scale. Remote evaluation of symptom severity provides for a substantial increase in the amount of data available about each individual patient's treatment. The eventual adoption of fully remote, data-driven programming of aDBS systems can only take place after optimization through automated programming has been firmly established.

Above all, we have demonstrated that any approach to designing aDBS control systems and neural data analysis algorithms should be fundamentally patient-centric. Top-down strategies and population scale analyses have their place in medicine, but as the evidence shows time and again, treatment design must ultimately be based on the person being treated. The popular conception that machine learning in medicine intrinsically removes the human aspect of treatment is rendered false only so long as researchers and clinicians maintain this vital mindset. Only by applying machine learning methods that reinforce the individualization of treatment can scientists, researchers, and clinicians meet the challenges posed by this newly arrived era of personalized medicine.

BIBLIOGRAPHY

[1] A. Schrag, "Psychiatric aspects of parkinson's disease," *J Neurol*, vol. 251, pp. 795 – 804, 2004.

[2] M. Zurowski, W. M. McDonald, S. Fox, and L. Marsh, "Psychiatric comorbidities in dystonia: emerging concepts," *Mov Disord*, vol. 28, pp. 914–20, 2013.

[3] E. Louis and J. Ferreira, "How common is the most common adult movement disorder? update on the worldwide prevalence of essential tremor," *Mov Disord*, vol. 25, p. 534–41, 2010.

[4] G. Alves, E. Forsaa, K. Pedersen, M. Dreetz-Gjerstad, and J. Larsen, "Epidemiology of parkinson's disease," *J Neurol*, vol. 255, no. Suppl 5, pp. 18–32, 2008.

[5] T. D. Steeves, L. Day, J. Dykeman, N. Jette, and T. Pringsheim, "The prevalence of primary dystonia: a systematic review and meta-analysis," *Mov Disord*, vol. 27, no. 14, pp. 1789–96, 2012.

[6] A. Gironell and J. Kulisevsky, "Review: Diagnosis and management of essential tremor and dystonic tremor," *Therapeut Adv in Neurolog Disord*, vol. 2, no. 4, pp. 215–222, 2009.

[7] M. C. Rodriguez-Oroz, J. A. Obeso, A. E. Lang, J.-L. Houeto, P. Pollak, S. Rehncrona, J. Kulisevsky, A. Albanese, J. Volkmann, M. I. Hariz, N. P. Quinn, J. D. Speelman, J. Guridi, I. Zamarbide, A. Gironell, J. Molet, B. Pascual-Sedano, B. Pidoux, A. M. Bonnet, Y. Agid, J. Xie, A.-L. Benabid, A. M. Lozano, J. Saint-Cyr, L. Romito, M. F. Contarino, M. Scerrati, V. Fraix, and N. Van Blercom, "Bilateral deep brain stimulation in parkinson's disease: a multicentre study with 4 years follow-up," *Brain*, vol. 128, no. 10, pp. 2240–49, 2005.

[8] J. Baizabal-Carvallo, M. Kagnoff, J. Jimenez-Shahad, R. Fekete, and J. Jankovic, "The safety and efficacy of thalamic deep brain stimulation in essential tremor: 10 years and beyond," *J Neurol Neurosurg Ps*, vol. 85, no. 5, pp. 567–72, 2014.

[9] J. Krauss, J. Yianni, T. Loher, and T. Aziz, "Deep brain stimulation for dystonia," *Clin Neurophysiol*, vol. 21, no. 1, pp. 18–30, 2004.

[10] B. Greenberg, D. Malone, G. Friehs, A. Rezai, C. Kubu, P. Malloy, S. Salloway, M. Okun, W. Goodman, and S. Rasmussen, "Three-year outcomes in deep brain stimulation for highly resistant obsessive–compulsive disorder," *Neuropsychopharmacology*, vol. 31, p. 2384–93, 2006.

[11] H. Mayberg, A. Lozano, V. Voon, H. McNeely, D. Seminowicz, C. Hamani, J. Schwalb, and S. Kennedy, "Deep brain stimulation for treatment-resistant depression," *Neuron*, vol. 45, no. 5, pp. 651–60, 2005.

[12] D. Martinez-Ramirez, J. Jimenez-Shahed, J. F. Leckman, M. Porta, D. Servello, F. G. Meng, J. Kuhn, D. Huys, J. Baldermann, T. Foltynie, M. Hariz, E. Joyce, L. Zrinzo, Z. Kefalopoulou, P. Silburn, T. Coyne, A. Mogilner, M. Pourfar, S. Khandhar, M. Auyeung, J. L. Ostrem, V. Visser-Vandewalle, M. Welter, L. Mallet, C. Karachi, J. L. Houeto, B. T. Klassen, L. Ackermans, T. Kaido, Y. Temel, R. E. Gross, H. C. Walker, A. M. Lozano, B. L. Walter, Z. Mari, W. S. Anderson, B. K. Changizi, E. Moro, S. E. Zauber, L. E. Schrock, J. G. Zhang, W. Hu, K. Rizer, E. H. Monari, K. D. Foote, I. A. Malaty, W. Deeb, A. Gunduz, and M. S. Okun, "Efficacy and safety of deep brain stimulation in tourette syndrome: The international tourette syndrome deep brain stimulation public database and registry," *JAMA Neurol*, vol. 75, no. 3, pp. 353–359, 2018.

[13] A. S. Widge, D. A. Malone Jr, and D. D. Dougherty, "Closing the loop on deep brain stimulation for treatment-resistant depression," *Front Neurosci*, vol. 12, p. 175, 2018.

[14] M. Bin-Mahfoodh, C. Hamani, E. Sime, and A. Lozano, "Longevity of batteries in internal pulse generators used for deep brain stimulation," *Stereotact Funct Neurosurg*, vol. 80, no. 1-4, pp. 56–60, 2003.

[15] W. Ondo, C. Meilak, and K. Vuong, "Predictors of battery life for the activa soletra 7426 neurostimulator," *Parkinsonism & Relat Disord*, vol. 13, no. 4, pp. 240–42, 2007.

[16] K. Fakhar, E. Hastings, C. Butson, K. Foote, P. Zeilman, and M. Okun, "Management of deep brain stimulator battery failure: battery estimators, charge density, and importance of clinical symptoms," *PLOS ONE*, vol. 8, no. 3, 2013.

[17] G. Deuschl, J. Herzog, G. Kleiner-Fisman, C. Kubu, A. M. Lozano, K. E. Lyons, M. C. Rodriguez-Oroz, F. Tamma, A. I. Tröster, J. L. Vitek, J. Volkmann, and V. Voon, "Deep brain stimulation: Postoperative issues," *Movement Disorders*, vol. 21, no. S14, pp. S219–S237, 2006.

[18] D. Aldridge, D. Theodoros, A. Angwin, and A. P. Vogel, "Speech outcomes in parkinson's disease after subthalamic nucleus deep brain stimulation: A systematic review," *Parkinsonism & Related Disorders*, vol. 33, pp. 3–11, 2016.

[19] C. Buhmann, T. Huckhagel, K. Engel, A. Gulberti, U. Hidding, M. Poetter-Nerger, I. Goerendt, P. Ludewig, H. Braass, C.-u. Choe, K. Krajewski, C. Oehlwein, K. Mittmann, A. K. Engel, C. Gerloff, M. Westphal, J. A. Köppen, C. K. E. Moll, and W. Hamel, "Adverse events in deep brain stimulation: A retrospective long-term analysis of neurological, psychiatric and other occurrences," *PLOS ONE*, vol. 12, pp. 1–21, 07 2017.

[20] D. Mücke, A. Hermes, T. B. Roettger, J. Becker, H. Niemann, T. A. Dembek, L. Timmermann, V. Visser-Vandewalle, G. R. Fink, M. Grice, and M. T. Barbe, "The effects of thalamic deep brain stimulation on speech dynamics in patients with essential tremor: An articulographic study," *PLOS ONE*, vol. 13, pp. 621–25, 01 2018.

[21] M. Reich, J. Brumberg, N. Pozzi, G. Marotta, J. Roothans, M. Åström, T. Musacchio, L. Lopiano, M. Lanotte, R. Lehrke, A. Buck, J. Volkmann, and I. Isaias, "Progressive gait ataxia following deep brain stimulation for essential tremor: adverse effect or lack of efficacy?," *Brain*, vol. 139, no. 11, pp. 2948–56, 2016.

[22] B. Appleby, P. Duggan, A. Regenberg, and P. Rabins, "Psychiatric and neuropsychiatric adverse events associated with deep brain stimulation: A meta-analysis of ten years' experience," *Mov Disord*, vol. 22, no. 12, pp. 1722–28, 2007.

[23] A. Castrioto, E. Lhommée, E. Moro, and P. Krack, "Mood and behavioural effects of subthalamic stimulation in parkinson's disease," *Lancet Neurol*, vol. 13, no. 3, pp. 287 – 305, 2014.

[24] E. B. J. Montgomery, *Deep brain stimulation programming: mechanisms, principles, and practice*. Oxford University Press, 2016.

[25] K. Witt, C. Daniels, and J. Volkmann, "Factors associated with neuropsychiatric side effects after STN-DBS in Parkinson's disease," *Parkinsonism & Relat Disord*, vol. 18, pp. S168–S170, 2012.

[26] S. Little, E. Tripoliti, M. Beudel, A. Pogosyan, H. Cagnan, D. Herz, S. Bestmann, T. Aziz, B. Cheeran, L. Zrinzo, M. Hariz, J. Hyam, P. Limousin, T. Foltynie, and P. Brown, "Adaptive deep brain stimulation for Parkinson's disease demonstrates reduced speech side effects compared to conventional stimulation in the acute setting," *J Neurol, Neurosurg PS*, vol. 87, no. 12, pp. 1388–1389, 2016.

[27] R. Bhidayasiri, "Differential diagnosis of common tremor syndromes," *Postgrad Med J*, vol. 81, pp. 756–762, 2005.

[28] A. Haddock, K. Mitchell, A. Miller, J. Ostrem, H. Chizeck, and S. Miocinovic, "Automated deep brain stimulation programming for tremor," *IEEE TNSRE*, vol. 26, no. 8, pp. 1618–25, 2018.

[29] E. Moro, Y.-Y. Poon, A. Lozano, J. Saint-Cyr, and A. Lang, "Subthalamic nucleus stimulation - improvements in outcome with reprogramming," *Archives of neurology*, vol. 63, pp. 1266–72, 2006.

[30] D. A. Heldman, C. L. Pulliam, E. Urrea Mendoza, M. Gartner, J. P. Giuffrida, E. B. Montgomery Jr., A. J. Espay, and F. J. Revilla, "Computer-guided deep brain stimulation programming for parkinson's disease," *Neuromod.*, vol. 19, no. 2, pp. 127–132, 2016.

[31] A. Ozanne, D. Johansson, U. Hällgren Graneheim, K. Malmgren, F. Bergquist, and M. Alt Murphy, "Wearables in epilepsy and parkinson's disease—a focus group study," *Acta Neurologica Scandinavica*, vol. 137, no. 2, pp. 188–194, 2018.

[32] K. Pratt, *Brain Computer Interfaces: Privacy, Ethics, and Policy*. PhD thesis, University of Washington, 2019.

[33] S. Fahn, "Classification of movement disorders," *Mov Disord*, vol. 26, pp. 947 – 957, 2011.

[34] O. Tysnes and A. Storstein, "Epidemiology of Parkinson's disease," *J Neural Transm*, vol. 124, no. 8, 2017.

[35] E. Louis and R. Ottman, "How many people in the usa have essential tremor? deriving a population estimate based on epidemiological data," *Tremor Other Hyperkinet Mov (NY)*, vol. 4, p. 259, 2014.

[36] E. D. Louis, "Essential tremor," *Handb Clin Neurol*, vol. 100, pp. 433–48, 2011.

[37] G. Fabbrini, I. Berardelli, M. Falla, G. Moretti, M. Pasquini, M. Altieri, G. Defazio, M. Biondi, and A. Berardelli, "Psychiatric disorders in patients with essential tremor," *Parkinsonism Related Disorders*, vol. 18, no. 8, pp. 971 – 973, 2012.

[38] A. L. Benabid, P. Pollak, A. Louveau, S. Henry, and J. de Rougemont, "Combined (thalamotomy and stimulation) stereotactic surgery of the vim thalamic nucleus for bilateral parkinson disease," *Appl Neurophysiol*, vol. 50, p. 344–346, 1987.

[39] A. L. Benabid, P. Pollak, D. Gao, D. Hoffmann, P. Limousin, E. Gay, I. Payen, and A. Benazzouz, "Chronic electrical stimulation of the ventralis intermedius nucleus of the thalamus as a treatment of movement disorders," *J Neurosurg*, vol. 84, pp. 203–14, 1996.

[40] W. Ondo, J. Jankovic, K. Schwartz, M. Almaguer, and R. Simpson, "Unilateral thalamic deep brain stimulation for refractory essential tremor and parkinson's disease tremor," *Neurolog*, vol. 51, no. 4, pp. 1063–9, 1998.

[41] W. C. Koller, K. E. Lyons, S. B. Wilkinson, and R. Pahwa, "Efficacy of unilateral deep brain stimulation of the vim nucleus of the thalamus for essential head tremor," *J Neurol Neurosurg Ps*, vol. 14, pp. 447–50, 1999.

[42] W. C. Koller, K. E. Lyons, S. B. Wilkinson, A. I. Troster, and R. Pahwa, "Long-term safety and efficacy of unilateral deep brain stimulation of the thalamus in essential tremor," *Mov Disord*, vol. 16, pp. 464–8, 2001.

[43] C. Kenney, R. Simpson, C. Hunter, W. Ondo, M. Almaguer, A. Davidson, and J. Jankovic, "Short-term and long-term safety of deep brain stimulation in the treatment of movement disorders," *J Neurosurg*, vol. 106, no. 4, pp. 621 – 625, 2007.

[44] S. Paschen, J. Forstenpointner, J. Becktepe, S. Heinzel, H. Hellriegel, K. Witt, A. K. Helmers, and G. Deuschl, "Long-term efficacy of deep brain stimulation for essential tremor: An observer-blinded study," *Neurology*, vol. 92, no. 12, pp. 95–99, 2019.

[45] S. Fahn, E. Tolosa, and C. Marín, "Clinical rating scale for tremor," *Parkinson's Disease and Mov Disord*, pp. 225–234, 1993.

[46] D. A. Heldman, J. P. Giuffrida, R. Chen, M. Payne, F. Mazzella, A. P. Duker, A. Sahay, S. J. Kim, F. J. Revilla, and A. J. Espay, "The modified bradykinesia rating scale for parkinson's disease: Reliability and comparison with kinematic measures," *Mov Disord*, vol. 26, no. 10, pp. 1859–1863, 2011.

[47] C. G. Goetz, B. C. Tilley, S. R. Shaftman, G. T. Stebbins, S. Fahn, P. Martinez-Martin, W. Poewe, C. Sampaio, M. B. Stern, R. Dodel, *et al.*, "Movement disorder society-sponsored revision of the unified parkinson's disease rating scale (mds-updrs): scale presentation and clinimetric testing results," *Mov Disord*, vol. 23, no. 15, pp. 2129–2170, 2008.

[48] J. L. Palmer, M. A. Coats, C. M. Roe, S. M. Hanko, C. Xiong, and J. C. Morris, "Unified parkinson's disease rating scale-motor exam: Inter-rater reliability of advanced practice nurse and neurologist assessments," *J Adv Nurs*, vol. 66, no. 6, pp. 1382–1387, 2010.

[49] M. A. Stacy, R. J. Elble, W. G. Ondo, S. C. Wu, and J. Hulihan, "Assessment of interrater and intrarater reliability of the fahn-tolosa-marin tremor rating scale in essential tremor," *Mov Disord*, vol. 22, no. 6, pp. 833–838, 2007.

[50] J.-W. Kim, J.-H. Lee, Y. Kwon, C.-S. Kim, G.-M. Eom, S.-B. Koh, D.-Y. Kwon, and K.-W. Park, "Quantification of bradykinesia during clinical finger taps using a gyrosensor in patients with parkinson's disease," *Med Biol Eng Comput*, vol. 49, pp. 365–371, Mar 2011.

[51] H. Dai, H. Lin, and T. C. Lueth, "Quantitative assessment of parkinsonian bradykinesia based on an inertial measurement unit," *Biomedical engineering online*, vol. 14, no. 1, p. 68, 2015.

[52] S. Das, L. Trutoiu, A. Murai, D. Alcindor, M. Oh, F. De la Torre, and J. Hodgins, "Quantitative measurement of motor symptoms in parkinson's disease: A study with full-body motion capture data," in *Engineering in Medicine and Biology Society, EMBC, 2011 Annual International Conference of the IEEE*, pp. 6789–6792, IEEE, 2011.

[53] A. Haddock, A. Velisar, J. Herron, H. Bronte-Stewart, and H. J. Chizeck, "Model predictive control of deep brain stimulation for Parkinsonian tremor," in *Proc 8th IEEE/EMBS NER*, pp. 358–362, IEEE, 2017.

[54] L. Cleeves and L. J. Findley, "Variability in amplitude of untreated essential tremor," *J Neurol Neurosurg Ps*, vol. 50, no. 6, pp. 704–708, 1987.

[55] J. J. Van Hilten, G. Hoogland, E. A. Van Der Velde, H. A. M. Middelkoop, G. A. Kerkhof, and R. A. C. Roos, "Diurnal effects of motor activity and fatigue in Parkinson's disease," *J Neurol Neurosurg Ps*, vol. 56, no. 8, pp. 874–877, 1993.

[56] G. M. Halliday and H. McCann, "The progression of pathology in parkinson's disease," *Annals of the New York Academy of Sciences*, vol. 1184, no. 1, pp. 188–195, 2010.

[57] H. A. Shill, C. H. Adler, and T. G. Beach, "Pathology in essential tremor," *Parkinsonism & related disorders*, vol. 18, pp. S135–S137, 2012.

[58] S. Papapetropoulos, "Patient diaries as a clinical endpoint in parkinson's disease clinical trials," *CNS Neuroscience & Therapeutics*, vol. 18, no. 5, pp. 380–387, 2012.

[59] A. J. Lees, "Unresolved issues relating to the shaking palsy on the celebration of james parkinson's 250th birthday," *Movement Disorders*, vol. 22, no. S17, pp. S327–S334, 2007.

[60] D. J. Lanska, "Chapter 33 the history of movement disorders," in *History of Neurology* (M. J. Aminoff, F. Boller, and D. F. Swaab, eds.), vol. 95 of *Handbook of Clinical Neurology*, pp. 501 – 546, Elsevier, 2009.

[61] C. G. Goetz, "Jean-martin charcot and movement disorders: Neurological legacies to the 21st century."

[62] J. G. Greenfield and F. D. Bosanquet, "The brain-stem lesions in parkinsonism," *J Neurol Neurosurg Psychiatry*, vol. 16, no. 4, pp. 213–226, 1953.

[63] V. HORSLEY and R. H. CLARKE, "THE STRUCTURE AND FUNCTIONS OF THE CEREBELLUM EXAMINED BY A NEW METHOD.," *Brain*, vol. 31, no. 1, pp. 45–124, 1908.

[64] J. M. Schwalb and C. Hamani, "The history and future of deep brain stimulation," *Neurotherapeutics*, vol. 5, pp. 3–13, 2008.

[65] R. Meyers, "The modification of alternating tremors, rigidity and festination by surgery of the basal ganglia," *RESEARCH PUBLICATIONS-ASSOCIATION FOR RESEARCH IN NERVOUS AND MENTAL DISEASE*, vol. 21, pp. 602–665, 1940.

[66] T. RIECHERT

[67] H. Ehringer and O. Hornykiewicz, "Verteilung von noradrenalin and dopamin im gehirn des menschen und ihr verhalten bei erkrankungen des extrapyramidalen systems," *Klin Wschr*, vol. 38, p. 1126–1239, 1960.

[68] A. Lozano, N. Lipsman, H. Bergman, P. Brown, S. Chabardes, J. Chang, K. Matthews, C. McIntyre, T. Schlaepfer, M. Schulder, Y. Temel, J. Volkmann, and J. Krauss, "Deep brain stimulation: current challenges and future directions," *Nature Rev Neurol*, vol. 13, no. 3, pp. 148–60, 2019.

[69] A. Meidahl, G. Tinkhauser, D. Herz, H. Cagnan, J. Debarros, and P. Brown, "Adaptive deep brain stimulation for movement disorders: the long road to clinical therapy," *Mov Disord*, vol. 32, no. 6, pp. 810–19, 2017.

[70] M. Arlotti, M. Rosa, S. Marceglia, S. Barbieri, and A. Priori, "The adaptive deep brain stimulation challenge," *Parkinsonism & Relat Disord*, vol. 28, pp. 12–17, 2016.

[71] M. Kronenbuerger, C. Fromm, F. Block, V. A. Coenen, I. Rohde, V. Rohde, and J. Noth, "On-demand deep brain stimulation for essential tremor: A report on four cases," *Mov Disord*, vol. 21, no. 3, pp. 401–5, 2006.

[72] H. Ackermann, I. Hertrich, I. Daum, G. Scharf, and S. Spieker, "Kinematic analysis of articulatory movements in central motor disorders," *Movement Disorders*, vol. 12, no. 6, pp. 1019–1027, 1997.

[73] A. de los Reyes-Guzmán, I. Dimbwadyo-Terrer, F. Trincado-Alonso, F. Monasterio-Huelin, D. Torricelli, and A. Gil-Agudo, "Quantitative assessment based on kinematic measures of functional impairments during upper extremity movements: A review," *Clinical Biomechanics*, vol. 29, no. 7, pp. 719 – 727, 2014.

[74] J. Herron, T. Denison, and H. J. Chizeck, "Closed-loop dbs with movement intention," in *Proc. 7th IEEE/EMBS Conf NER*, pp. 844–847, 2015.

[75] D. Graupe, I. Basu, D. Tuninetti, P. Vannemreddy, and K. Slavin, "Adaptively controlling deep brain stimulation in essential tremor patient via surface electromyography," *Neurol Res*, vol. 32, no. 9, pp. 899–904, 2010.

[76] J. A. Herron, M. C. Thompson, T. Brown, H. J. Chizeck, J. G. Ojemann, and A. L. Ko, "Cortical brain–computer interface for closed-loop deep brain stimulation," *IEEE TNSRE*, vol. 25, no. 11, pp. 2180–2187, 2017.

[77] W.-J. Neumann, R. S. Turner, B. Blankertz, T. Mitchell, A. A. Kühn, and R. M. Richardson, "Toward electrophysiology-based intelligent adaptive deep brain stimulation for movement disorders," *Neurotherapeutics*, vol. 16, no. 1, pp. 105–118, 2019.

[78] E. Opri, J. Shute, R. Molina, K. Foote, M. Okun, and A. Gunduz, "Closing the loop in deep brain stimulation: A responsive treatment for essential tremor," *Neurology*, vol. 86, no. 16 Supplement, 2016.

[79] N. Swann, C. de Hemptinne, M. Thompson, S. Miocinovic, A. Miller, J. Ostrem, H. Chizeck, and P. Starr, "Adaptive deep brain stimulation for parkinson's disease using motor cortex sensing," *J Neural Eng*, vol. 15, no. 4, p. 046006, 2018.

[80] B. Houston, M. Thompson, A. L. Ko, and H. J. Chizeck, "A machine-learning approach to volitional control of a closed-loop deep brain stimulation system," *J Neural Eng*, vol. 16, no. 1, 2018.

[81] J. Herron, M. Thompson, T. Brown, H. Chizeck, J. Ojemann, and A. Ko, "Chronic electrocorticography for sensing movement intention and closed-loop deep brain stimulation with wearable sensors in an essential tremor patient," *J Neurosurg*, vol. 127, no. 4, pp. 1–8, 2017.

[82] M. Rosa, M. Arlotti, G. Ardolino, F. Cogiamanian, S. Marceglia, A. Di Fonzo, F. Cortese, P. M. Rampini, and A. Priori, "Adaptive deep brain stimulation in a freely moving parkinsonian patient," *Mov Disord*, vol. 30, no. 7, pp. 1003–1005, 2015.

[83] A. Velisar, J. Syrkin-Nikolau, Z. Blumenfeld, M. Trager, M. Afzal, V. Prabhakar, and H. Bronte-Stewart, "Dual threshold neural closed loop deep brain stimulation in parkinson disease patients," *Brain Stimulation*, vol. 12, no. 4, pp. 868–876, 2019.

[84] S. Little, A. Pogosyan, S. Neal, B. Zavala, L. Zrinzo, M. Hariz, T. Foltynie, P. Limousin, K. Ashkan, J. FitzGerald, A. Green, T. Aziz, and P. Brown, "Adaptive deep brain stimulation in advanced parkinson disease," *Ann Neurol*, vol. 74, no. 3, pp. 449–57, 2013.

[85] T. Mera, J. L. Vitek, J. L. Alberts, and J. P. Giuffrida, "Kinematic optimization of deep brain stimulation across multiple motor symptoms in parkinson's disease," *Journal of Neuroscience Methods*, vol. 198, no. 2, pp. 280 – 286, 2011.

[86] S. M. Rissanen, V. Ruonala, E. Pekkonen, M. Kankaanpää, O. Airaksinen, and P. A. Karjalainen, "Signal features of surface electromyography in advanced parkinson's disease during different settings of deep brain stimulation," *Clin Neurophysiol*, vol. 126, no. 12, pp. 2290–2298, 2015.

[87] V. Kremen, B. H. Brinkmann, I. Kim, H. Guragain, M. Nasseri, A. L. Magee, T. Pal Attia, P. Nejedly, V. Sladky, N. Nelson, S. Chang, J. A. Herron, T. Adamski, S. Baldassano, J. Cimbalnik, V. Vasoli, E. Fehrmann, T. Chouinard, E. E. Patterson, B. Litt, M. Stead, J. Van Gompel, B. K. Sturges, H. J. Jo, C. M. Crowe, T. Denison, and G. A. Worrell, "Integrating brain implants with local and distributed computing devices: a next generation epilepsy management system," *IEEE JTEHM*, vol. 6, pp. 1–12, 2018.

[88] B. Houston, Z. Blumenfeld, E. Quinn, H. Bronte-Stewart, and H. Chizeck, "Long-term detection of parkinsonian tremor activity from subthalamic nucleus local field potentials," in *2015 37th Annual International Conference of the IEEE Engineering in Medicine and Biology Society (EMBC)*, 2015.

[89] B. Ferleger, B. Houston, M. Thompson, S. Cooper, K. Sonnet, A. Ko, J. Herron, and H. Chizeck, "Fully implanted adaptive deep brain stimulation infreely moving essential tremor patients," *J Neural Eng*, 2020.

[90] C. Brücke, A. Bock, J. Huebl, J. K. Krauss, T. Schönecker, G. H. Schneider, P. Brown, and A. A. Kühn, "Thalamic gamma oscillations correlate with reaction time in a Go/noGo task in patients with essential tremor," *Neuroimage*, vol. 75, pp. 36–45, 2013.

[91] E. Opri, S. Cernera, M. Okun, K. Foote, and A. Gunduz, "The functional role of thalamocortical coupling in the human motor network," *Neurosci*, vol. 39, no. 41, pp. 8124–34, 2019.

[92] A. L. Crowell, E. S. Ryapolova-Webb, J. L. Ostrem, N. B. Galifianakis, S. Shimamoto, D. A. Lim, and P. A. Starr, "Oscillations in sensorimotor cortex in movement disorders: An electrocorticography study," *Brain*, vol. 135, no. 2, pp. 615–630, 2012.

[93] E. D. Kondylis, M. J. Randazzo, A. Alhourani, W. J. Lipski, T. A. Wozny, Y. Pandya, A. S. Ghuman, R. S. Turner, D. J. Crammond, and R. M. Richardson, "Movement-related dynamics of cortical oscillations in parkinson's disease and essential tremor," *Brain*, vol. 139, no. 8, pp. 2211–2223, 2016.

[94] A. M. Koss, R. L. Alterman, M. Tagliati, and J. L. Shils, "Calculating total electrical energy delivered by deep brain stimulation systems," *Ann Neurol*, vol. 58, no. 1, pp. 168–168, 2005.

[95] P. Khanna, S. Stanslaski, Y. Xiao, T. Ahrens, D. Bourget, N. Swann, P. Starr, J. M. Carmena, and T. Denison, "Enabling closed-loop neurostimulation research with downloadable firmware upgrades," in *IEEE BioCAS*, pp. 1–6, 2015.

[96] M. Barbe, L. Liebhart, M. Runge, K. Pauls, L. Wojtecki, A. Schnitzler, N. Allert, G. Fink, V. Sturm, M. M, and L. Timmermann, "Deep brain stimulation in the nucleus ventralis intermedius in patients with essential tremor: habituation of tremor suppression," *J Neurol*, vol. 258, no. 12, p. 434–439, 2011.

[97] N. Patel, W. Ondo, and J. Jimenez-Shahed, "Habituation and rebound to thalamic deep brain stimulation in long-term management of tremor associated with demyelinating neuropathy," *Int'l J of Neurosci*, vol. 124, no. 12, pp. 919–925, 2014.

[98] A. Fasano and R. Helmich, "Tremor habituation to deep brain stimulation: Underlying mechanisms and solutions," *Mov Disord*, vol. 34, no. 12, pp. 1761–1773, 2019.

[99] A. Haddock, H. J. Chizeck, and A. L. Ko, "Deep neural networks for context-dependent deep brain stimulation," in *2019 9th Int'l IEEE NER*, pp. 957–960, 2019.

[100] M. M. Reich, J. Brumberg, N. G. Pozzi, G. Marotta, J. Roothans, M. Åström, T. Musacchio, L. Lopiano, M. Lanotte, R. Lehrke, A. K. Buck, J. Volkmann, and I. U. Isaias, "Progressive gait ataxia following deep brain stimulation for essential tremor: adverse effect or lack of efficacy?," *Brain*, vol. 139, no. 1, pp. 2948–2956, 2016.

[101] M. I. Hariz, P. Shamsgovara, F. Johansson, G. M. Hariz, and H. Fodstad, "Tolerance and tremor rebound following long-termchronic thalamic stimulation for parkinsonian and essential tre-mor.," *Stereotactic Func Neurosurg*, vol. 72, no. 2-4, pp. 208–218, 1999.

[102] S. E. Cooper, C. C. McIntyre, H. H. Fernandez, and J. L. Vitek, "Association of deep brain stimulation washout effects with parkinson disease duration," *Arch of Neurol*, vol. 70, no. 1, pp. 95–99, 2013.

[103] S. S. Cooper*, B. I. Ferleger*, A. L. Ko, J. A. Herron, and H. J. Chizeck, "Rebound effect in deep brain stimulation for essential tremor and symptom severity estimation from neural data," in *Proc. 42nd Conf IEEE EMBC*, (Montreal, Canada), 2020.

[104] E. Opri, S. Cernera, R. Molina, R. S. Eisinger, J. N. Cagle, L. Almeida, T. Denison, M. S. Okun, K. D. Foote, and A. Gunduz, "Chronic embedded cortico-thalamic closed-loop deep brain stimulation for the treatment of essential tremor," *Sci Transl Med*, vol. 12, no. 572, 2020.

[105] N. Khobragade, D. Graupe, and D. Tuninetti, "Towards fully automated closed-loop deep brain stimulation in parkinson's disease patients: A lamstar-based tremor predictor," *Proc 37th IEEE EMBS*, pp. 2616–19, 2015.

[106] S. Castaño Candamil, B. I. Ferleger, A. Haddock, S. S. Cooper, J. A. Herron, A. L. Ko, H. J. Chizeck, and M. Tangermann, "A pilot study on data-driven adaptive deep brain stimulation in chronically implanted essential tremor patients," *Front Hum Neurosci*, 2020.

[107] F. Panov, E. Levin, C. de Hemptinne, N. Swann, S. Qasim, S. Miocinovic, J. Ostrem, and P. Starr, "Intraoperative electrocorticography for physiological research in movement disorders: principles and experience in 200 cases," *J Neurosurg*, vol. 126, no. 1, pp. 122–31, 2017.

[108] K. Hoang, I. Cassar, W. Grill, and D. Turner, "Biomarkers and stimulation algorithms for adaptive brain stimulation," *Front Neurosci*, vol. 11, no. 564, 2017.

[109] S. Little and P. Brown, "What brain signals are suitable for feedback control of deep brain stimulation in Parkinson's disease?: Brain signals for control of DBS in PD," *Ann NY Acad Sci*, vol. 1265, pp. 9–24, Aug. 2012.

[110] A. Priori, G. Foffani, L. Rossi, and S. Marceglia, "Adaptive deep brain stimulation (adbs) controlled by local field potential oscillations," *Exp Neurol*, vol. 245, pp. 77–86, 2013.

[111] D. Whitmer, C. de Solages, B. Hill, H. Yu, J. Henderson, and H. Bronte-Stewart, "High frequency deep brain stimulation attenuates subthalamic and cortical rhythms in parkinson's disease," *Front Hum Neuro*, vol. 6, no. 155, 2012.

[112] C. Cao, K. Zeng, D. Li, S. Zhan, X. Li, and B. Sun, "Modulations on cortical oscillations by subthalamic deep brain stimulation in patients with parkinson disease: A meg study," *Neurosci Letters*, vol. 636, pp. 95–100, 2017.

[113] A. A. Kühn, A. Tsui, T. Aziz, N. Ray, C. Brücke, A. Kupsch, G.-H. Schneider, and P. Brown, "Pathological synchronisation in the subthalamic nucleus of patients with Parkinson's disease relates to both bradykinesia and rigidity," *Exp Neurol*, vol. 215, no. 2, pp. 380–387, 2009.

[114] A. A. Kühn, F. Kempf, C. Brücke, L. G. Doyle, I. Martinez-Torres, A. Pogosyan, T. Trottenberg, A. Kupsch, G.-H. Schneider, M. I. Hariz, *et al.*, "High-frequency stimulation of the subthalamic nucleus suppresses oscillatory β activity in patients with parkinson's disease in parallel with improvement in motor performance," *J Neurosci*, vol. 28, no. 24, pp. 6165–6173, 2008.

[115] Z. Blumenfeld and H. Brontë-Stewart, "High Frequency Deep Brain Stimulation and Neural Rhythms in Parkinson's Disease," *Neuropsych Rev*, vol. 25, pp. 384–397, Dec. 2015.

[116] W.-J. Neumann, F. Staub-Bartelt, A. Horn, J. Schanda, G.-H. Schneider, P. Brown, and A. A. Kühn, "Long term correlation of subthalamic beta band activity with motor impairment in patients with Parkinson's disease," *Clin Neurophysiol*, vol. 128, no. 11, pp. 2286–2291, 2017.

[117] D. Weiss, R. Klotz, R. B. Govindan, M. Scholten, G. Naros, A. Ramos-Murguialday, F. Bunjes, C. Meisner, C. Plewnia, R. Krüger, and A. Gharabaghi, "Subthalamic stimulation modulates cortical motor network activity and synchronization in Parkinson's disease," *Brain*, vol. 138, pp. 679–693, Mar. 2015.

[118] B. Rosin, M. Slovik, R. Mitelman, M. Rivlin-Etzion, S. N. Haber, Z. Israel, E. Vaadia, and H. Bergman, "Closed-loop deep brain stimulation is superior in ameliorating parkinsonism," *Neuron*, vol. 72, no. 2, pp. 370–384, 2011.

[119] S. Little, M. Beudel, L. Zrinzo, T. Foltynie, P. Limousin, M. Hariz, S. Neal, B. Cheeran, H. Cagnan, J. Gratwicke, *et al.*, "Bilateral adaptive deep brain stimulation is effective in parkinson's disease," *J Neurol Neurosurg Ps*, pp. jnnp–2015, 2015.

[120] L. Johnson, S. Nebeck, A. Muralidharan, M. Johnson, K. Baker, and J. Vitek, "Closed-loop deep brain stimulation effects on parkinsonian motor symptoms in a non-human primate–is beta enough?," *Brain Stimulation*, vol. 9, no. 6, pp. 892–896, 2016.

[121] B. Blankertz, S. Lemm, M. Treder, S. Haufe, and K. Müller, "Single-trial analysis and classification of erp components—a tutorial," *NeuroImage*, vol. 56, no. 2, pp. 814–825, 2011.

[122] M. Tangermann, K. R. Müller, A. Aertsen, N. Birbaumer, C. Braun, C. Brunner, R. Leeb, C. Mehring, K. J. Miller, and G. Mueller-Putz, "Review of the bci competition iv," *Front Neurosci*, vol. 6, p. 55, 2012.

[123] A. Meinel, S. Castaño-Candamil, J. Reis, and M. Tangermann, "Pre-trial eeg-based single-trial motor performance prediction to enhance neuroergonomics for a hand force task," *Front Hum Neurosci*, vol. 10, p. 170, 2016.

[124] A. T. Connolly, A. L. Jensen, K. B. Baker, J. L. Vitek, and M. D. Johnson, "Classification of pallidal oscillations with increasing parkinsonian severity," *Journal of neurophysiology*, vol. 114, no. 1, pp. 209–218, 2015.

[125] H. Tan, J. Debarros, S. He, A. Pogosyan, T. Z. Aziz, Y. Huang, S. Wang, L. Timmermann, V. Visser-Vandewalle, D. J. Pedrosa, *et al.*, "Decoding voluntary movements and postural tremor based on thalamic lfps as a basis for closed-loop stimulation for essential tremor," *Brain Stimulation*, vol. 12, no. 4, pp. 858–867, 2019.

[126] L. Yao, P. Brown, and M. Shoaran, "Improved detection of parkinsonian resting tremor with feature engineering and kalman filtering," *Clin Neurophysiol*, vol. 131, no. 1, pp. 274–284, 2020.

[127] G. Tinkhauser, A. Pogosyan, S. Little, M. Beudel, D. M. Herz, H. Tan, and P. Brown, "The modulatory effect of adaptive deep brain stimulation on beta bursts in parkinson's disease," *Brain*, vol. 140, no. 4, pp. 1053–1067, 2017.

[128] E. M. Moraud, G. Tinkhauser, M. Agrawal, P. Brown, and R. Bogacz, "Predicting beta bursts from local field potentials to improve closed-loop dbs paradigms in parkinson's patients," in *2018 40th Annual International Conference of the IEEE Engineering in Medicine and Biology Society (EMBC)*, pp. 3766–3796, IEEE, 2018.

[129] D. Piña-Fuentes, J. C. van Zijl, J. M. C. van Dijk, S. Little, G. Tinkhauser, D. M. Oterdoom, M. A. Tijssen, and M. Beudel, "The characteristics of pallidal low-frequency and beta bursts could help implementing adaptive brain stimulation in the parkinsonian and dystonic internal globus pallidus," *Neurobiology of disease*, vol. 121, pp. 47–57, 2019.

[130] I. Adamchic, C. Hauptmann, U. B. Barnikol, N. Pawelczyk, O. Popovych, T. T. Barnikol, A. Silchenko, J. Volkmann, G. Deuschl, W. G. Meissner, *et al.*, "Coordinated reset neuromodulation for Parkinson's disease: proof-of-concept study," *Mov Disord*, vol. 29, no. 13, pp. 1679–1684, 2014.

[131] J. Wang, S. Nebeck, A. Muralidharan, M. D. Johnson, J. L. Vitek, and K. B. Baker, "Coordinated reset deep brain stimulation of subthalamic nucleus produces long-lasting, dose-dependent motor improvements in the 1-methyl-4-phenyl-1, 2, 3, 6-tetrahydropyridine non-human primate model of Parkinsonism," *Brain stimulation*, vol. 9, no. 4, pp. 609–617, 2016.

[132] H. Cagnan, D. Pedrosa, S. Little, A. Pogosyan, B. Cheeran, T. Aziz, A. Green, J. Fitzgerald, T. Foltynie, P. Limousin, *et al.*, "Stimulating at the right time: phase-specific deep brain stimulation," *Brain*, vol. 140, no. 1, pp. 132–145, 2016.

[133] S. E. Cooper, C. C. McIntyre, H. H. Fernandez, and J. L. Vitek, "Association of deep brain stimulation washout effects with Parkinson disease duration," *JAMA neurology*, vol. 70, no. 1, pp. 95–99, 2013.

[134] R. J. Elble, H. Hellriegel, J. Raethjen, and G. Deuschl, "The essential tremor rating assessment scale," *J Neurol Neuromed*, vol. 1, no. 4, pp. 34–38, 2016.

[135] S. Fahn, E. Tolosa, and C. Marín, "Clinical rating scale for tremor," *Parkinson's disease and Mov Disord*, vol. 2, pp. 271–80, 1993.

[136] A. Gramfort, M. Luessi, E. Larson, D. A. Engemann, D. Strohmeier, C. Brodbeck, R. Goj, M. Jas, T. Brooks, L. Parkkonen, *et al.*, "Meg and eeg data analysis with mne-python," *Frontiers in neuroscience*, vol. 7, p. 267, 2013.

[137] J. Raethjen and G. Deuschl, "The oscillating central network of essential tremor," *Clin Neurophysiol*, vol. 123, no. 1, pp. 61–64, 2012.

[138] B. van Wijk, P. J. Beek, and A. Daffertshofer, "Neural synchrony within the motor system: what have we learned so far?," *Front Hum Neurosci*, vol. 6, p. 252, 2012.

[139] K. A. Neely, A. S. Kurani, P. Shukla, P. J. Planetta, A. Wagle Shukla, J. G. Goldman, D. M. Corcos, M. S. Okun, and D. E. Vaillancourt, "Functional brain activity relates to 0–3 and 3–8 hz force oscillations in essential tremor," *Cerebral Cortex*, vol. 25, no. 11, pp. 4191–4202, 2014.

[140] T. C. Bulea, S. Prasad, A. Kilicarslan, and J. L. Contreras-Vidal, "Sitting and standing intention can be decoded from scalp eeg recorded prior to movement execution," *Front Neurosci*, vol. 8, p. 376, 2014.

[141] B. Pollok, V. Krause, W. Martsch, C. Wach, A. Schnitzler, and M. Südmeyer, "Motor-cortical oscillations in early stages of Parkinson's disease: Suppression of motor cortical beta oscillations is altered in early PD," *J Physiol*, vol. 590, pp. 3203–3212, July 2012.

[142] J. Bollinger, *Bollinger on Bollinger bands*. McGraw Hill Professional, 2001.

[143] A. Kane, W. D. Hutchison, M. Hodaie, A. M. Lozano, and J. O. Dostrovsky, "Enhanced synchronization of thalamic theta band local field potentials in patients with essential tremor," *Exp Neurol*, vol. 217, no. 1, pp. 171–176, 2009.

[144] C. Pulliam, S. Eichenseer, C. Goetz, O. Waln, C. Hunter, J. Jankovic, D. Vaillancourt, J. Giuffrida, and D. Heldman, "Continuous in-home monitoring of essential tremor," *Parkinsomism & Relat Disord*, vol. 20, pp. 37–40, 2014.

[145] B. Ferleger, K. Sonnet, T. Morriss, A. Ko, H. Chizeck, and J. Herron, "A tablet- and mobile-based application for remote diagnosis and analysis of movement disorder symptoms," in *Proc. 42nd Conf IEEE EMBC*, 2020.

[146] T. Morishita, K. D. Foote, S. S. Wu, C. E. Jacobson, R. L. Rodriguez, I. U. Haq, M. S. Siddiqui, I. A. Malaty, C. J. Hass, and M. S. Okun, "Brain penetration effects of microelectrodes and deep brain stimulation leads in ventral intermediate nucleus stimulation for essential tremor," *J Neurosurg*, 2010.

[147] C. Granziera, C. Pollo, H. Russmann, C. Staedler, J. Ghika, J.-G. Villemure, P. Burkhard, and F. Vingerhoets, "Sub-acute delayed failure of subthalamic dbs in parkinson's disease: The role of micro-lesion effect," *Parkinsonism Related Disorders*, vol. 14, no. 2, pp. 109 – 113, 2008.

[148] S. Farris and M. Giroux, "Retrospective review of factors leading to dissatisfaction with subthalamic nucleus deep brain stimulation during long-term management," 2013.

[149] C. L. Pulliam, D. A. Heldman, T. H. Orcutt, T. O. Mera, J. P. Giuffrida, and J. L. Vitek, "Motion sensor strategies for automated optimization of deep brain stimulation in parkinson's disease," *Parkinsonism Relat Disord*, vol. 21, no. 4, pp. 378–382, 2015.

[150] C. Ramaker, J. Marinus, A. M. Stiggelbout, and B. J. van Hilten, "Systematic evaluation of rating scales for impairment and disability in Parkinson's disease," *Mov Disord*, vol. 17, pp. 867–876, Sept. 2002.

[151] A. Siderowf, M. McDermott, K. Kieburtz, K. Blindauer, S. Plumb, and I. Shoulson, "Test–retest reliability of the unified parkinson's disease rating scale in patients with early parkinson's disease: Results from a multicenter clinical trial," *Movement Disorders*, vol. 17, no. 4, pp. 758–763, 2002.

[152] J. P. Giuffrida, D. Riley, B. Maddux, and D. Heldman, "Clinically deployable kinesia technology for automated tremor assessment," *Mov Disord*, vol. 24, 2009.

[153] P. Lin, K.-H. S. Chen, B.-S. Yang, and Y. jung Chen, "A digital assessment system for evaluating kinetic tremor in essential tremor and parkinson's disease," *BMC Neurology*, vol. 18, 2018.

[154] M. San Luciano, C. Wang, R. A. Ortega, Q. Yu, S. Boschung, J. Soto-Valencia, S. B. Bressman, R. B. Lipton, S. Pullman, and R. Saunders-Pullman, "Digitized spiral drawing: A possible biomarker for early parkinson's disease," *PLOS ONE*, vol. 11, no. 10, pp. 1–11, 2016.

[155] M. E. Isenkul, B. E. Sakar, and O. Kursun, "Improved spiral test using digitized graphics tablet for monitoring parkinson's disease," 2014.

[156] D. Surangsrirat and C. Thanawattano, "Android application for spiral analysis in parkinson's disease," *Conference Proceedings - IEEE SOUTHEASTCON*, 03 2012.

[157] P. Drotár, J. Mekyska, I. Rektorová, L. Masarová, Z. Smékal, and M. Faundez-Zanuy, "Evaluation of handwriting kinematics and pressure for differential diagnosis of parkinson's disease," *AI in Medicine*, vol. 67, pp. 39 – 46, 2016.

[158] J. Solé-Casals, I. Anchustegui-Echearte, P. Marti-Puig, P. Calvo, A. Bergareche, J. Sánchez-Méndez, and K. Lopez-de Ipina, "Discrete cosine transform for the analysis of essential tremor," *Front. in Physio.*, vol. 10, 2019.

[159] K. Sonnet, B. Ferleger, A. Ko, H. Chizeck, and J. Herron, "Multi-class classification and feature analysis of ftm drawing tasks in a digital assessment of tremor," in *IEEE BIBE*, 2020.

[160] S. Little, A. Pogosyan, S. Neal, B. Zavala, L. Zrinzo, M. Hariz, T. Foltynie, P. Limousin, K. Ashkan, J. FitzGerald, *et al.*, "Adaptive deep brain stimulation in advanced parkinson disease," *Ann Neurol*, vol. 74, no. 3, pp. 449–457, 2013.